INFORMATION-USE STRATEGIES IN ANTS

by

Andrew James Basinski

A dissertation submitted to the faculty of
The University of Utah
in partial fulfillment of the requirements for the degree of

Doctor of Philosophy

Department of Mathematics

The University of Utah

December 2016

The University of Utah Graduate School

STATEMENT OF DISSERTATION APPROVAL

The dissertation of **Andrew James Basinski**

has been approved by the following supervisory committee members:

Frederick R. Adler ,	Chair(s)	**29 July 2016** Date Approved
Alla R. Borisyuk ,	Member	**29 July 2016** Date Approved
Donald H. Feener Jr. ,	Member	**29 July 2016** Date Approved
James P. Keener ,	Member	**29 July 2016** Date Approved
John T. Longino ,	Member	Date Approved

by **Peter Trapa** , Chair/Dean of

the Department/College/School of **Mathematics**

and by **David B. Kieda** , Dean of The Graduate School.

ABSTRACT

Chapter 1 introduces a classic question from optimal foraging theory regarding space-use strategies of a forager, and gives context for addressing similar questions in groups of foraging ants.

Chapter 2 generalizes the marginal value theorem (MVT) model by describing a rate-maximizing forager searching for pointwise resources with a specific searching distribution around previous resource finds, and giving-up value (GUV) strategy at resources. The model shows that the optimal ARS breadth increases, and the optimal GUV decreases, with increased dispersion of the resource distribution.

Chapter 3 builds an agent-based model (ABM) and corresponding PDE model derived from an isotropic diffusion limit. The model links individual movement biases in the presence of pheromone to the colony-wide searching distribution. Parameterized with movement data obtained from *Tetramorium caespitum* (the pavement ant), the model predicts bistability in pheromonal recruitment at resource distances of 3 - 6 m; the onset-distance of bistability increases with colony size.

Data collected from the field are used to estimate parameters of the PDE model for *T. caespitum* in Chapter 4. The ability of *T. caespitum* to find autocorrelated resources during recruitment is analyzed using a Cox proportional hazards model, the results of which are compared to those predicted by the PDE model developed in Chapter 3. Finally, Chapter 5 develops a simulation to assess the effect of individual trail fidelity on the ability of a colony to capitalize on autocorrelated resources in different resource scenarios; the results suggest that *T. caespitum* is tuned to exploit large, nonautocorrelated resource distributions.

For my family.

CONTENTS

ABSTRACT . . . . . **iii**

LIST OF FIGURES . . . . . **vii**

LIST OF TABLES . . . . . **viii**

CHAPTERS

1. INTRODUCTION **1**

2. A SPATIALLY EXPLICIT MARGINAL VALUE MODEL **5**

2.1 Methods 8
2.1.1 Exploitation phase 8
2.1.2 1-D environment 9
2.1.2.1 Deriving the discovery-time distribution 10
2.1.2.2 Deriving the finding location distribution 10
2.1.2.3 Continuous space limit 11
2.1.2.4 longterm searching time average $\hat{T}$ 12
2.1.3 Extension to 2-D 12
2.1.4 Parameter values and functional forms 13
2.2 Algorithms to Find the Expected Collection Rate 14
2.2.1 Using analytical calculations 14
2.2.2 Stochastic simulation 15
2.2.2.1 Resource falls into the environment 16
2.2.2.2 Resource disappears 16
2.2.2.3 The forager finds a resource 16
2.3 Results 17
2.4 Discussion 19

3. PHEROMONAL RECRUITMENT MODEL **28**

3.1 Methods 32
3.1.1 Habitat 32
3.1.2 States, transitions, and movement 32
3.1.3 Continuum limit of ABM in the absence of the resource 35
3.1.4 Continuum limit with resource present 37
3.1.5 Parameter Set 39
3.1.6 Bifurcation Simulations 40
3.2 Results 41
3.3 Discussion 42

4. MODEL PARAMETERIZATION AND VALIDATION **56**

4.1 Parameters obtained from literature 56

4.2 Movement parameter estimation 57
4.3 v estimate 60
4.4 Experiment 1: null searching state 60
4.5 Experiment 2: ARS searching state 60
4.6 Data Analysis 61
4.7 Results 62
4.8 Model prediction 63
4.9 q_S Estimate 63
4.10 Discussion 64

5. MECHANISM AND BENEFITS OF COLONY-WIDE ARS 70

5.1 Methods 72
5.1.1 Simulation overview 73
5.1.2 Non-ARS strategy 73
5.1.3 ARS simulation 74
5.1.4 PDE steady states and searching distributions 75
5.1.5 Parameter values 75
5.1.6 Simulations 76
5.1.7 Data analysis 76
5.2 Results 76
5.3 Discussion 77

APPENDICES

A. NUMERICAL CALCULATIONS IN CHAPTER 2 87

B. COMPUTATION AND DIFFUSION LIMIT OF CHAPTER 3 89

C. SIMULATION ADD-ON TO CHAPTER 5 102

REFERENCES 104

LIST OF FIGURES

2.1 Collection rate vs. searching strategy 23
2.2 Optimal GUV for various resource dynamics and search strategy 24
2.3 Optimal σ_f vs. σ_r 25
2.4 Relative collection rate vs. σ_r 25
2.5 Collection rate vs. search strategy in the memoryless case 26
3.1 Bifurcation diagrams of the ABM 45
3.2 Bistable searching distributions 46
3.3 Bifurcation diagrams of the ABM 47
3.4 Bifurcation diagrams of the ABM 48
3.5 Bifurcation diagrams of the PDE 49
3.6 Bifurcation diagrams of the PDE 50
3.7 Searching distributions of the PDE and ABM 51
3.8 Searching distributions of the PDE and ABM 52
3.9 Searching distributions of the PDE and ABM 53
3.10 Bifurcation diagrams of *T. caespitum* 53
4.1 Boxplots of κ and ρ estimates 67
4.2 Histograms of ρ estimates 67
4.3 Survival plots of empirical data 68
5.1 Collection rate boxplots with variable environment, $\sigma_r = 5$, $r_c = 2$ 81
5.2 Collection rate boxplots with variable environment, $\sigma_r = 1$, $r_c = 2$ 82
5.3 Collection rate boxplots with variable environment, $\sigma_r = 1$, $r_c = 5$ 83
5.4 Optimal trail fidelity and colony size 84
5.5 Collection rate boxplots with variable environment, $\sigma_r = 1$, $r_c = 5$ 85

LIST OF TABLES

2.1 Parameter values used in the simulations 27
3.1 State space of ABM 54
3.2 Transition rates in the ABM 54
3.3 Parameter values in the ABM 54
3.4 ABM movement parameters 55
3.5 PDE parameter values 55
4.1 Maximum likelihood estimates of κ and ρ 68
4.2 Cox model of experiment 2 69
5.1 Parameters of the search-recruit simulation 86

CHAPTER 1

INTRODUCTION

Optimal foraging theory (OFT) seeks to understand how foraging behavior has been tuned by natural selection to optimize food collection. Two major goals of OFT are to understand the optimal foraging strategy given a particular resource scenario, and to determine how that strategy can be realized from the perspective of the forager using information from its environment [65]. The latter goal is especially important when applying OFT-based questions to an ant colony; here, a strategy that is optimal at the colony level may require the coordination of thousands of individuals. Understanding how individual behavior is tuned to facilitate this coordination and attain a desired colony-wide response is a major challenge in applying OFT to colonies of ants.

A classic question in OFT concerns how foraging effort should be allocated by a solitary forager in space when the resource distribution is heterogeneous [65]. One of the earliest mathematical descriptions of space use strategies is given by Charnov's 1976 patch exploitation model. The model describes a rate-maximizing forager that must decide how much time to spend in a patch before traveling to another, with diminishing returns at each patch providing the impetus to leave. The optimal strategy is given by the so-called marginal value theorem (MVT), which states that an optimal forager will leave a patch when its instantaneous collection rate is equal to its longterm average collection rate. The MVT result gives several qualitative predictions of foraging trends: a forager should remain in a patch until its marginal rate of return is equal to its longterm collection rate, and all patches should be depleted to the same giving-up density (GUD) [15].

Though useful in predicting a diversity of foraging trends, the MVT does not describe the individual behaviors that gives rise to the optimal strategy [4]. A more mechanistic development of space use in a rate-maximizing forager comes from the concept of area-restricted search (ARS), a strategy in which a forager intensifies its search effort around a

previous resource find by modifying attributes of its random walk [10, 13, 40]. Computer simulation models have been used to understand how the forager's search strategy should vary with the resource distribution being foraged, and generally show that a smaller breadth ARS around a previous find is optimal in more autocorrelated resource environments [61,79]. These models are able to qualitatively predict how aspects of the forager's movements should vary with its typical resource distribution to optimize collection.

Continuing this line of research, Chapter 2 presents a spatially explicit version of Charnov's patch exploitation model. The model describes a forager that searches for pointwise resources in explicit 2D space and faces diminishing returns at a resource; the strategy it uses is its ARS breadth and giving-up value (GUV) at a resource. The results show that the optimal search breadth increases with spatial autocorrelation of the resource distribution, and that the optimal GUV at a resource decreases with increased resource dispersion. This model improves upon previous ARS work in that it contains both analytical and simulation components, and includes a description of exploitation dynamics (the GUV) at the resource; previous work assumes resource collection is instantaneous [61].

Ant colonies also benefit by directing searching effort to profitable regions of space; however, coordinating the movements of many individual ants is a challenge, as individual ants lack central leadership, operate on simple behavioral rules, and have small perceptual radii that limit the amount of the environment that can be tracked, as well as communication between individuals [35]. The behavioral response of a colony is realized by local information transmitted between individuals, along with subsequent changes in individual behavior [24]. Of course, natural selection operates at the colony level; predicting the optimal individual behavior that scales up to the optimal colony-wide behavior is a major challenge of applying OFT to an ant colony.

Pheromonal recruitment is an example of a colony-wide behavior that serves as an efficient means of directing individuals to a resource. During recruitment, an ant that discovers a resource returns to the nest, laying a pheromone trail. At the nest, she prompts nestmates to leave via "antennal beating" and trophollaxis (food sharing) [72]. The so-called recruited nestmates follow the pheromone trail and repeat the recruitment process [35].

More generally, pheromonal recruitment is a means to efficiently spread information through the colony. The rate at which information spreads is influenced by positive feed-

back as more individuals become recruiters, information decay as a result of pheromone evaporation, and noise from differential success in following the pheromone trail. These three factors give pheromonal recruitment the potential to act as a bistable system in 2D space. If bistable, the longterm dynamics of the process can either equilibrate at high levels of recruitment, with a strong pheromone trail and high levels of workers moving between the nest and resource or low levels of recruitment, with a weak trail and few foragers outside the nest. The equilibrial dynamics that are realized depend on the initial state of the colony [9]. If present, bistability influences the ability of a colony to generate a colony-wide foraging response, and has also been implicated in the evolution of group recruitment in *Tetramorium caespitum* [18].

Understanding whether positive feedback, information decay, and noise give rise to bistability requires a mathematical model. Though some experimental results suggest bistability being prevalent in certain species during pheromonal recruitment, it is generally difficult to untangle the effects of a particular experimental setup (i.e., a 1D or otherwise limited foraging arena) [9, 18]. A mathematical model built from movement behavior can be implemented on any foraging arena and used to understand the existence of bistability from the perspective of an individual's behavioral program.

Chapter 3 builds an agent-based model (ABM) and partial differential equation (PDE) model that links individual movement biases in the presence of pheromone to the colony-wide searching distribution, as well as exploitation dynamics at the resource. The ABM allows the modeling description to start at the individual level, and incorporates stochasticity in behavioral responses. The PDE model allows the results of the ABM to be clearly interpreted without relying on the averages of many simulations. The model improves upon past work by being spatially explicit, parameterized by individual behavior, and tracking the positions and behavioral states of all individuals. The model result shows that pheromonal recruitment is bistable in 2D space, and gives quantitative predictions of the distribution of foragers at both high and low recruiting equilibria. Parameterized with *T. caepsitum* movement parameters, the model shows that bistability is present in this system with an onset at 3 - 6 m, depending on colony size.

A classic tradeoff in OFT applied to ants is between exploitation, or an efficient response to an environmental opportunity, and exploration, the ability to quickly learn about new

environmental opportunities that appear. The scout-recruit tradeoff, for example, seeks to understand the optimal fraction of the colony that should be scouting the environment for new finds, and the complement that stay at the nest ready to aid in exploitation [39]. The tradeoff also appears in the optimal number of nests to divide a colony into; a colony divided into many nests is on average better at exploring its environment and tracking newly appearing resources, but at a cost to recruitment capabilities due to smaller nest sizes [19].

Another example of the exploration-exploitation tradeoff concerns the trail fidelity of individuals during pheromonal recruitment. Ants following a pheromone trail make errors; some become lost, and do not move directly from the nest to the resource [23]. Deneubourg et al. (1983) hypothesized that this noise in the pheromonal recruitment process could be tuned by natural selection to allow a colony to simultaneously exploit a resource and search for spatially autocorrelated resources, generating a colony-wide ARS. In this scenario, individual error in trail-following increases the spread of searching ants around a resource being exploited, resulting in efficient finding of autocorrelated resources [23]. Though Deneubourg et al. (1983) give empirical measurements of ants that differ in trail fidelity, the experiment does not determine whether lost ants actually contribute to autocorrelated resource finds.

This hypothesis is investigated with empirical experiments in Chapter 4. Using *T. caespitum* as the study organism, empirical work shows that autocorrelated resources are found more quickly during recruitment than the initial resource find. The parameterized PDE model is validated by simulating scenarios similar to the empirical work, and is shown to qualitatively match the empirical finding trends. In Chapter 5, a simulation model is used to understand how trail fidelity could tune the recruitment process to capitalize on autocorrelated resource distributions. The results indicate that *T. caespitum*'s trail fidelity is tuned to maximize exploitation of single, large resources.

CHAPTER 2

A SPATIALLY EXPLICIT MARGINAL VALUE MODEL

The marginal value theorem (MVT) provides an important framework for understanding animal foraging behavior in patchy environments. The MVT describes a rate-maximizing forager that must choose its foraging duration in a patch of food items before seeking out another patch, and states that a forager should leave a patch when its marginal rate of food collection in the patch is equal to its longterm average collection rate in the environment [15]. The impetus to leave comes from diminishing returns of food collection, attributed to patch depletion and the subsequent increased search time to find resources within the patch. If the forager remains in the patch for too long, this decreased collection rate becomes an opportunity cost; the forager would be better off paying the travel time cost of moving to a new patch [15].

The MVT gives three testable predictions of how organisms should forage in patchy environments: 1) an organism should spend more time in higher quality patches before departing; 2) patches should be depleted to the same "giving-up density" before departure, regardless of their starting value; and 3) foragers should spend more time in patches when the average travel travel time between patches is large. The MVT has been used to interpret foraging behavior in a wide range of organisms, including ants [42], parasitoids [68, 74], plants [49], and birds [58]. However, while it may be evident that a forager is following qualitative predictions of the MVT (i.e., staying longer in more profitable regions of the environment), the MVT gives little insight into how such a strategy is realized [4].

A more mechanistic development of the MVT comes from the concept of an area-restricted search (ARS), where a forager searches with higher intensity after finding a resource. Many organisms modify the intensity of search in response to information collected from the environment, including nematodes searching for bacteria [34], ants searching

for carbohydrate and protein food sources [30], bees searching for flowers [20], and birds searching for marine prey [54,77]. In these examples, foraging success is a cue for animals to adjust movement attributes so as to slow net displacement as the animal continues to search, thus focusing searching activity on profitable parts of the environment. ARS provides a link between qualitative foraging patterns that resemble predictions of the MVT with individual movement behavior.

Random walk models have given insight into the value of particular individual search strategies in different resource distributions. The search strategy is modeled as a series of steps whose length and changes in direction are random variables. ARS results when a forager reduces its net displacement, either by taking smaller steps or by increasing its turning angle after locating a resource [10,13,40]. Simulations of solitary foragers following a random walk show that the optimal movement rules of an individual depend on the resource distribution in the environment; a more restricted search strategy performs better when searching for patchier resources [61,79].

Empirical evidence shows that some organisms adjust the intensity of ARS according to the type of resource that is encountered. For example, the Namaqua sand lizard's (*Pedioplanis namaquensis*) searching intensity (as measured by first passage times) is significantly higher after consuming termite prey when compared to fly prey [27]. Searching intensity is influenced by the anticipated distribution of other termites nearby; because termite colonies are a clumped resource, ARS is more likely to result in subsequent finds. As a less clumped resource, fly prey do not give information on the location of subsequent fly finds, decreasing the benefits of subsequent ARS. Similarly, individual ants can adjust the breadth of their ARS in response to the food type they are searching for [30,63,70]. Schultheiss and Cheng (2012) presented *Melophorus bagoti* colonies with either a protein source (mealworm) or carbohydrate resource (cookie crumbs). The ants were allowed to learn the resource's position for 2 days, after which the resource was removed and ant searching behavior was observed. Foragers that had experienced cookie crumbs had tighter ARS's than foragers that experienced mealworms. In the field, *M. bagoti* encounters carbohydrate resources in the form of plant exudates or aphid secretions; these sources are typically clustered on a plant, and renewable. Protein resources are typically dead insects, and are not spatially clustered or renewable. Schultheiss and Cheng argue that natural selection has primed the ants to

better remember the spatial location of carbohydrate sources than protein sources [63].

Foragers that follow the MVT might benefit from an ARS strategy when a patch has been depleted to its giving-up density or is rejected upon encounter. Though giving-up densities of ants at a resource have not been directly measured, it is known that ants reject sucrose and protein solutions below a threshold concentration [42]. An ant foraging on an aphid's honeydew secretions, for example, must decide a threshold intake rate at which to abandon the aphid and seek out another; however, little is known of how a resource encounter influences subsequent searching behavior once a resource is abandoned. The goal of this paper is to build a spatially explicit model of a forager that exploits pointwise resources in its environment, and link predictions of the MVT, such as the relationship between giving-up density and inter-resource travel time, to predictions of the optimal ARS intensity following the abandonment of a depleted resource. Specifically, this model will connect the inter-resource travel time to a specific ARS search strategy.

Resource scenarios can pose different kinds of challenges for foragers: resources may appear infrequently or disappear quickly, be dispersed throughout the environment (lack a spatial signal), or be difficult to locate when present. This paper uses simulation and a mathematical model, centered around a general, solitary forager, to investigate the optimal search intensity following a resource find in each of these scenarios. Previous models of optimal ARS have focused on resources that are collected instantaneously [61, 79]; however, resource exploitation by small organisms, such as ants on aphids or bees on flowers, can represent a significant fraction of time spent foraging. This paper shows that the optimal amount of time to spend foraging at a particular resource is influenced by the search strategy chosen and the spatial distribution of resources in the environment. The mathematical model describes an iterative process that ignores resource depletion by the focal forager. To test the validity of the results under this assumption, they are compared to a nonrenewal process version of our model that accounts for forager depletion. Comparison of the two highlights when a forager's strategy will be most influenced by the depletion that it causes.

Specifically, the model will address (1) how the optimal standard deviation of searching spread depends on the resource distribution and the rate of resource appearance and disappearance, (2) the payoff of this optimal strategy compared to a null searching strategy, (3) the optimal resource value to cease foraging at a resource and search for another (the

giving-up value, hereafter referred to as the GUV), and (4) how the optimal collection rate of the renewal process compares to a process with forager-induced depletion.

2.1 Methods

This section models a renewal process describing an individual forager that switches between two nonoverlapping phases: exploiting a resource, and an area-restricted search centered around the resource until the next resource is found.

2.1.1 Exploitation phase

During the exploitation phase, the forager collects food at rate $b\,A(t)$, where $A(t)$ is the fraction of food remaining at the resource t hours into collection, and b is the collection rate (measured as fraction of resource collected per time) at the resource. Resource items all begin with initial value $A_0 = 1$. If $C(t)$ denotes the amount of food collected by time t, then $C(t) = A_0 - A(t)$, where

$$\frac{dA}{dt} = -bA \tag{2.1}$$

Solving Equation (2.1) with $A(0) = 1$ yields collection as a function of time:

$$C(t) = 1 - e^{-bt}. \tag{2.2}$$

The forager is assumed to switch from exploitation to searching at some critical time t_{crit}. Mechanistically, this sudden quitting represents the individual abandoning the resource when its intake rate falls below some threshold b_{crit}. At time t, the collection rate is $\frac{dC}{dt} = be^{-bt}$, so formulating the model in terms of either t_{crit} or b_{crit} is equivalent. For ease of presentation, work with t_{crit}. Define C_{crit} as the amount of food collected by time t_{crit}, and $\hat{T}$ as the average time taken to locate the next resource. With these assumptions, the longterm collection rate is

$$\frac{C_{crit}}{t_{crit} + \hat{T}} \tag{2.3}$$

The marginal value theorem states that the optimal quitting time, t^*, and food collected, $C^* = C(t^*)$ satisfies [15]

$$\left.\frac{dC}{dt}\right|_{t^*} = \frac{C^*}{t^* + \hat{T}} \tag{2.4}$$

$$be^{-bt^*} = \frac{1 - e^{-bt^*}}{t^* + \hat{T}} \tag{2.5}$$

The optimal leaving time can be found by numerically solving Equation (2.5). The optimal leaving time depends on $\hat{T}$, the average time spent searching for the next resource, and $\hat{T}$ in turn depends on the rate at which resources fall into the environment, the rate at which they disappear, the way in which resources are distributed throughout the environment, and the searching strategy of the forager. Determining $\hat{T}$ requires a more thorough description of these attributes, and is the goal of the remainder of the methods section. The 1-D environment case is addressed first, then extended to 2-D.

2.1.2 1-D environment

The environment is assumed to consist of infinitely many independent, nonoverlapping patches, indexed by $i = \{-\infty, ..., -2, -1, 0, 1, 2, ..., \infty\}$, each of width $\triangle y$ and centered at $y_i = i\triangle y$. Patches may contain 1 or 0 resources, and switch between these states according to probabilistic rates. Resources fall into the entire environment at rate r, and fall into patch i at rate $r_i = rB(y_i)\triangle y$, where $B(y_i)$ is a discrete probability distribution ($\sum_i B(y_i)\triangle y = 1$) describing where resources land. While unexploited, resources are instantly removed at probabilistic rate δ by agents other than the focal forager.

Once the threshold C_{crit} is reached, the forager ceases collecting and performs an area-restricted search centered around the most recently exploited resource. Throughout this section, $\hat{y_i}$ refers to the position of the resource most recently exploited. After exploitation at resource $\hat{y_i}$ has ceased, the probability of the forager searching at patch y_j immediately obeys the distribution $f(\hat{y_i}, y_j)$, where $\sum_j f(\hat{y_i}, y_j)\triangle y = 1$ for all t, and f is symmetric around $\hat{y_i}$. $f(\hat{y_i}, y_j)$ represents an equilibrium concentration of search effort, given some random walk model of movement. If patch j contains a resource, it is found at a rate proportional to the probability that the forager is searching the patch. Denoting v as the constant of proportionality, the finding rate is $vf(\hat{y_i}, y_j)$.

To find the optimal strategy of this iterative scheme of finding and eating, the following are derived: (1) the distribution of times until the next resource is found, given that search effort is centered around $\hat{y_i}$, and (2) the longterm distribution of locations at which exploitation occurs.

2.1.2.1 Deriving the discovery-time distribution

The forager searches the environment according to $f(\hat{y}_i, y_j)$ until a resource is found. For now, consider each patch as being in one of three states: E, the patch is empty; P, a resource is present in the patch; and F, the patch has been discovered by the forager. Let $E_{ij}(t), P_{ij}(t), F_{ij}(t)$ denote the probability of patch j being in the respective states at time t, given that the individual's search effort is centered around patch i. These probabilities obey the differential equations

$$\begin{aligned} \dot{E}_{ij} &= -r_j E_{ij} + \delta P_{ij} \\ \dot{P}_{ij} &= r_j E_{ij} - (\delta + v f_{ij}) P_{ij} \\ \dot{F}_{ij} &= v f_{ij} P_{ij} \end{aligned} \tag{2.6}$$

where $f_{ij} = f(\hat{y}_i, y_j)$. For initial conditions when the search begins, assume that patch j is at its quasisteady state equilibrium; $E_{ij}(0) = \frac{\delta}{r_j+\delta}, P_{ij}(0) = \frac{r_j}{r_j+\delta}$, and $F_{ij}(0) = 0$. This system of linear equations can be solved, giving the probability of finding a resource in patch j by time t as

$$F_{ij}(t) = \frac{r_j f_{ij}}{(r_j+\delta)(\lambda_2-\lambda_1)} \left(\frac{\lambda_2 + f_{ij}}{\lambda_1}(e^{\lambda_1 t} - 1) - \frac{\lambda_1 + f_{ij}}{\lambda_2}(e^{\lambda_2 t} - 1) \right) \tag{2.7}$$

where $\lambda_{1,2} = \frac{1}{2}(-\delta - f_{ij} - r_j) \pm \sqrt{-4 f_{ij} r_j + (\delta + f_{ij} + r_j)}$ are the eigenvalues of the system (2.6).

The next patch that is exploited is the first one found during this process. Referring to the cumulative distribution of time to first find from patch $\hat{y}_i$ as $\mathscr{F}(t, \hat{y}_i)$, and using the initial condition that no patch is found at time 0, $\mathscr{F}(0, \hat{y}_i) = 0$,

$$\mathscr{F}(t, \hat{y}_i) = 1 - \prod_j \left(1 - F_{ij}(t)\right). \tag{2.8}$$

In words, $\mathscr{F}(t, \hat{y}_i)$ is one minus the probability that nothing has been discovered up to time t.

2.1.2.2 Deriving the finding location distribution

Now, the next-resource find location is derived. Let $P(\hat{y}_i, y_j)$ be the probability that the next resource found is at position y_j, given that searching is centered around position $\hat{y}_i$ according to $f(\hat{y}_i, y_j)$. Let τ_{ij} denote the random finding time of patch j in isolation. The

probability of patch j being found next is the probability that $\tau_{ij} < \tau_{ik}$ for $k \neq j$, summed over all possible τ_{ij}. Thus

$$P(\hat{y}_i, y_j) = \int_0^\infty \left.\frac{dF_{ij}}{dt}\right|_{\tau_{ij}} \prod_{k \neq j} (1 - F_{ik}(\tau_{ij}))\, d\tau_{ij} \tag{2.9}$$

In words, the integrand is the probability that patch j is found at time τ_{ij}, times the probability that no other patch has been found up to time τ_{ij}. The integral sums all the ways in which this can occur.

2.1.2.3 Continuous space limit

Letting the width of each patch $\triangle y \to 0$ gives continuous forms of $P(\hat{y}_i, y_j)$ and $\mathscr{F}(t, \hat{y}_i)$. In this limit, both the searching and resource distributions become continuous functions: $f(\hat{y}, y)$, with $\int_{-\infty}^{\infty} f(\hat{y}, y)\, dy = 1$, and $B(y)$ with $\int_{-\infty}^{\infty} B(y)\, dy = 1$.

First, we derive the continuous form of the cumulative finding time distribution, $\mathscr{F}(\hat{y}, t)$. Taylor expanding $F_{ij}(t)$ around $\triangle y = 0$ and using $r_j = rB(y_j)\triangle y$ yields

$$F_{ij}(t) = \frac{rB(y_j)f_{ij}}{\delta(\delta + f_{ij})} \left(\delta t + \frac{f_{ij}}{\delta + f_{ij}} \left(1 - e^{-(\delta + f_{ij})t}\right)\right) \triangle y + \mathcal{O}(\triangle y^2) \tag{2.10}$$

as $\triangle y \to 0$.

From Equation (2.8), let $M = \prod_{j=1} (1 - F_{ij}(t))$. Equation (2.10) shows that $F_{ij}(t)$ is small for each j as $\triangle y \to 0$, justifying a Taylor expansion of $\ln M$ around $F_{ij}(t) = 0$.

$$\begin{aligned} \ln M &= \ln\left(\prod_j (1 - F_{ij}(t))\right) \\ &= \sum_j \ln\left(1 - F_{ij}(t)\right) \\ &\approx -\sum_j F_{ij}(t) \\ &\approx -\sum_j F(t, \hat{y}, y)\triangle y \end{aligned} \tag{2.11}$$

where $F(t, \hat{y}, y)$ is the $\mathcal{O}(\triangle y)$ term of $F_{ij}(t)$, $y = j\triangle y$ is the continuous variable representing the location of each patch as $\triangle y \to 0$, and $\hat{y}$ for the patch position most recently occupied. As $\triangle y \to 0$, $\ln M = -\int_{-\infty}^{\infty} F(t, \hat{y}, y)dy$. By Equation (2.11), $M = e^{-R(\hat{y}, t)}$, where $R(t, \hat{y}) = \int_{-\infty}^{\infty} F(t, \hat{y}, y)dy$. Combining Equations (2.8) and (2.11), the cumulative distribution of the time until the finding of the first resource while searching from position $\hat{y}$, $\mathscr{F}(t, \hat{y})$, is

$$\mathscr{F}(t, \hat{y}) = 1 - e^{-R(t, \hat{y})} \tag{2.12}$$

The expected search time after exploiting a resource at position $\hat{y}$ is then

$$T(\hat{y}) = \int_0^\infty e^{-R(t,\hat{y})} dt \tag{2.13}$$

Similarly, the discrete finding location distribution from Equation (2.9) becomes the continuous distribution,

$$P(\hat{y}, y) = \int_0^\infty \frac{f(\hat{y}, y) r B(y)}{\delta(\delta + f(\hat{y}, y))} \left(\delta + f(\hat{y}, y) e^{-(\delta + f(\hat{y}, y))t}\right) e^{-R(t,\hat{y})}\, dt \tag{2.14}$$

2.1.2.4 longterm searching time average $\hat{T}$

Define $\chi_n(\hat{y})$ as the probability distribution of the location of the n^{th} resource found. These distributions obey the recursion

$$\chi_{n+1}(y) = \int_{-\infty}^\infty \chi_n(\hat{y})\, P(\hat{y}, y)\, d\hat{y} \tag{2.15}$$

which is a sum of the transitions from $\hat{y}$ to y multiplied by the probability of being at position $\hat{y}$. To find the longterm average collection rate, we must find the equilibrium distribution of resource finds, χ^*, which satisfies

$$\chi^*(y) = \int_{-\infty}^\infty \chi^*(\hat{y})\, P(\hat{y}, y)\, d\hat{y} \tag{2.16}$$

Thus far, we have derived the finding time distribution given the forager is searching around a resource at position $\hat{y}$ (Equation (2.13)), and have an expression for the equilibrium distribution of resource finds (Equation (2.16)). The longterm average time to find the next resource is an expectation of average finding times given position $\hat{y}$, weighted by the probability that a resource is found at position $\hat{y}$

$$\hat{T} = \int_{-\infty}^\infty \chi^*(\hat{y})\, T(\hat{y})\, d\hat{y} \tag{2.17}$$

2.1.3 Extension to 2-D

The 2-D case follows quite naturally with sums over two dimensions instead of one. Patch i's position is now of the form (x_i, y_i), and its area is $(\triangle y)^2$. The resource probability distribution becomes $B(x_i, y_i)$, and the probabilistic rate at which resources fall into the patch located at (x_i, y_i) is $r\, B(x_i, y_i)(\triangle y)^2$.

Each patch's state during the finding phase is still given by the system (2.6). Let $(\hat{x}, \hat{y})$ denote the continuous space position of the most recently foraged patch. The approximation technique performed in Equation (2.11) can be applied again, yielding a double integral form for the 2-D version of $R(t, \hat{x}, \hat{y})$

$$R(t, \hat{x}, \hat{y}) = \int_{-\infty}^{\infty} \int_{-\infty}^{\infty} F(t, \hat{x}, \hat{y}, x, y) dx\, dy$$

Likewise, the rest of the calculations in the 1-D case extend naturally, with

$$T(\hat{x}, \hat{y}) = \int_{0}^{\infty} e^{-R(t,\hat{x},\hat{y})}\, dt \tag{2.18}$$

as the equation for the finding time after exploiting a resource at $\hat{x}, \hat{y}$, and

$$P(\hat{x}, \hat{y}, x, y) = \int_{0}^{\infty} \frac{f(\hat{x}, \hat{y}, x, y) r B(x, y)}{\delta(\delta + f(\hat{x}, \hat{y}, x, y))} \left(\delta + f(\hat{x}, \hat{y}, x, y) e^{-(\delta + f(\hat{x},\hat{y},x,y))t}\right) e^{-R(t,\hat{x},\hat{y})}\, dt \tag{2.19}$$

as the pdf describing the probability of exploiting a resource at (x, y) on the next iterate. Likewise, the equilibrium distribution of resource discovery locations satisfies

$$\chi^*(x, y) = \int_{-\infty}^{\infty} \int_{-\infty}^{\infty} \chi^*(\hat{x}, \hat{y})\, P(\hat{x}, \hat{y}, x, y)\, d\hat{x}\, d\hat{y} \tag{2.20}$$

and the longterm average finding time between patches is

$$\hat{T} = \int_{-\infty}^{\infty} \int_{-\infty}^{\infty} \chi^*(\hat{x}, \hat{y})\, T(\hat{x}, \hat{y})\, d\hat{x}\, d\hat{y} \tag{2.21}$$

2.1.4 Parameter values and functional forms

All parameter values are summarized in Table 2.1. The searching and resource distributions are assumed to be Gaussian with standard deviations σ_f and σ_r, respectively. The resource distribution is always centered at the origin, the searching distribution is centered around the position of the last discovery. In two dimensions,

$$f(\hat{x}, \hat{y}, x, y) = \frac{1}{2\pi\sigma_f^2} \mathrm{Exp}\left[-\frac{1}{2\sigma_f^2}\left((x - \hat{x})^2 + (y - \hat{y})^2\right)\right] \tag{2.22}$$

$$B(x, y) = \frac{1}{2\pi\sigma_r^2} \mathrm{Exp}\left[-\frac{1}{2\sigma_r^2}(x^2 + y^2)\right] \tag{2.23}$$

These forms are chosen to allow a direct comparison between the spread in the resource distribution and the spread in the optimal search strategy. The resource dynamics are

completely determined by the three parameters r, δ, and σ_r. σ_r values range from 0.5 to 3 m^2 with a step-size of 0.25, and r takes on the values 1,3,5 and 10 $\frac{1}{hr}$.

The constant v relates the finding rate to the probability density distribution of the forager, and may depend on several factors; in a foraging ant, for example, v depends on searching attributes, such as velocity, perceptual radius, and the parameters of individuals' correlated random walk [1,55], the terrain that the forager is searching [11], and the resource that is being searched for [56]. We set $v = 0.5$ or $2\ \frac{m^2}{hr}$ to investigate the optimal strategy in scenarios with slow and fast discovery.

The fractional collection rate parameter b depends on food type, size, and feeding rate. Instead of trying to incorporate all of these factors, we set $b = 0.5$ or $2\ \frac{1}{hr}$ to investigate the optimal strategy when resource consumption is slow and fast.

The optimal foraging strategy is given by t^*, the optimal leaving time at a resource item, and σ_f, the standard deviation of its searching distribution. t^* is determined by numerically solving Equation (2.5), and depends on the choice of σ_f through $\hat{T}$. Large values of σ_f result in a wide searching distribution and smaller values produce high levels of area-restricted search.

2.2 Algorithms to Find the Expected Collection Rate

Given a resource distribution $B(x, y)$ and renewal and disappearance rates r and δ, the optimal giving-up value and search strategy can be found by using the analytical equations derived above, or by stochastic simulation.

2.2.1 Using analytical calculations

For given resource dynamics, find the equilibrium collection rate for a given σ_f by calculating

1. $\hat{T}$ for that choice of σ_f by numerically solving Equation (2.21) (see Appendix A)
2. The best GUV, using Equation (2.5)
3. The corresponding equilibrium collection rate with Equation (2.3)

The optimal σ_f produces the largest longterm collection rate in an environment. This algorithm requires substantial numerical calculations, but provides a method of verifying

the average longterm collection rate of the stochastic process without relying on the mean of many simulations. All integration was performed numerically in R [59].

To compare the value of the optimal search strategy across different resource scenarios, we divide the optimal collection rate by the collection rate when $\sigma_f = \sigma_r$. This latter collection rate represents a null strategy, where the forager searches for a resource according to its distribution in space.

2.2.2 Stochastic simulation

The mathematical model presented above is an iterative process that does not include the effects of depletion of resources in the environment due to the forager; instead, the environment "resets" to its equilibrial dynamics after each resource exploitation. Two stochastic simulations, termed the "memoryless" and "true" simulations, were built to verify the longterm average collection rate C in a 2-D environment. In the memoryless simulation, the resource distribution is reinitialized after each resource exploitation event; thus the local depletion caused by exploitation is forgotten by the environment. In the "true" simulation, the resource dynamics are not reset after each exploitation; local depletion can occur and may have an impact on the optimality of the foraging strategy. Parameters were varied as outlined above.

Both simulations use a Gillespie-like algorithm to determine the waiting time until the next event [31]. The simulation differs from the Gillespie algorithm in that the exploitation event takes a fixed amount of time to complete. Events are (1) A resource falls into the environment, (2) A resource disappears from the environment, and (3) The forager finds a resource, and exploits it deterministically for a time t_{crit}. During the exploitation time, only resource appearance and disappearance events are allowed to occur, but not to the exploited resource. For a given set of resource parameters, t_{crit} is set to t^* from Equation (2.5), using $\hat{T}$ determined by Equation (2.21).

As in the mathematical derivation, the forager switches between exploitation and exploration as resources appear and disappear in the environment. Collected food and position of resource finds were tracked for 10000 hours of simulation time. The simulations were initialized by laying down n resources in the habitat; n was chosen from a Poisson distribution with mean $\frac{r}{\delta}$. The random initial position of the forager, $(\hat{x}, \hat{y})$, was drawn

from the resource distribution $B(x, y)$.

2.2.2.1 Resource falls into the environment

Resources fall into the environment at rate r. The new resource's position is determined in polar coordinates, (ρ, θ). θ is chosen from a uniformly distributed distribution between 0 and 2π. The probability of a resource falling in an annulus with radii $(\rho, \rho + \triangle\rho)$ is

$$2\pi\rho B(\rho)\triangle\rho = \frac{1}{\sigma_r^2}\rho \text{ Exp}\left[-\frac{\rho^2}{2\sigma_r^2}\right]\triangle\rho \tag{2.24}$$

We use the cumulative distribution of (2.24) to draw a random radial distance. The cumulative distribution of Equation (2.24) is found by integrating the density from 0 to ρ:

$$B_{cdf}(\rho) = 1 - e^{-\frac{\rho^2}{2\sigma_r^2}} \tag{2.25}$$

A uniformly distributed random number X is chosen between 0 and 1 and plugged into the inverse of the cumulative distribution, $B_{cdf}^{-1}(X) = \sqrt{-2\sigma_r^2 \ln(1 - X)}$. The resulting (ρ, θ) coordinate is randomly distributed according to the pdf $B(x, y)$. The position of the i^{th} resource is tracked in the i^{th} row of a matrix called ResMat.

2.2.2.2 Resource disappears

The resource disappearance event occurs at rate δN, where N is the number of resources currently present in the environment. When this event occurs, a random integer between 1 and N is generated, and the corresponding row of ResMat is deleted.

2.2.2.3 The forager finds a resource

The resource discovery rate is the sum of the finding rates of each of the resources present. Letting $(\hat{x}, \hat{y})$ denote the position of the resource last exploited, the finding rate of a resource at position (x, y) is given by $vf(\hat{x}, \hat{y}, x, y)$. Suppose the finding event occurs, and the environment has $N > 0$ resources at positions (x_k, y_k), $k \in \{1, 2, ..., N\}$; the exploited resource is chosen from the probability distribution

$$P(K = k) = \frac{vf(\hat{x}, \hat{y}, x_k, y_k)}{\sum_{i=1}^{N} vf(\hat{x}, \hat{y}, x_i, y_i)} \tag{2.26}$$

where K is the chosen resource. When a resource is found it is exploited for a time t^*, resulting in $C(t^*)$ resource being collected. After exploitation, the resource is removed from the environment.

2.3 Results

The analytical calculations and memoryless numerical simulation of the collection rate agree well over the range of parameter values. Figure 2.1 shows the results of the memoryless stochastic simulation, as well as analytical calculations outlined in Section 2.2.1, for all resource scenarios with $\delta = 0.25$; the cases with $\delta = 1$ give similar agreement. In each resource scenario, a unique σ_f^* value exists that maximizes the collection rate; this optimum becomes less sharp with increasing σ_r. For fixed r, the maximum possible collection rate decreases as σ_r increases (Figure 2.1). Thus, the degree of autocorrelation influences the maximum collection rate a forager can achieve in any environment.

For fixed resource autocorrelation, the optimal GUV increases with r and decreases with δ (Figure 2.2). Stated another way, resources are consumed more completely when they are more scarce at equilibrium, either through appearing slowly or disappearing quickly, in the environment. The optimal GUV also decreases with increasing σ_r; thus, resources should be consumed more completely when they are more dispersed in the environment. These results are more explicit analogues of the classic MVT's prediction that the giving-up density should decrease with increasing travel time between patches [15].

The optimal degree of ARS, σ_f^*, increases in a concave-down manner with σ_r in all resource scenarios (Figure 2.3). The initial increase was greater with smaller resource appearance rates than with larger appearance rates. Larger δ values decrease the rate at which σ_f^* increases with σ_r. Taken together, these imply that a forager's search strategy should respond to changes in the resource distribution most when the resource appearance rate and disappearance rate are small. σ_f^* increases with σ_r more quickly when v is large.

Because the environment is set to its equilibrial dynamics after exploitation, the subsequent search dynamics are the same regardless of how long the forager stays at the resource. Thus, the fractional resource consumption rate b has no effect on the optimal search strategy in the memoryless scenario; Figure 2.3 corroborates this, as only the GUVs change when b is increased from 0.5 to 2 with v fixed. GUVs are smaller for larger values of b, meaning

resources that can be exploited quickly should be exploited more thoroughly.

To compare the relative value of autocorrelated search to a null search strategy, the collection rate of the optimal strategy was divided by the collection rate when $\sigma_f = \sigma_r$ and the GUV was set to that which maximized collection for the σ_f used (Figure 2.4). This relative collection rate measures the benefit of adopting the optimal ARS compared to the search strategy that matches the resource distribution's autocorrelation. For $\delta = 1$ and $v = 0.5$, a concave-down relationship occurs for most of the resource appearance rates in the range of σ_r values used. At small values of σ_r, the optimal search strategy (σ_f^*) is very similar to the resource distribution (σ_r), so the collection rates are also similar and the relative collection rate is close to 1. As σ_r increases, so does the relative collection rate; intermediate values of σ_r give the most benefit in adopting the optimal strategy over the null. For larger values of σ_r the relative benefit decreases; the optimal search strategy still yields a higher collection rate than the null, but relatively lower than for smaller σ_r values. $\delta = 0.25$ yields similar results. Simulations with larger σ_r show that concave-down relationships exist for all resource scenarios (not shown).

Simulations with memory were run to determine the effect of ignoring resource depletion caused by the focal forager. As expected, collection rates are always smaller. Figure 2.5 compares the collection rates with memory to the memoryless model for all environments with $\delta = 0.25$. In this case, environments in which resources are easier to exploit or find ($b = 2$ or $v = 2$) exhibit the greatest disparity between the true stochastic and memoryless results. For any given b, v combination, smaller σ_r values yield a greater disparity than larger σ_r. Stochastic simulations with $\delta = 1$ exhibit much less of a difference in collection rates, compared to memoryless simulations (not shown). Thus, resource depletion is an important influence on longterm collection rate when the resource distribution is autocorrelated, and when resources appear quickly and disappear slowly and are easy to find and exploit.

The memoryless stochastic simulations are noisy, but in many cases the optima are shifted towards larger σ_f values compared to the memoryless simulations (Figure 2.5). This matches with intuition; a more dispersed search avoids the risk of becoming trapped in a region that is locally depleted. The optimal GUV likely differs as well because resource depletion increases the time it takes to find the next resource.

2.4 Discussion

The MVT gives a broad framework for interpreting foraging behavior. The MVT predicts that organisms foraging in a patchy environment should remain in a patch until the marginal rate of food collection in that patch is equal to their longterm average. This study extends this result to explicit 2D space; both resources and searching effort are modeled as specific spatial distributions. The optimal search strategy includes both a spatial distribution of search effort and a GUV at a resource that depends on specific resource dynamics, as well as forager consumption rate and finding ability. Analytical calculations agree with a memoryless environment simulation in which the resource distribution "resets" after each resource exploitation (Figure 2.1). Analytical calculations have the advantage of giving time between resource finds, the distribution of resource finds, and collection rates for a given strategy without averaging over many simulations.

Different resource scenarios pose different types of challenges; resources may be dispersed through the environment (high σ_r), hard to find (low v), appear infrequently (low r), or disappear quickly (high δ). Generally, a forager faced with any of these challenges should decrease its GUV, resulting in more time spent at each resource (Figure 2.3). A relatively dispersed search strategy is best in dispersed resource distributions. Figure 2.3 shows that the effect of resource dispersion on search strategy weakens when resources disappear quickly, or when they are difficult to find. The optimal strategy in these cases is to intensify search effort to find resources before they vanish. Higher searching dispersion is optimal in resource distributions that have a low renewal rate (r); this allows the forager to search the environment broadly, increasing the chance that a resource is discovered.

Modification of search strategy based on prior foraging experience, such as the type of resource found previously, is probably common in the animal kingdom, although more empirical research needs to be conducted to investigate the extent that animals understand and use the distribution of their resources in their search strategy. Ants, for example, engage in lower intensity searches when expecting a protein resource in a location, while ants expecting a carbohydrate resource exhibit higher intensity searches [63]. Here, we show that such a strategy is optimal if resources are abandoned when their quality falls below a threshold. Protein sources encountered by ants are likely dispersed and renewed infrequently; Figure 2.3 implies that a dispersed strategy is optimal, as observed in several studies [30, 63, 70].

Carbohydrate resources (aphids, plant exudates) tend to be autocorrelated and renewable; the model shows that an intense search strategy is indeed optimal in this case. Because recruitment at the nest typically requires trophollaxis, or food sharing, between recruiter and recruit, naive ants in the nest might be primed to search in a particular way after receiving a particular type of food when prompted to help with collection [35].

The analytical calculations were compared to a null strategy to investigate the relative value of the optimal ARS in different resource scenarios with different types of challenges (Figure 2.4). In most environments with low disappearance rates, the value of using the optimal strategy over the null strategy increases with increased resource dispersion. The benefits increase further when resources are consumed quickly ($b = 2$) or are difficult to find ($v = 0.5$). When resources disappear quickly (high δ) and searching is difficult, the relative benefit becomes unimodal; in these poor conditions the relative benefit of the optimal strategy decreases for large σ_r. For the smallest resource appearance rate, the optimal strategy provides little advantage over the null for high values of σ_r (Figure 2.4). These results imply that the search strategy of a forager should differ most from the resource distribution's when resources are dispersed.

The model also shows that the spatial distribution of resources affects the GUV at individual resources (Figure 2.2). The fact that carbohydrates and proteins represent different nutrients makes an empirical comparison between types difficult [42]. The model could provide valuable insight for foragers that have evolved to efficiently exploit different types of carbohydrate or protein sources with differing spatial distributions; the model predicts that the type that is spread more uniformly will be exploited to a greater extent than the other. *Lasius niger* ants routinely exploit nectaries and honeydew secretions of aphids, both of which are carbohydrate sources; the searching attributes of ants expecting either type of resource has not yet been compared to the distribution of each resource.

Two stochastic simulations were built to understand the impact of resource depletion on an optimal strategy. In the "memoryless" simulation, the resource distribution was redrawn from its equilibrium distribution following an exploitation event; in the "true" simulation, resources were continually tracked during the exploitation event. Comparison of the true stochastic process with the memoryless process highlights how resource depletion by the focal forager's strategy modifies a strategy's realized collection rate (Figure 2.5), and

in turn might modify the optimal search strategy and GUV. The greatest discrepancy in collection rate occurs when the resource distribution is highly autocorrelated, and disappearance rates are low. Intuitively, these environmental conditions allow for structure in the resource distribution to be present, and in turn destroyed by a forager capitalizing on that structure. Resource scenarios with high δ should essentially act as memoryless environments. Generally, an optimal strategy should result in a reduction of autocorrelation in the resource distribution due to depletion. This comparison motivates the question of how a forager's search strategy should be altered due to nonrandom resource depletion caused by itself, as well as other optimal foragers in a population.

This model has several simplifying assumptions. The searching distribution is assumed constant in time, and realized immediately after exploitation. A more explicit approach would connect movement attributes of the forager to the probability distribution of searching location. Modification of sinuosity in the search path of a simple individual forager can result from changes in velocity (orthokinesis) or turning rate (klinokinesis) [10]. For example, ladybugs, *Coccinella septempunctata*, increase their turning rate in response to food capture, resulting in a tendency to stay in areas of high food concentration [40]. When searching for a carbohydrate food source, individual *Melophorus bagoti* ants appear to search in loops that repeatedly bring them back to the expected location of a resource [63]. A random walk model of movement would allow the optimal strategy to be presented in terms of diffusive and centralizing tendencies of individual foragers [41, 50, 73]. In this context, the results of this paper provide an approximation to the case where the equilibrium probability distribution of searching locations is reached quickly.

Despite these simplifying assumptions, this modeling framework bridges the gap between patch-based MVT models that predict a giving-up density, and explicit 2D space models that investigate the optimal ARS after a resource encounter. The methods section provides analytical expressions of collection rates, given a spatially explicit environment, resource dynamics, and searching strategy. Model development was motivated with innate ARS strategies of ants, however this framework would apply equally well to other solitary foragers as well. Experimental conditions could be used to carefully modify the autocorrelation of resources, their renewal rate, and disappearance rate in an environment, and observe how a forager's strategy responds. These results could also serve as a null comparison when

the forager does not take into account the depletion that its strategy causes. Such studies will extend understanding of how natural selection has tuned information use strategies in foragers.

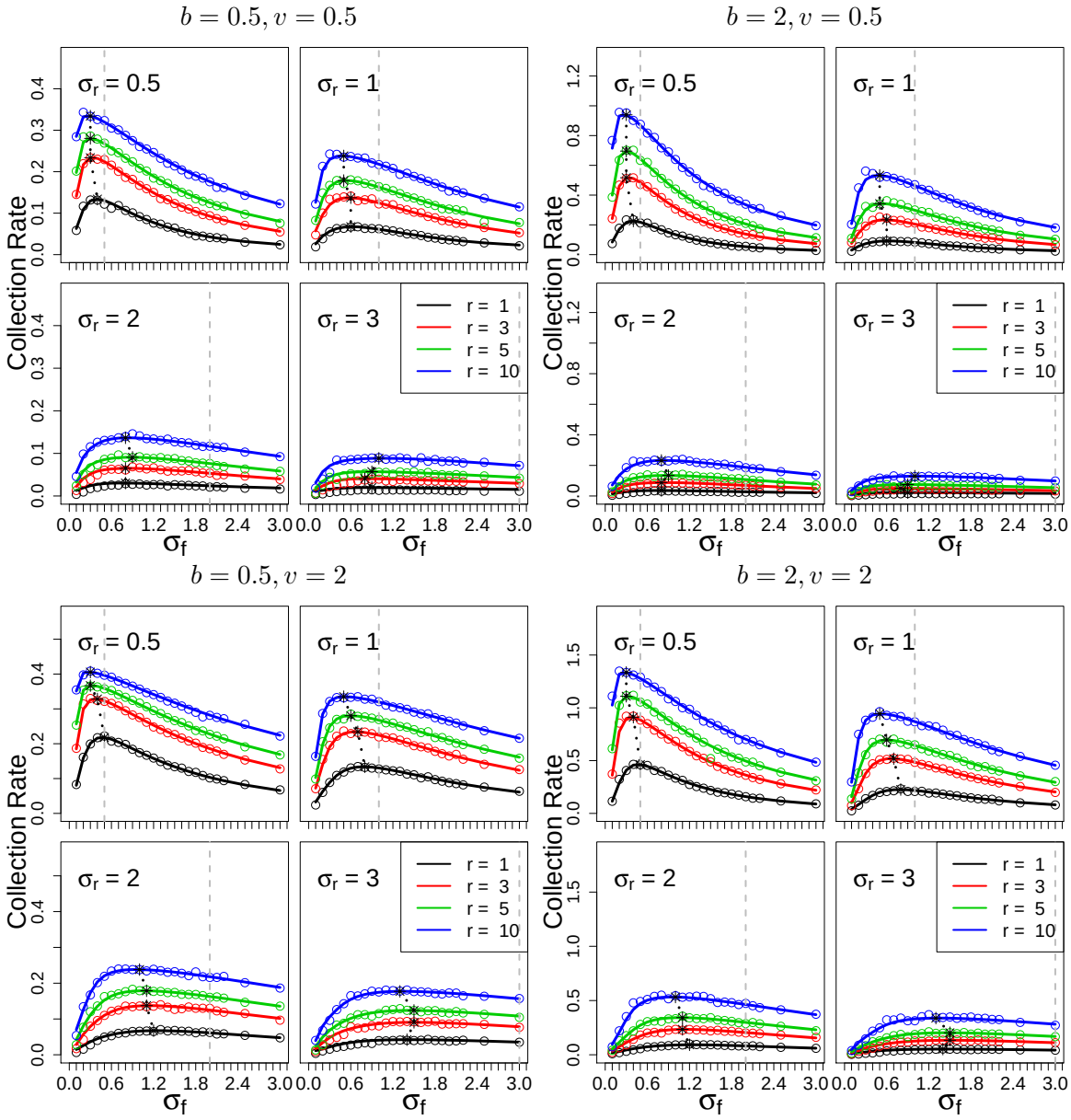

Figure 2.1: Each graph shows collection rate vs. searching strategy σ_f with a specific σ_r, various values of r, and $\delta = 0.25$. Lines represent collection rates obtained from analytical calculations outlined in Section 2.2.1, dots are output from the memoryless stochastic simulation. For each r, the optimal σ_f value is marked with an asterisk. A vertical dashed line is placed at $\sigma_f = \sigma_r$ for comparison of the optimal search strategy to the resource distribution.

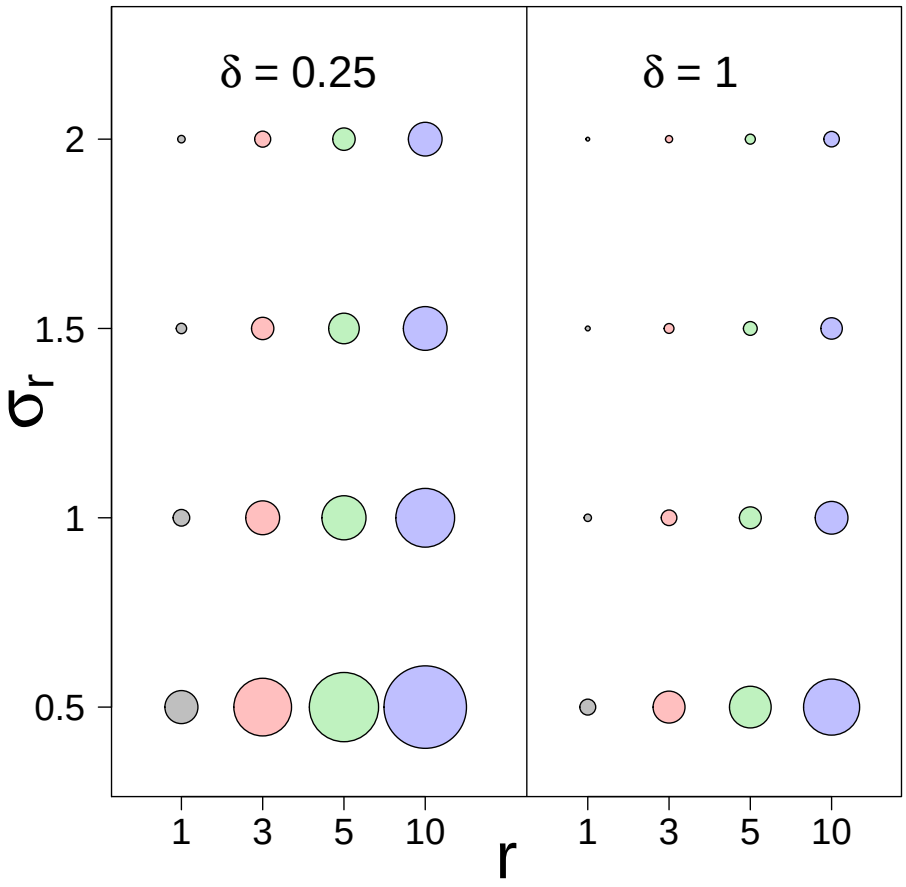

Figure 2.2: GUV for various resource dynamics with $b = 0.5, v = 0.5$; other cases follow similar trends. Dot size indicates the amount of food remaining (GUV) when the resource is abandoned, given the optimal foraging strategy.

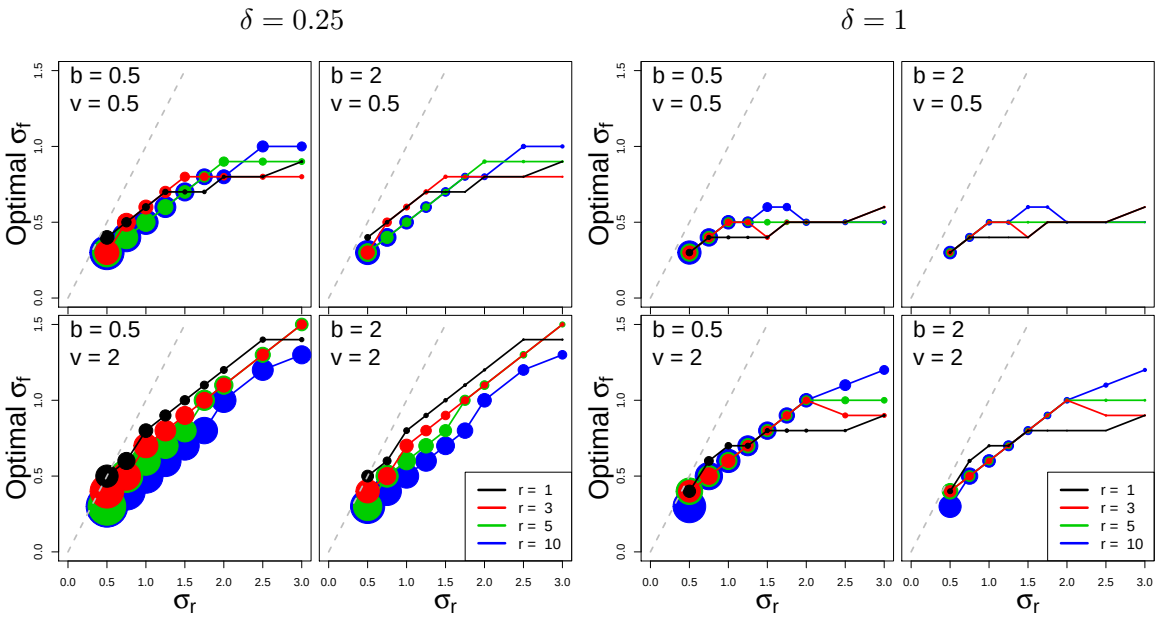

Figure 2.3: Graph of the optimal σ_f vs. σ_r. Dot size indicates the optimal GUV for each (σ_r, σ_f^*) coordinate. The dashed gray line is the diagonal.

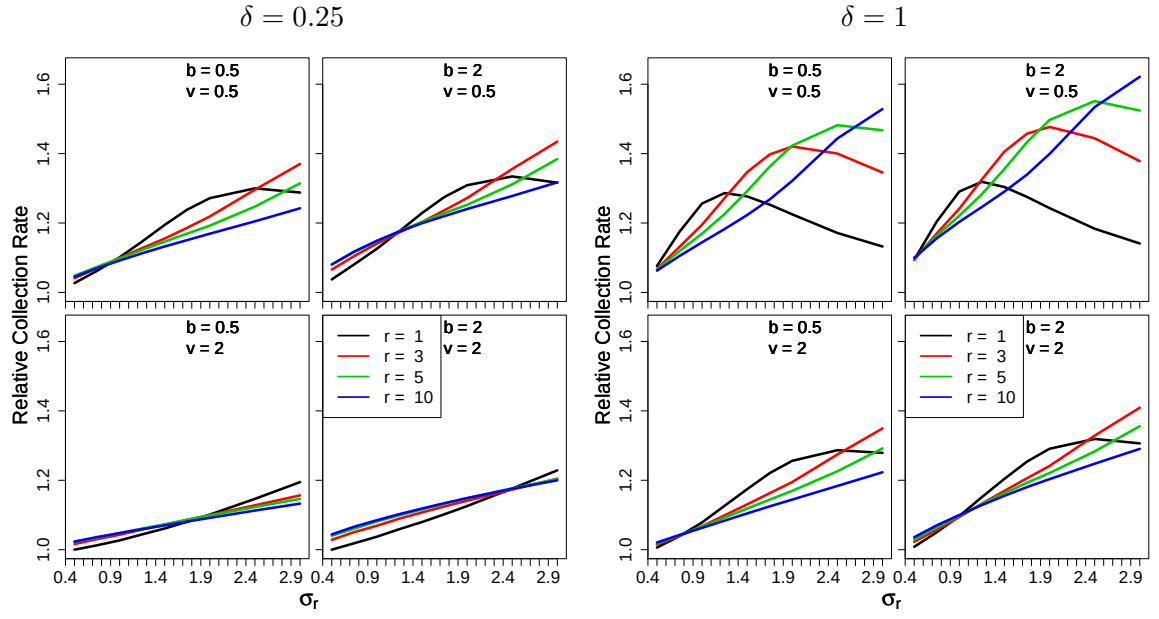

Figure 2.4: Graph of the relative collection rate vs. σ_r. The relative collection rate is defined as the collection rate with the optimal strategy divided by the collection rate with $\sigma_f = \sigma_r$, with the best choice of GUV for each σ_f.

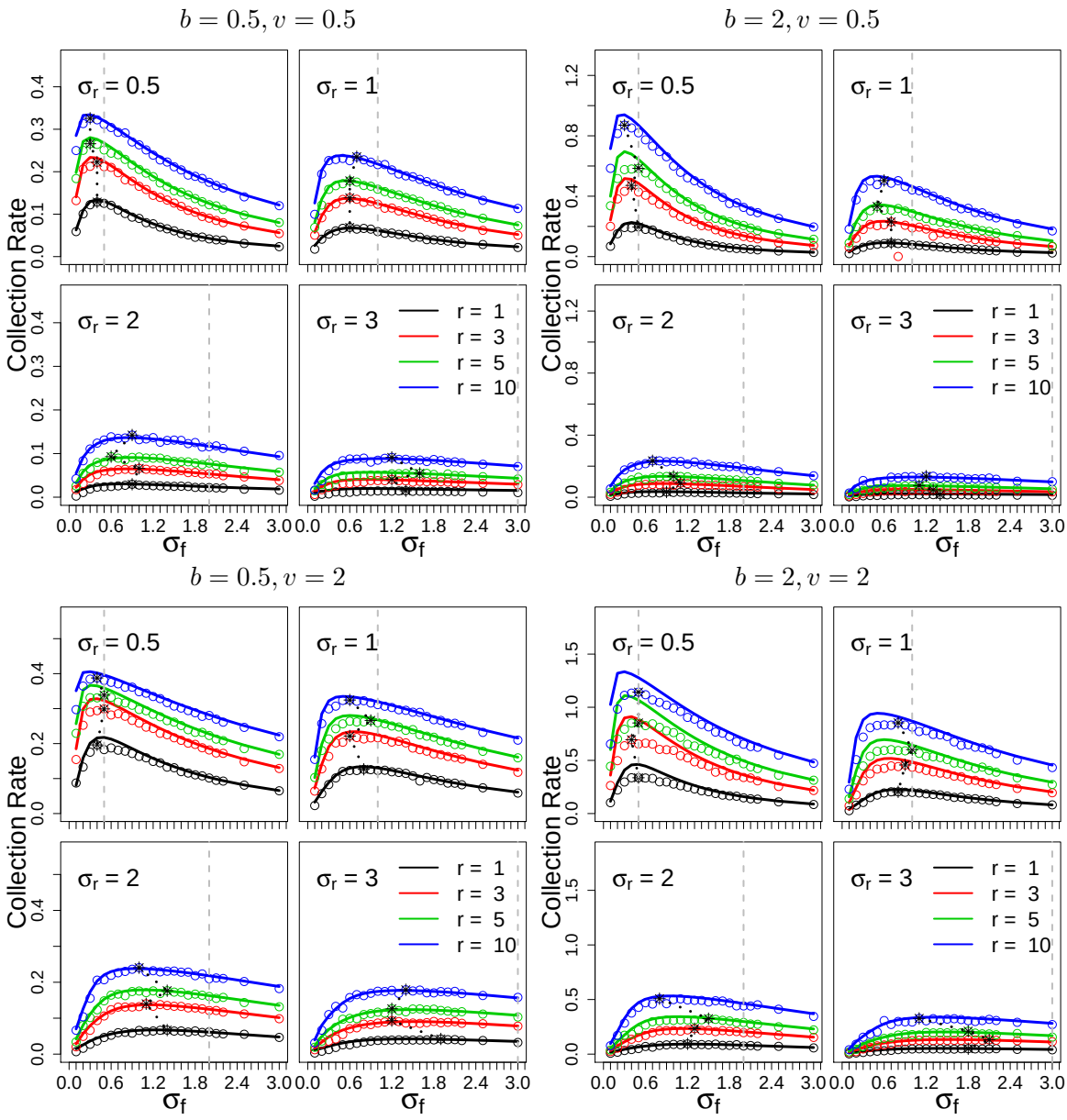

Figure 2.5: Collection rate vs. searching strategy σ_f with a specific σ_r, various values of r, and $\delta = 0.25$. Lines represent collection rates obtained from analytical calculations outlined in Section 2.2.1, dots are output from the true stochastic simulation. For each r, the optimal σ_f value of the stochastic simulation is marked with an asterisk. A vertical dashed line is placed at $\sigma_f = \sigma_r$ for comparison of the optimal search strategy to the resource distribution.

Table 2.1: Parameter values used in the simulations.

Param.	Description	Value(s)	Units
σ_f	Standard deviation of searching distribution	0.1 to 3	m
σ_r	Standard deviation of resource distribution	0.5 to 3	m
r	Rate at which resources appear in the environment	{1, 3, 5, 10}	$\frac{1}{\text{hr}}$
δ	Rate at which resources disappear when unoccupied	{0.25, 1}	$\frac{1}{\text{hr}}$
b	Fractional collection rate	{0.5, 2}	$\frac{1}{\text{hr}}$
v	Relationship between search effort and finding rate	{0.5, 2}	$\frac{\text{m}^2}{\text{hr}}$

CHAPTER 3

PHEROMONAL RECRUITMENT MODEL

Spatial organization is an important function of many biological processes. For example, the internal environment of cells becomes polarized in order to initiate directed motion and budding [53]. Dictyostelium amoebae organize spatially to collectively form a reproductive structure as part of their life cycle [43]. In many cases, spatial organization is a switch-like, or bistable, process, in which the biological system moves from an unstable spatially homogeneous steady-state to an inhomogeneous steady-state due to some endogenous signal [43,53]. In general, bistable switches are built from positive or negative feedbacks that amplify or repress excitatory signals [16]; in the case of Dictyostelium, acrasin acts as the signal that simultaneously attracts amoebas and induces acrasin production.

Many social insects, and in particular ants, must also spatially organize to respond to colony intruders [78], direct searching effort along trails [32], and efficiently collect large resources [35]. Ant colonies, like amoebas, do not rely on central leadership; any spatial organization must arise out of individual responses to information in the environment, and information passed between individuals via chemical signals or direct antennation. A classic example is the process of pheromonal recruitment, whereby ants direct their movement along an established pheromone trail leading to a resource. Ants that successfully exploit the resource reinforce the pheromone trail as they return to the nest, and prompt other nestmates at the nest to follow the pheromone trail to the resource and repeat the process [35].

With regard to pheromonal recruitment to a resource, the positive feedback involved in trail-use, combined with the tendency for pheromone trails to evaporate when not reinforced, gives pheromonal recruitment the potential to exhibit spatial bistability when a resource is present. Empirically, bistability of recruitment has been demonstrated in *Monomorium pharaonis* ants, and noted in *Tetramorium caespitum*, the pavement ant [9, 17]. Beekman

et al. (2001) show that small *M. pharaonis* colonies are not able to initiate high levels of recruitment to a bait 50 cm from the nest; however, when recruitment is "helped" by initially placing the bait near the colony, then gradually moved away to the 50 cm distance, high levels of recruitment do occur. Thus, the colony can only reach the high branch of the recruiting equilibrium when the initial state of the system is close to that equilibrium, with high numbers of ants on or near the resource.

Collignon and Detrain (2010) argue that the bistable nature of pheromonal recruitment has led to the evolution of group recruitment in *T. caespitum* [17]. In group recruitment, the ant that first encounters a resource directly leads a group of its nestmates back to the resource; this process continues, with returning ants laying and establishing a pheromone trail back to the nest. As the pheromone trail becomes established, the ants gradually reduce the tendency to participate in group recruitment, and instead rely on pheromone trails for directional cues [17]. Group recruitment thus acts as a mechanism to drive the dynamics of the colony away from the low branch of a bistable system.

Though informative, the empirical experiments of Beekman et al. (2001) limit ant movement to essentially a 1D foraging arena; the first goal of this manuscript is to create a mathematical framework to understand how various colony parameters contribute to the spatial distribution of ants during the recruitment process in 2D, the second is to understand whether bistability is predicted in a 2D foraging arena for the pavement ant, *T. caespitum*. This is shown in Collignon and Detrain (2010); however, their model does not describe explicit 2D space, but instead describes rate transitions to behavioral states and points in space. Using a spatially explicit model, we find parameters that allow bistability, and describe how the bistable regime qualitatively changes with behavioral parameters.

Mathematical models have been crucial in understanding how individual behavioral parameters allow for spatial organization in biological processes [33, 51, 52]. With regard to ants, agent-based models (ABM) allow explicit assumptions of individual behavior to be modeled. By analyzing ABM output, or dynamical systems derived from ABMs, an understanding of how individual behavioral parameters influence the colony-wide response can be gained. This process allows researchers to infer what behavioral parameters are most important in generating colony-wide responses, and suggest novel experiments that further understanding. However, a major challenge in spatial ant models has been mathematically,

and mechanistically, describing trail following in explicit 2D space.

Edelstein-Keshet et al. (1995), for example, use a spatially implicit system of ODEs to understand how individual responses to trail strength, such as trail fidelity and trail recruitment, result in spatial bistability as observed in a phase plane diagram [26]. This model simplifies trail following by only considering two behavioral classes of ants: those following a trail, and "lost" ants laying new trails. Bistability occurs when stronger trails exhibit more attraction to nontrailing ants than weaker ones; in this case, the ants' equilibrial distribution can form erractic, weak trailing activity, or organized trailing along few strong trails; the equilibrium state reached is determined by the initial state of the system. Edelstein-Keshet et al. (1995) argue that behavioral parameters of ants should be tuned, or behaviorally adaptable, to allow ants to switch quickly from their homogeneous steady-state to the ordered, trailing state so that a quick, colony-wide response can be generated to various events requiring collective organization [25].

Watmough and Edelstein-Keshet (1995) develop a PDE system analogous to Edelstein-Keshet et al. (1995) in 1D space to understand how the shape and propagation speed of a raiding column of army ants is influenced by individual behavioral parameters. The results include traveling wave velocities used to estimate the ratio of lost and trail-following ants [75].

These modeling papers rely on a vague classification of ants into lost and following behavioral states. In reality, these states represent two points on a continuum of pheromone-induced bias during a random walk. More recent papers of pheromone-induced bias have developed models incorporating this continuum in explicit 2D space. Boissard et al. (2013) construct an agent-based model (ABM) based on a velocity-jump process with jump transitions as a function of pheromone vectors, and show that the ABM can exhibit spontaneous trail formation in 2D. A continuum description of the ABM model is derived by assuming that the velocity jumps instantly relax to their equilibrium distribution; thus, many velocity-jumps occur on the macroscopic timescale. The PDE model derived from the ABM, however, possesses only the homogeneous steady-state, highlighting the differences that can arise in ABM and continuum descriptions of biological processes [12].

Amorim (2015) modeled pheromonal recruitment to a resource using a phenomenological system of PDEs based on chemotaxis, and show that such a system can generate spatial

organization typical of recruitment trails [3]. Chemotaxis models have proven successful in understanding chemical-based migration of cells; in these models, a sensing body detects and biases its movement along a chemical gradient [33, 44]. The trailing mechanism in Amorim (2015) requires the assumption that ants establish a trail of pheromone that increases in density with distance from the nest, resulting in trail polarity. However, evidence for chemotaxis, or pheromone gradient following in ants during pheromone recruitment to a resource, does not exist; a more likely mechanism is osmotropotaxis, where an ant walks with constant velocity and continually adjusts its direction to align with the trail using inputs from its antennae [14].

Here, a mechanistic ABM in continuous 2D space is built, and a corresponding ODE/PDE system is derived. We use the models to: 1) determine the general circumstances under which pheromonal recruitment acts as a bistable system; 2) understand the ability of the PDE to predict the searching distribution of the ABM; 3) understand how the distribution of searching ants depends on a specific set of behavioral parameters. Finally, the model will be parameterized with movement data to understand the conditions under which bistability could be observed in *T. caespitum* (see Chapter 4 for a description of the movement data). This model differs from previously cited work in that it tracks a full set of behavioral states, tracks individuals across space, and presents a model of pheromone following not based on chemotaxis. Deriving the ODE/PDE system from an ABM ensures that the model is based on explicit individual behaviors; all of the parameters of the model can be estimated to investigate the presence of bistability in various species by watching individual ants. The ODE/PDE system output will be used to better understand the stochastic output of the ABM.

A space-jump process in explicit 2D space is developed, after which a diffusion limit is used to derive a dynamical system. In a space-jump process, an organism's continuous path is broken up into discrete positional changes, or jumps, at randomly distributed times; this is different than a velocity-jump process, where an organism undergoes continuous motion punctuated with sudden random changes in velocity. Velocity-jump models are deemed more realistic, as they explicitly account for autocorrelation between directional changes, and do not describe organisms with infinite velocity and zero momentum in a continuum limit [36]. However, diffusion models are generally more tractable in two spatial

dimensions, and have been successful in describing oriented movement in response to a signal similar to osmotropotaxis [48, 50, 52]. The model presented below was inspired by Lewis and Moorecraft (2013), which describes models of wolves and red fox reacting to urine marking. Although the diffusion limit in our model derivation closely follows Lewis and Moorecraft (2013), it is included in appendix B for completeness.

The methods section begins with a derivation of the ABM space-jump process, after which the continuum limit is derived. Steady states of the PDE are numerically calculated and compared to corresponding simulations of the ABM in the results section to demonstrate the potential for bistability.

3.1 Methods

The agent-based model tracks transitions in the behavioral state and location for each of n ants in the focal colony over time.

3.1.1 Habitat

Define $\Omega_H = \{(x, y) : -\frac{L^H}{2} \leq x \leq \frac{L^H}{2}, -\frac{L^H}{2} \leq y \leq \frac{L^H}{2}\}$ as the habitat, an $L^H \times L^H$ square region with outer boundary $\partial\Omega_H$. Define $\Omega_N \in \Omega_H$ as the nest region: an $L^N \times L^N$ square, and $\partial\Omega_N$ as its boundary. Define the indicators

$$I_N(x,y) = \begin{cases} 1 & \text{if } (x,y) \in \Omega_N \\ 0 & \text{otherwise} \end{cases} \qquad \hat{I}_N(x,y) = \begin{cases} 0 & \text{if } (x,y) \in \Omega_N \\ 1 & \text{otherwise} \end{cases} \tag{3.1}$$

and area $A_N = \iint_{\Omega_N} 1\, dA$. Finally, define $\Omega_B \in \Omega_H$ as the resource region and $\partial\Omega_B$ its boundary; similar to previous regions, it is chosen as a square with side length L^B, with the constraint $\Omega_B \cap \Omega_N = \varnothing$. Define the resource region indicator I_B similarly to those defined above with area $A_B = \iint_{\Omega_B} 1\, dA$.

3.1.2 States, transitions, and movement

The full simulation tracks ants' transitions among seven behavioral states: waiting at the nest (N), recruiting at the nest (E), searching (S), returning to the nest after quitting searching (T), waiting for a feeding spot at the resource (Q), exploiting (taking a bite out of) the resource (B), and returning to the nest to recruit nestmates (R).

Ants not involved in recruitment are either at the nest (N), outside the nest searching (S), or returning to the nest unexcited (T). The ants undergo the following dynamics: N ants spontaneously leave the nest at rate w_N and transition to the S state. Ants in the searching state search the environment with movement generated by a random walk (described below), quit searching at rate q_S, and transition to returning ants (state T), which bias their random movements in the direction of the nest relative to their position. T ants that touch the nest boundary, $\partial\Omega_N$, transition into nest ants (N). S ants that quit searching while in the region Ω_N transition directly into N ants.

During each time step τ, nest ants transition to state S with probability τw_N, and are positioned at a random location chosen uniformly over Ω_N. An ant in state S quits searching (switches to the T state) with probability τq_S; if it does not quit searching it takes a step with steplength chosen from an exponential distribution with mean $\hat{\rho}_S$, and movement angle chosen from a uniform distribution on $(-\pi, \pi]$ in the absence of pheromone.

Ants in state T move according to a random walk with steplength chosen from an exponential distribution with mean $\hat{\rho_T}$. Let $\hat{\theta}_N$(x,y) denote the angular direction of the center of the nest region relative to position (x,y); for simplicity, the spatial argument is dropped. The movement angle of a state T ant is drawn from the von Mises distribution with mean $\hat{\theta}_N$ and fixed bias parameter κ_T, denoted $k_T(\theta, \hat{\theta}_N)$. A T ant that contacts any point in Ω_N instantly transitions to state N. The von Mises distribution is commonly used to model random motion with directional bias and has well-studied properties [5, 29, 50], and is discussed further in appendix B.

A searching ant in Ω_B transitions to waiting for a feeding spot near the resource (state Q) at rate v hr^{-1}. Ants in state Q return unexcited to the nest at rate w_Q, and transition to feeding on the resource (state B) at a rate dependent on the number of ants currently exploiting the resource. Letting B_{tot} denote the number of ants in state B, the $Q \to B$ transition rate is $\alpha(B_{tot}) = \alpha_0(A_0 - B_{tot})$, where A_0 denotes the number of feeding sites on the resource and α_0 describes the rate at which available sites are found by state Q ants. An ant takes a bite at rate w_B, and transitions to returning to the nest (state R).

An ant in state R moves according to a random walk biased towards the nest similar to state T ants, with analogous average step length, concentration parameter and direction angle distribution $\hat{\rho}_R$, κ_R, and $k_R(\theta, \hat{\theta}_N)$. State R ants transition to the E state upon

contact with $\partial\Omega_N$. Ants in state E transition to state S at rate w_E. In addition to N ants spontaneously leaving to search at rate w_N, an ant in state E can motivate an ant in state N to begin searching. This occurs at a rate proportional to the total number of ants in state E; given E_{tot} E state ants are present, this rate is ξE_{tot}. For example, during any timestep, an ant in state N transitions to searching with probability $(w_N + \xi E_{tot})\tau$.

Finally, no moving ant is allowed to cross the outer boundary $\partial\Omega_H$. Any step that results in this crossing is truncated to keep the individual in Ω_H. The behavioral states of individual ants are summarized in Table 3.1; state transition rate parameters are summarized in Table 3.2.

To track pheromone, Ω_H is divided equally into squares of area $\triangle A$, with pheromone dynamics tracked in each square. Pheromone density levels for the current timestep are tracked in a matrix ($Pmat$), with each entry representing the density of pheromone present in a specific corresponding square. During every timestep, the discretized positions of R ants are mapped to corresponding entries of $Pmat$, and the levels in each square are updated during each timestep. It is assumed that only R state ants lay pheromone. Let $R_{tot}^{i,j}$ be the total number of R ants in square (i, j); at the end of each timestep, $Pmat$ is updated as

$$Pmat[i,j] \leftarrow Pmat[i,j] + \ell \frac{R_{tot}^{i,j}}{\triangle A}\tau - \delta\tau Pmat[i,j]. \tag{3.2}$$

ℓ is the rate at which pheromone marks are laid by each R ant, and δ is the rate at which pheromone marks disappear. The division by $\triangle A$ converts $R_{tot}^{i,j}$ into a density.

The angular direction of movement of an S ant at (x,y) is chosen from a von Mises Distribution $k_S(\theta, \hat{\theta}_B)$, where $\hat{\theta}_B(x, y)$ is the direction of the resource relative to current position. The S ants' von Mises bias parameter is a function of the entry in $Pmat$ corresponding to its spatial location; for an S ant in square (i, j) the bias parameter used is $\kappa_S(Pmat_{i,j})$, for which the following functional form is assumed:

$$\kappa_S(P) = \frac{k_m P}{P_0 + P}. \tag{3.3}$$

The parameter k_m is the maximal response possible, and P_0 is the value at which response is half of the maximum. Thus, an S ant in a square with high levels of pheromone has high levels of bias in its direction-angle distribution; this bias is in the direction of the resource relative to its position, $\hat{\theta}_B$.

3.1.3 Continuum limit of ABM in the absence of the resource

In this section, the ODE/PDE system is derived from the ABM dynamics described above. Begin by focusing on the nonrecruitment behavioral states: N, S, T. The behavioral states are described mathematically as probability distributions with function names corresponding to the different states. $N(t)$, for example, describes the probability that a particular ant of the colony is in behavioral state N at time t. The expected number of ants in state N at time t is $nN(t)$. $S(t,x,y)$ and $T(t,x,y)$ are probability densities defined over Ω_H at each time t. $S(t,x,y)$, for example, is the probability density of a particular ant searching at location (x,y) at time t, while $nS(t,x,y)$ is the number density of individuals at location (x,y) and time t. For ease of presentation, function arguments will typically be omitted.

To derive the probability of being in state N at a given time t, start by mathematically describing all of the ways the focal ant could arrive in state N at time $t+\tau$. The probability of being in state N at time $t+\tau$ is

$$N(t+\tau) = N(t)\,(1 - w_N\tau) + j^T(t)\tau + q_S\tau \iint\limits_{\Omega_N} S(t,x,y)\,dA. \tag{3.4}$$

The first term on the right-hand side corresponds to the case in which the ant was in state N at time t and did not transition out of state N during the interval $[t, t+\tau)$. j^T is the probabilistic rate of being in the T state and running into the nest boundary, thus transitioning to state N. The last term corresponds to switching from state S directly into the N state. Expanding the right-hand side, dividing through by τ, and rearranging terms yields

$$\frac{N(t+\tau) - N(t)}{\tau} = -w_N N(t) + j^T(t) + q_S \iint\limits_{\Omega_N} S(t,x,y)\,dA. \tag{3.5}$$

Finally, taking the limit of both sides as $\tau \to 0$ gives

$$\frac{dN}{dt} = -w_N N - \oint\limits_{\partial\Omega_N} \mathbf{J}_T \cdot \vec{n}_N\,ds + q_S \iint\limits_{\Omega_N} S\,dA, \tag{3.6}$$

with function arguments omitted. Here, $\mathbf{J}_T(t)$ is the diffusion-limit flux vector of state T ants (described further below), and $\vec{n}_N$ is the *outward* normal vector (hence the minus sign), parameterized by dummy variable s, around $\partial\Omega_N$; the contour integral sums the probabilistic flux from state T into state N from all points along the nest region boundary.

The S and T states are more involved, as these probability distributions are functions of space and time. Proceeding as before, the probability of being at position (x, y) at time $t + \tau$ is

$$S(t+\tau, x, y) = \frac{I_N(x,y)}{A_N} w_N N(t)\tau + (1 - q_S\tau) \iint_{\Omega_H} K_S(x', y', x, y) S(t, x', y')\, dA. \tag{3.7}$$

The first term on the right-hand side describes the probability of being in state N at time t and transitioning into state S at a position chosen uniformly within Ω_N. $K_S(x', y', x, y)$ is the S state movement kernel, describing the probability density of hopping from position (x', y') to (x, y). The second term incorporates the probability of being in state S at time t and hopping to position (x, y) in time τ; for this to occur, the ant must not quit state S, hence the $(1 - q_S\tau)$ term. Expanding and rearranging as before gives

$$\begin{aligned} S(t+\tau, x, y) = \frac{I_N(x,y)}{A_N} w_N N(t)\tau + \iint_{\Omega_H} K_S(x', y', x, y) S(t, x', y')\, dA \\ - q_S\tau \iint_{\Omega_H} K_S(x', y', x, y) S(t, x', y')\, dA, \end{aligned} \tag{3.8}$$

From here, use the standard isotropic diffusion limit procedure (see appendix B) to find

$$\frac{\partial S}{\partial t} = \frac{I_N}{A_N} w_N N - q_S S + D_S \Delta S. \tag{3.9}$$

This step used the assumption that searchers' walks have no bias ($\kappa_S = 0$) in the absence of pheromone; thus the advection term is 0. In the diffusion limit, the diffusion constant is related to the timestep and average step length as $D_S = \lim_{\tau \to 0} \frac{\hat{\rho}_S^2}{2\tau}$.

The probability distribution describing state T is similar to that of S, but assumes a nonzero bias κ_T and thus results in a nonzero advection term $\mathbf{c}_T$. In the diffusion limit (see appendix B) it was necessary to assume that the bias scaled with average steplength. Define this scaling parameter as b_T; thus $\kappa_T = b_T \hat{\rho}_T$. D_T is defined similarly to D_S.

The full set of equations describing the searching process in the absence of a resource are

$$\frac{dN}{dt} = q_S \iint_{\Omega_N} S\, dA - \oint_{\partial\Omega_N} \mathbf{J}_T \cdot \vec{n}_N\, ds - w_N N \qquad \text{Nest Ants} \tag{3.10a}$$

$$\frac{\partial S}{\partial t} = D_S \Delta S - q_S S + \frac{I_N}{A_N} w_N N \qquad \text{Searching Ants} \tag{3.10b}$$

$$\frac{\partial T}{\partial t} = D_T \Delta T - \nabla \cdot (\mathbf{c}_T T) + q_S \hat{I}_N S \qquad \text{Returning Ants} \tag{3.10c}$$

The double integral term $q_S \iint_{\Omega_N} S\,dA$ is the rate at which probability mass moves directly from the S state to the N state. The term $q_S \hat{I}_N S$ describes the rate that S ants quit searching while outside the nest region. $-\oint_{\partial\Omega_N} \mathbf{J}_T \cdot \vec{n}_N\,ds$ sums the flux of returning ants into the nest state. $\mathbf{J}_T$ is the flux of returning ants, $\mathbf{J}_T = -D_T \nabla T + \mathbf{c}_T T$, and $\vec{n}_N$ is the unit outward normal vector along the nest boundary. The total flux is obtained by summing the dot product of $\mathbf{J}_T$ and $\vec{n}_N$ around the nest boundary, which is parameterized by s. The term $\frac{I_N}{A_N} w_N N$ represents the rate at which an ant in the N state spontaeously leaves and becomes an S ant in the region Ω_N. Finally, the transport terms of the S and T states arise from the random walk model outlined in Appendix B, Section B.4.

The process described by the system (3.10) is constrained to Ω_H by no-flux boundary conditions on S and T along $\partial\Omega_H$: $\mathbf{J}_T \cdot \vec{n}_H\big|_{\partial\Omega_H} = 0$, where $\vec{n}_H$ is the unit outward normal along $\partial\Omega_H$. Likewise, $\mathbf{J}_S \cdot \vec{n}_H\big|_{\partial\Omega_H} = 0$. In addition, T ants that encounter the nest boundary, $\partial\Omega_N$, are instantly absorbed into the N state. Thus, $T\big|_{\Omega_N} = 0$.

3.1.4 Continuum limit with resource present

Let $N(t)$, $E(t)$, $Q(t)$, and $B(t)$ be the probabilities of a focal ant being in state N, E, Q, B respectively, at time t. Let $S(t,x,y)$, $T(t,x,y)$, and $R(t,x,y)$ be the probability densities of location at time t defined on Ω_H. The ODE/PDE derivation is similar to the dynamics without a resource, with some key changes in states that interact with each other. The probability of being in the nest at time $t+\tau$ is

$$N(t+\tau) = N(t)\left(1 - w_N\tau - \xi\chi_E(t)\tau\right) + \tau j^T(t) + \tau q_S \iint_{\Omega_N} S(t,x,y)\,dA. \tag{3.11}$$

Here, $\chi_E(t)$ is a binomially distributed random variable describing the number of individuals in state E at time t, with probability of success $E(t)$, and $n-1$ as the number of ants (other than the focal ant in the N class) that represent trials. To avoid the complication of working with this random variable, assume $\chi_E(t)$ is well approximated by $\chi_E(t) \approx (n-1)E(t) \approx nE(t)$, since n is typically large. With this approximation, and the standard expansion, rearrangement, and $\tau \to 0$ limit, Equation (3.11) yields

$$\frac{dN}{dt} = -w_N N(t) - \xi n E(t) N(t) + j^T(t) + q_S \iint_{\Omega_N} S\,dA. \tag{3.12}$$

The Q and B state dynamics also have between-state interactions; the rate at which Q ants transition to state B depends on how many B ants are present. The Q state is derived as follows:

$$Q(t+\tau) = Q(t)\left(1 - w_Q\tau - \alpha_0(A_0 - \chi_B(t))\tau\right) + v\iint\limits_{\Omega_B} S\,dA\tau, \tag{3.13}$$

where $v\iint\limits_{\Omega_B} S\,dA$ is the probabilistic rate at which an ant in state S located in Ω_B transitions into state Q, and $\chi_B(t)$ is the number of ants at the resource at time t. Using the same approximation and limiting procedure,

$$\frac{dQ}{dt} = w_Q Q(t) - \alpha_0(A_0 - nB(t)) + v\iint\limits_{\Omega_B} S\,dA. \tag{3.14}$$

Let $P(t,x,y)$ be the *density* of pheromone marks at a point (x,y) and time t. The amount of pheromone in a small square of area $\triangle A$, centered at (x,y) is approximately

$$P(t+\tau,x,y)\triangle A = P(t,x,y)\triangle A + \ell\tau\chi_R(t,x,y) - \delta\tau P(t,x,y)\triangle A \tag{3.15}$$

Here, $\chi_R(t)$ is the number of ants in state R in the focal square. Using the approximation $\chi_R(t,x,y) \approx nR(t,x,y)\triangle A$, rearranging terms, and taking a limit as $\tau \to 0$ yields

$$\frac{\partial P}{\partial t} = \ell nR(t,x,y) - \delta P(t,x,y). \tag{3.16}$$

Ants in the S state have pheromone-induced bias described by the advection vector $\mathbf{c}_P(P)$, a function of the pheromone levels at time t and position (x,y). This advection vector arises from the diffusion limit with a pheromone-dependent directional bias. Incorporation of pheromone into the advection-diffusion terms is worked out in appendix B, and assumes that the maximal bias, k_m (presented in Equation (3.3)), is proportional to steplength: $k_m = b_m\hat{\rho}_S$. The equations for other states are derived similarly to what has been demonstrated. The entire system is

$$\frac{\partial N}{\partial t} = q_S \iint_{\Omega_N} S\, dA - \oint_{\partial\Omega_N} \mathbf{J}_T \cdot \vec{n}_N\, ds - w_N N - \xi n E N \qquad \text{Nest Ants} \tag{3.17a}$$

$$\frac{\partial S}{\partial t} = D_S \Delta S - \nabla\left(\mathbf{c}_P(P) S\right) - q_S S + \frac{I_N}{A_N}\left(w_N N + \xi n E N + w_E E\right) - v\, I_B\, S \qquad \text{Searching Ants} \tag{3.17b}$$

$$\frac{\partial T}{\partial t} = D_T \Delta T - \nabla\left(\mathbf{c}_T T\right) + q_S \hat{I}_N S + w_Q Q \frac{I_B}{A_B} \qquad \text{Ret., Unex.} \tag{3.17c}$$

$$\frac{\partial R}{\partial t} = D_R \Delta R - \nabla\left(\mathbf{c}_R R\right) + \frac{I_B}{A_B} w_B B \qquad \text{Ret., Excited} \tag{3.17d}$$

$$\frac{\partial E}{\partial t} = - \oint_{\partial\Omega_N} \mathbf{J}_R \cdot \vec{n}_N ds - w_E E \qquad \text{Excited Ants} \tag{3.17e}$$

$$\frac{\partial Q}{\partial t} = v \iint_{\Omega_B} S\, dA - \alpha_0 (A_0 - nB) Q - w_Q Q \qquad \text{Queued Ants} \tag{3.17f}$$

$$\frac{\partial B}{\partial t} = \alpha_0 (A_0 - nB) Q - w_B B \qquad \text{Exploiting Ants} \tag{3.17g}$$

$$\frac{\partial P}{\partial t} = \ell n R(t,x,y) - \delta P(t,x,y) \qquad \text{Pheromone} \tag{3.17h}$$

Similar to before, the terms $-\oint_{\partial\Omega_N} \mathbf{J}_T \cdot \vec{n}_N ds$ and $-\oint_{\partial\Omega_N} \mathbf{J}_R \cdot \vec{n}_N ds$ describe the probability flux of state T into N, and state R into N, respectively. $\mathbf{J}_I = -D_I \nabla I + \mathbf{c}_I I$ for I $\in$ {T, R}.

3.1.5 Parameter Set

Behavioral parameters of the ABM are listed in Tables 3.3 and 3.4 (discussed further in Chapter 4); parameters used in the PDE continuum model are listed in Table 3.5.

Behavioral parameters were varied to understand how species with different trail fidelities might have qualitatively different equilibrium recruitment dynamics; reasonable ranges for parameter values in ants were determined by field measurements with *T. caespitum* in Chapter 4. Distance was varied from 0.4 to 30 m to understand how recruiting steady states varied with distance. 100 resource sites were assumed (1000 resource sites gave very similar results to 100, and are thus omitted). P_0 was set to 10 or 100 to incorporate a wide

range of half-max trail fidelities. A timestep of $\tau = 10$ s was used, with measured average steplengths found in Chapter 4.

The upper value of k_m, 2.96 (corresponding to $b_m = 50.7$), was based on field measurements on *T. caepsitum*; to understand how a species with lower trail fidelity would differ, $k_m = 1.4$ (corresponding to $b_m = 22.6$) was also included.

The habitat Ω_H was chosen to be large enough to minimize boundary impacts on the foraging dynamics. The minimum region used was 4×4 m^2; this minimal region was necessarily expanded as the nest-resource distance increased. In all simulations, the nest was placed at the center of the habitat $(0, 0)$. The resource region was a 0.2 m$\times 0.2$ m square centered at $(R, 0)$, where R is the distance between the centers of the nest and resource regions. The habitat size was increased along the x-direction: the left and right boundaries were $(-4, 4 + R)$, while the top and bottom edges of the habitat were kept at $(-4, 4)$. The discretization (for both ABM and PDE) models was 0.2×0.2 m^2, which coincided with the nest and bait region sizes.

3.1.6 Bifurcation Simulations

Bifurcation diagrams of the PDE were numerically constructed to investigate the existence of bistability regarding the effect of distance (R) on the equilibrial number of B state ants over different behavioral parameter values. Finite-difference techniques were used to determine the steady states; the method is outlined in detail in Appendix B.

To detect whether a similar bifurcation structure was present in the ABM, simulations were run with the same parameter values; however, since an isotropic diffusion limit was used to derive the continuous time dynamics in the PDE and not the ABM, it is expected that the overall dynamics will differ. To check whether bistability exists in the ABM, the different PDE steady states were used as a sampling distribution for the states and positions of individuals in the ABM colony. After initializing the ABM to the PDE steady-state, the ABM was run for 5 hours of simulation time, and the first 3 hours of dynamics were removed to eliminate the effect of the initial condition; 10 ABM runs were completed for each parameter set.

To compare the steady-state searching distributions of the ABM to those of the PDE, 50 simulations of the ABM were run for 5 hours of simulation time, starting at each

equilibrium found in the PDE; the first 3 hours were discarded to remove the effect of the initial condition. Averaged plots of the 50 distributions of searching ants are compared to predictions of the PDE.

3.2 Results

For a range of parameter values, simulations of the ABM resulted in two generally different types of outcomes. In the first, the resource has few ants exploiting it, and the distribution of searching ants in sectors around the colony is relatively homogeneous. The second type of outcome featured high levels of ants exploiting the resource and a well-established pheromone trail from nest to resource, with a high density of searching ants moving toward the resource (Figure 3.1 and 3.2). The overall distribution of searching ants varied dramatically in these two outcomes, with the latter showing a highly biased distribution of searching effort around the trail and resource.

The ABM exhibited high levels of recruitment for large colony sizes, relatively close distances, small P_0, and large k_m. Figures 3.1, 3.3, and 3.4 illustrate this with histogram heatmaps. For a given heatmap, each column is a histogram with the shade of yellow indicating the frequency of numbers of B ants for the simulations. n and q_S had the greatest impact on the bistable nature; fixing $q_S = 1$, $\delta = 10$, $P_0 = 10$, and $k_m = 2.96$, the ABM model predicts bistability in distances from 6 - 20 m when $n = 2000$, compared to bistability between 4 - 8 m when $n = 500$ (Figure 3.1). When $q_S = 2$, the ABM model predicts bistability between 4 - 13 m when $n = 2000$. Increasing P_0 or δ had the effect of moving the onset of bistability to smaller resource distances (Figure 3.1 and 3.3, respectively), while increasing k_m increased the largest value for which bistability occurred (Figure 3.3).

Steady states of the expected number of exploiting ants (nB^*) in the PDE model (Figures 3.5 and 3.6) exhibited a similar form of bistability as the ABM (Figures 3.1 and 3.3). Generally, the PDE predicts bistability over a slightly greater range of distances than the ABM; however, bistability in the ABM may be difficult to observe at large distances due to the recruiting states being unstable to perturbations; in this case, the system is driven down to the lowest recruiting steady-state through random noise.

In the bistable regime, the distribution of S ants predicted by the PDE was strongly

biased along the trail and around the resource when high levels of recruitment occurred, and homogenously distributed around the nest when low levels of recruitment occurred (Figure 3.2). Figure 3.7 shows the dependence of the searching distribution on various parameter values in the PDE and ABM with $b_m = 22.6$ ($k_m = 1.4$), and $n = 2000$. In both the PDE and ABM searching distributions, increasing P_0 increased the spread of searching ants directly around the resource, especially when $\delta = 10$ and $q_S = 1$. Generally, the ABM graphs show a greater spread of searching ants than is predicted by the PDE; this increased spread is most prominent for parameter combinations with $P_0 = 10$ (Figure 3.7). Simulations with $n = 500$ were similar.

Increasing k_m from 1.4 to 2.96 results in a searching distribution with less spread around the resource in both the ABM and PDE (Figure 3.8). The same previous qualitative dependencies are found in the ABM and PDE models with regards to q_S, δ, and P_0. These qualitative differences in the searching distribution were also present at larger distances, but are harder to observe (Figure 3.9). Generally, the searching distributions matched least well when $n = 500$ and $P_0 = 10$.

Parameterizing the model with data from *T. caepsitum* shows bistability is persistent across a wide range of colony sizes, starting at resource distances of 3 - 7 m, depending on colony size (Figure 3.10), and extending beyond 10 m for larger colonies. Investigations on how bistability varied with changing bait attributes (A_0 and w_B) show almost no effect.

3.3 Discussion

This chapter develops a mechanistic, spatially explicit model of pheromonal trail recruitment in ants. The agent-based model (ABM) incorporates trail following as a biased space-jump random walk, with the amount of bias determined by the amount of pheromone laid by ants returning from the resource. This ABM includes a complete set of behavioral transitions involved in the recruitment process and was used to derive an analogous system of PDEs (partial differential equations) via a diffusion limit. Simulations with initial conditions from various steady states of the corresponding PDE model were used to understand the potential for bistability in this ABM. The PDE model allows investigation of how the bistable nature of the system varies with individual behavioral parameters, and is able to predict the bifurcation diagram of ants exploiting a resource in the ABM (Figures 3.1 and

3.5 for comparison of ABM and PDE).

The steady states observed can be classified as one of two types: the first (referred to as the "recruiting equilibrium") is typified by high levels of pheromone, trail following by ants, and resource exploitation. The second (referred to as the "null equilibrium") lacks all of those properties, and exhibits dynamics much like those that would be found with the resource absent (Figure 3.2). The general structure of the ABM steady states resembled that of the PDE; bistability was present at intermediate resource distances for many of the parameter combinations investigated. The PDE is useful in showcasing this, as it is a deterministic model that does not exhibit stochasticity or randomness in its output. This allows the bistable structure of the ABM to be understood more clearly. In this case, the PDE allowed predictions of the distances under which bistability is present.

The ABM generally predicts a greater spread of searching ants around the resource (Figure 3.8). Despite the discrepancies in the searching distributions of the ABM and PDE, the PDE was able to capture the general qualitative changes in the ABM with various parameter values. This included an increased spread of searching effort around resources when P_0 or δ was large, or q_S was small (Figure 3.7). The flexibility in the searching distribution in response to changes in these parameters is greatest when the maximal bias is small (Figure 3.7 vs. 3.8).

The discrepancies in the searching distributions may come from several sources. The errors are generally greatest when n is small (Figure 3.9), implying that the stochasticity in the ABM may be the cause. Averaging the searching distribution over more runs may help clarify the contour boundaries. In addition, the PDE uses a first-order upwind scheme to solve for the steady-state; using a second-order upwind scheme may increase the level of matching by reducing the local truncation error in the PDE solution. Preliminary results show that a second-order centered-difference scheme is unstable for this advection-diffusion parameter regime. Future work will employ a second-order upwind scheme.

Bistability plays an important role in determining an ant colony's ability to spatially organize, and thus must influence the ability of colonies to generate foraging activity [9, 12, 26]. Empirical experiments show that colony attributes, such as colony size, along with the initial configuration of the colony, determine whether *M. pharaonis* ants are able to initiate high levels of recruitment to a resource when ant movement is restricted to a 1D foraging

arena. This model predicts that spatial bistability is also present in a 2D foraging arena in a wide range of ants species; however, this bistability only occurs at relatively far distances from the nest.

When parameterized specifically to *T. caespitum*, the model predicts that bistability is present over a range of colony sizes, starting at resource distances of 3 - 7 m, and in large colonies, extending beyond 10 m. Foraging ranges of *T. caespitum* are typically much smaller than this (personal observation). It remains to be tested whether a large colony can sustain foraging distances beyond 10 m. At smaller distances (< 3 m), the model predicts no bistability in 2D space, which contradicts the theory that group recruitment has evolved to combat bistability. Other work investigated the effect of resource type on the propensity of ants to use group recruitment [17]; future empirical research needs to investigate whether the tendency for group recruitment varies with resource distance.

An alternative hypothesis is that group recruitment evolved to facilitate food processing, like cutting through exoskeleton to gain access to insect haemolymph [17]. An important addition to this model will be a nonlinear increase in the rate at which ants can take a bite out of the resource (w_B as a function of the number of ants in behavioral state B), which will model resource processing by multiple ants. It is expected that this addition will shift the region of bistability to closer resource distances; however, model simulations with a wide range of fixed w_B (6 - 180 $\frac{1}{\text{hr}}$) give similar bistability ranges with regards to resource distance to help elucidate its purpose.

This model allows measurable individual behavioral parameters to be tied with the dynamics of a foraging ant colony. The individual parameters of this model could be calibrated to any particular species that uses trailing. Future empirical studies need to verify the bistable nature of pheromonal recruitment when ants are allowed to forage in 2 spatial dimensions. While insightful, models and experiments on ants limited to 1 spatial dimension may lead to misinterpretation of the foraging dynamics that have evolved in nature.

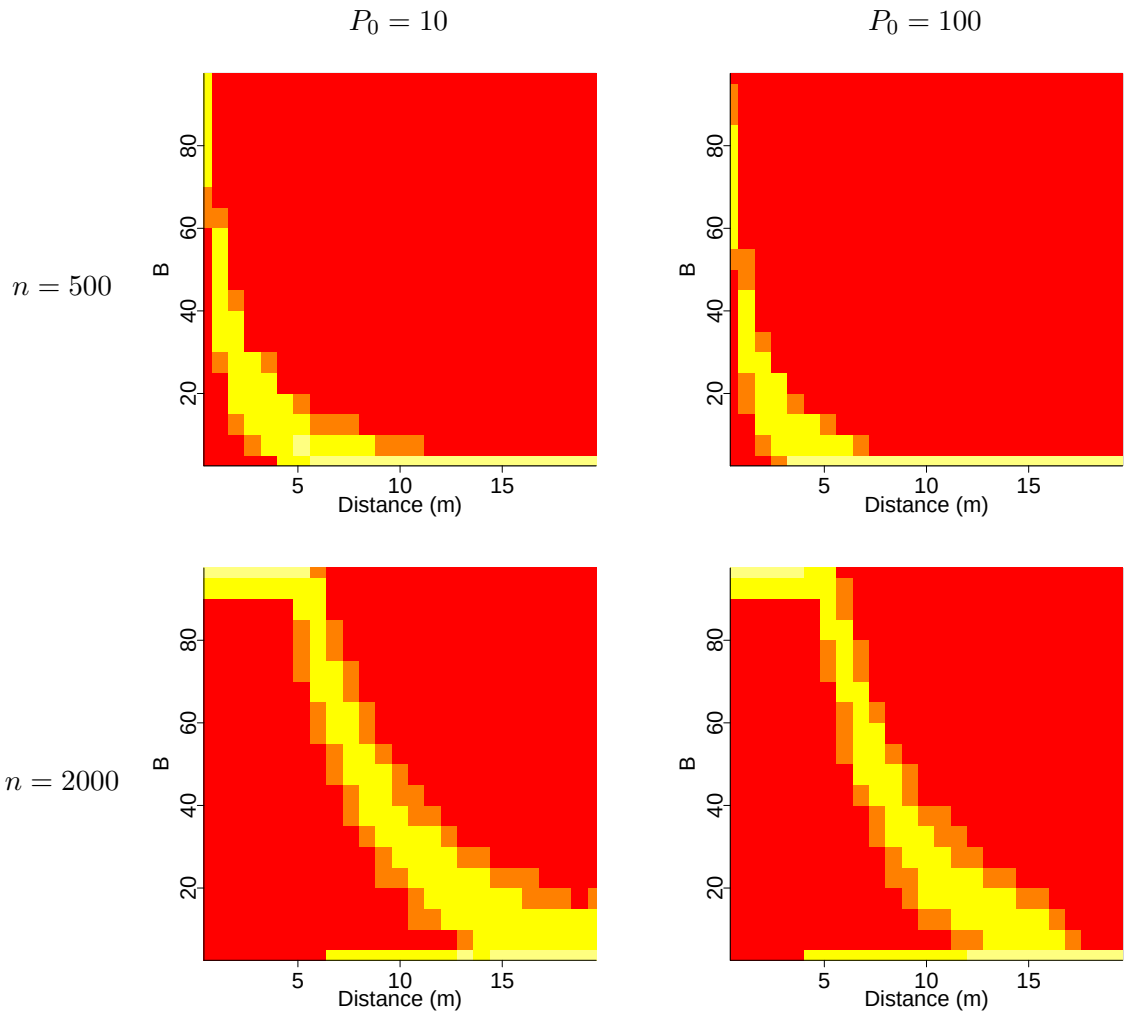

Figure 3.1: Bifurcation diagrams of the ABM. For each distance, 10 simulations were run for 5 hours of simulation time starting from the equilibria of the PDE model; the first three hours of simulation time were excluded from all runs to remove the effect of the initial condition. If multiple equilibria were present for a distance, 10 each were started from the high and low equilibria. All simulations were performed with $\delta = 10$, $k_m = 2.96$, and $q_S = 1$.

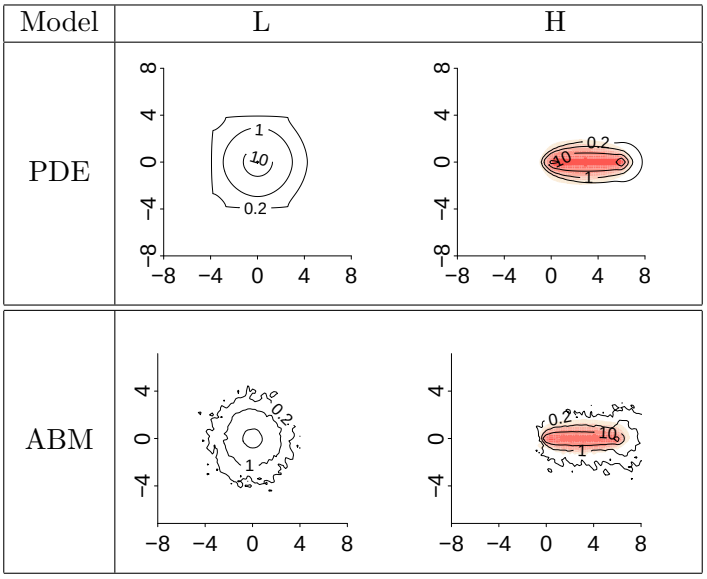

Figure 3.2: Representative searching distributions of the PDE and ABM at high ("H") and low ("L") steady states in bistable parameter regime. All results in this figure were obtained with $b_m = 24$ ($k_m = 1.4$), $R = 6$, $q_S = 1$, and $n = 2000$.

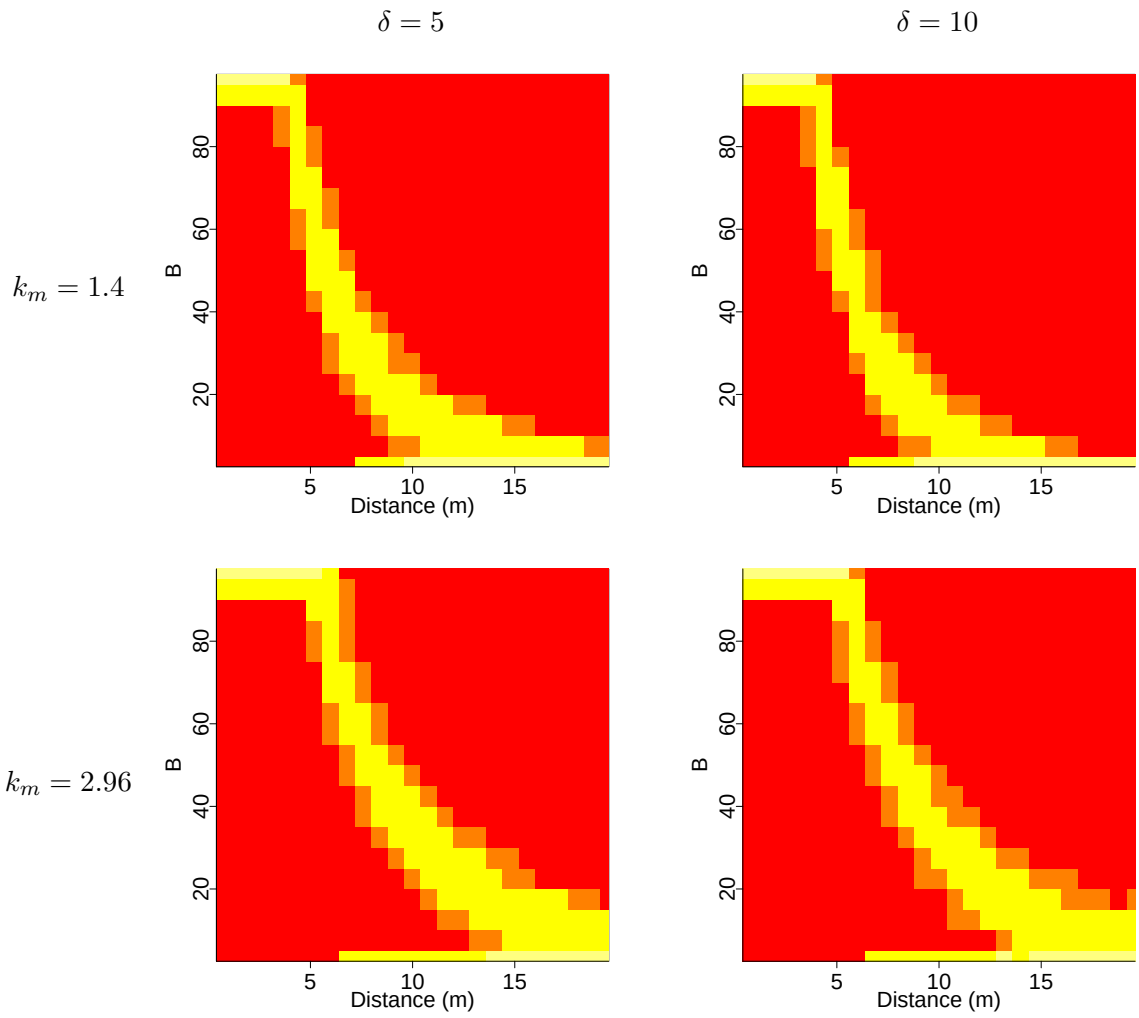

Figure 3.3: Bifurcation diagrams of the ABM constructed as in Figure 3.1. All simulations were performed with $P_0 = 10$, and $q_S = 1$.

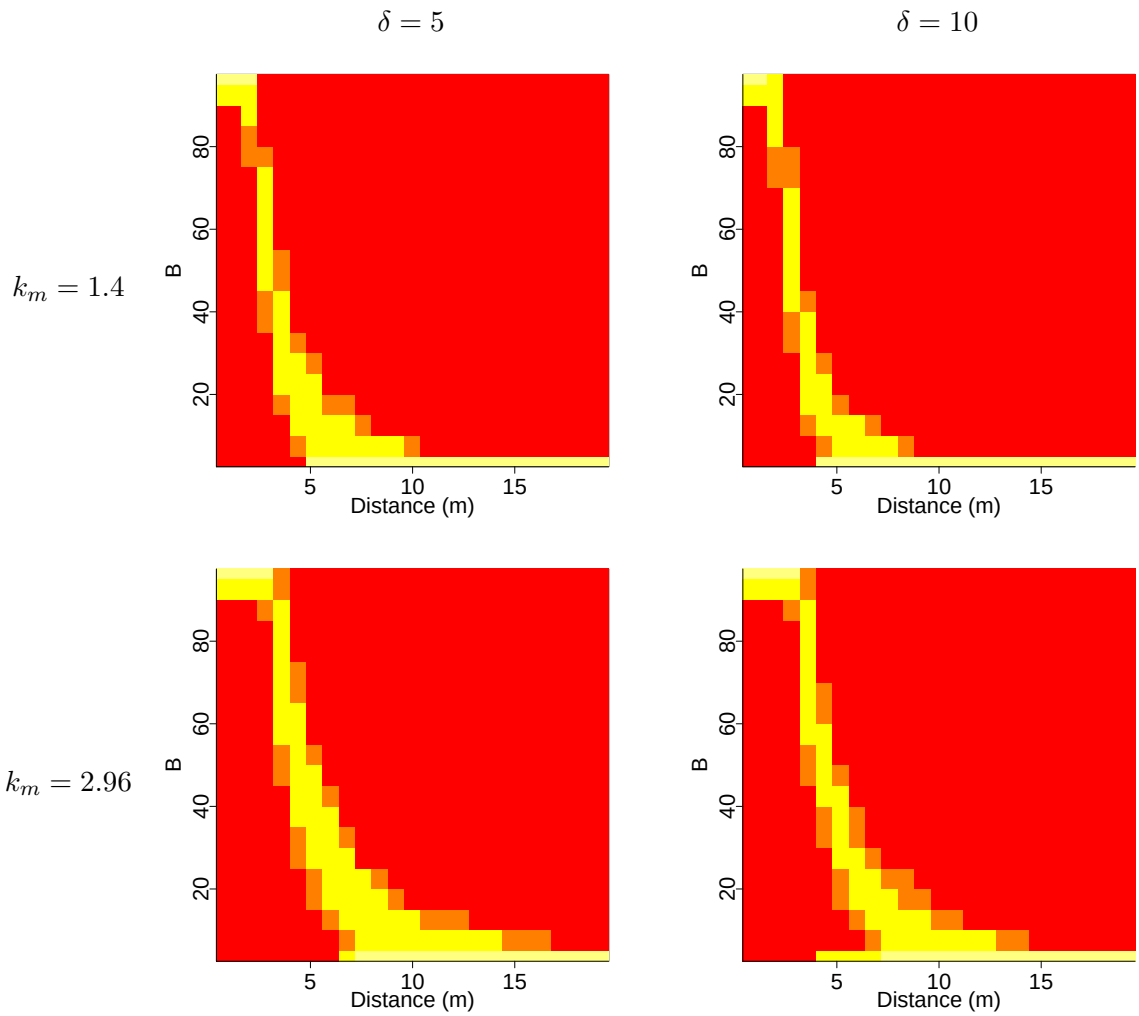

Figure 3.4: Bifurcation diagrams of the ABM constructed as in Figure 3.1. All simulations were performed with $P_0 = 10$, and $q_S = 2$.

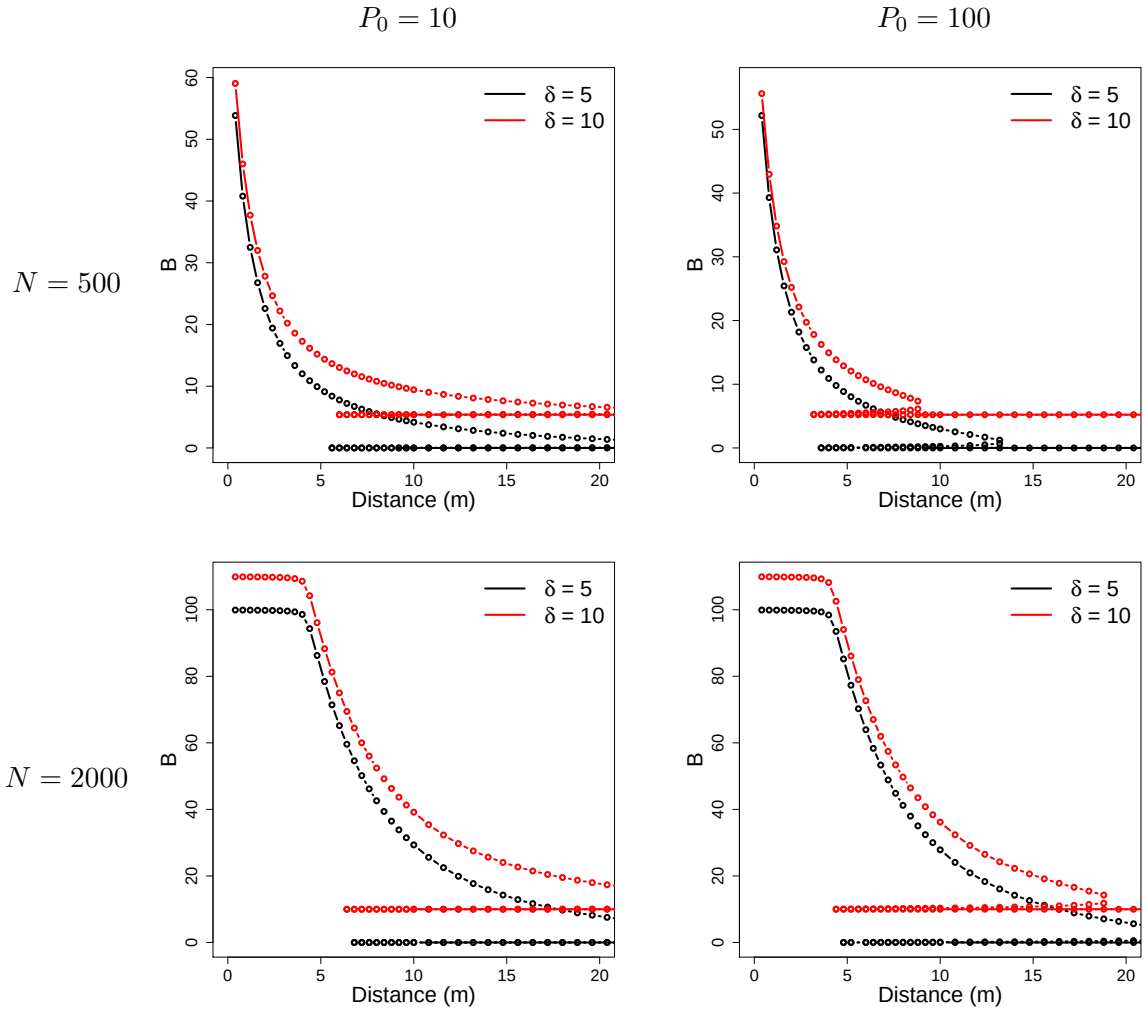

Figure 3.5: Plots of the PDE equilibrial number of B-state ants vs. distance of resource from the nest in meters with $q_S = 1$. B-values corresponding to $\delta = 10$ are shifted up a tenth of the maximum value present in the graph to better display the bistable nature of these graphs. All curves exhibit two saddle-node bifurcations with respect to distance.

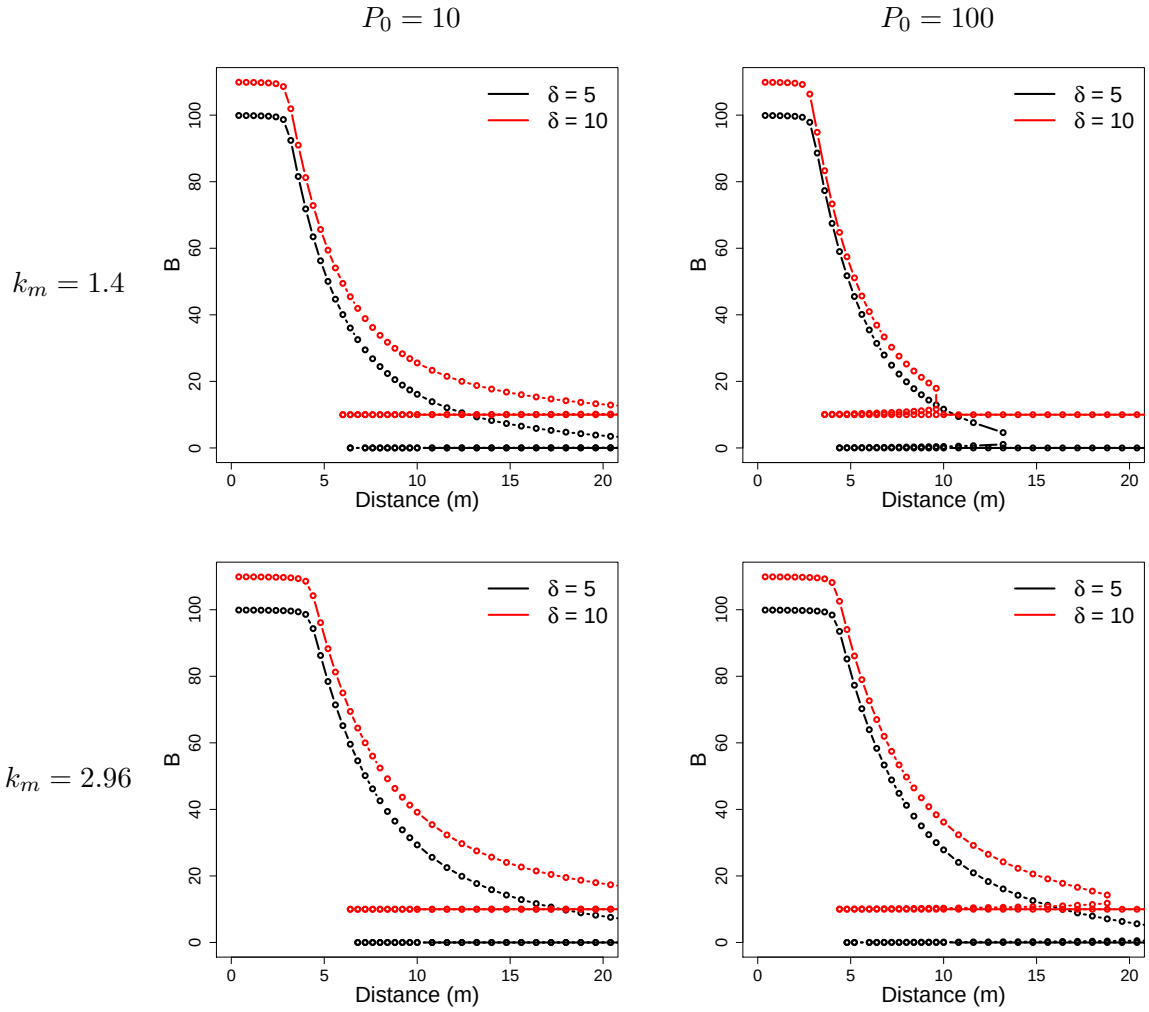

Figure 3.6: Plots of PDE equilibrial number of B-state ants vs. distance of resource from the nest in meters with $q_S = 1$. B-values corresponding to $\delta = 10$ are shifted up a tenth of the maximum value present in the graph to better display the bistable nature of these graphs. All curves exhibit two saddle-node bifurcations with respect to distance.

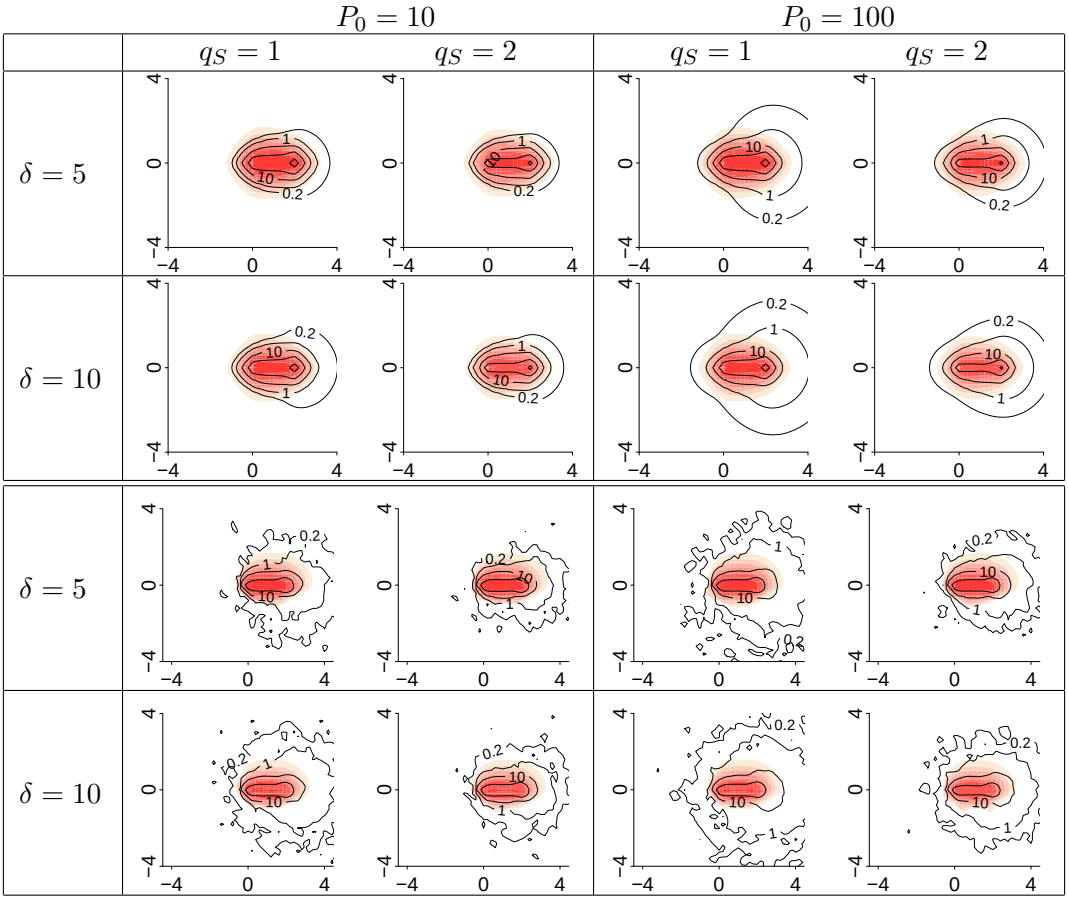

Figure 3.7: Searching distributions of the PDE and ABM above and below the double line break, respectively. For parameter combinations that have multiple equilibria, only the high equilibrium was plotted. All results in this figure were obtained with $b_m = 24$ ($k_m = 1.4$), $R = 2$, and $n = 2000$.

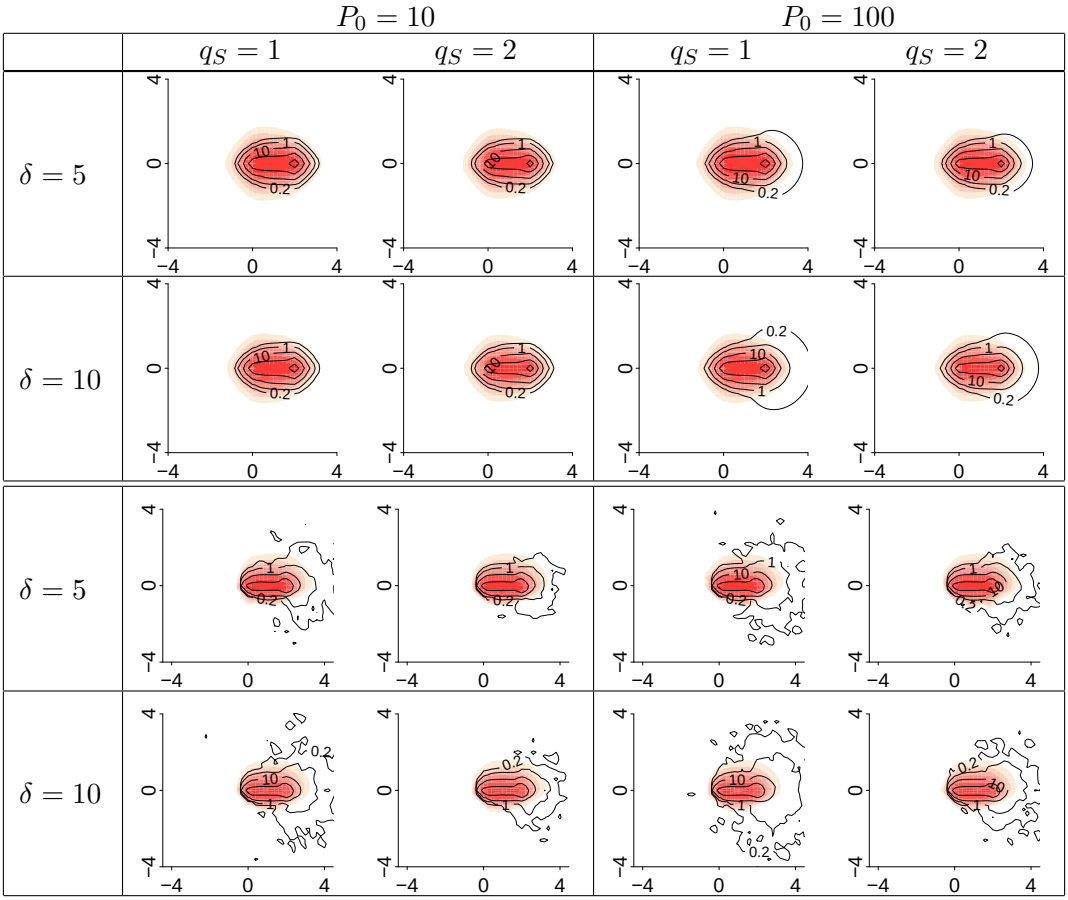

Figure 3.8: Searching distributions of the PDE and ABM above and below the double line break, respectively. For parameter combinations that have multiple equilibria, only the high equilibrium was plotted. All results in this figure were obtained with $b_m = 50.7$ ($k_m = 2.96$), $R = 2$, and $n = 2000$.

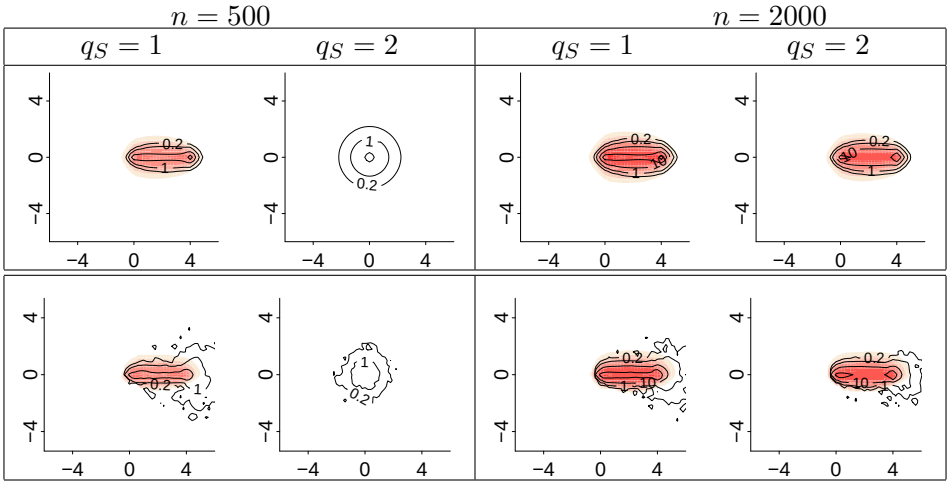

Figure 3.9: Searching distributions of the PDE and ABM above and below the double line break, respectively. For parameter combinations that have multiple equilibria, only the high equilibrium was plotted. All results in this figure were obtained with $b_m = 50.7$ ($k_m = 2.96$), $R = 4$, $P_0 = 10$, and $\delta = 10$.

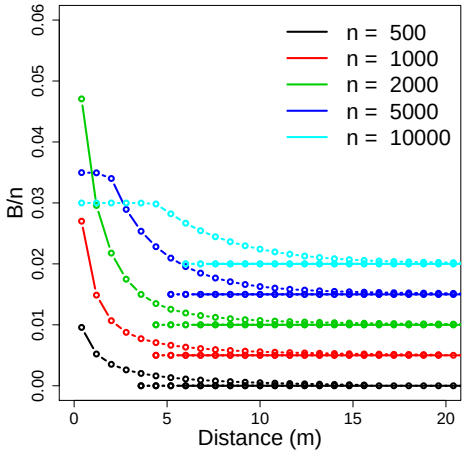

Figure 3.10: Plots of the PDE equilibrial number of B-state ants relative to colony size vs. distance with parameters found from empirical work on *T. caepsitum*. B-values for different colony sizes were shifted up to better reveal the bistable nature of these curves.

Table 3.1: Behavioral state space of the agent-based model.

State	Description	Transitions to
N	Nest ants	S
S	Searching ants	N,T, or Q
T	Nest-bound, unexcited	N
E	Recruiting at nest	S
R	Nest-bound, excited	E
Q	Queued at resource	B
B	Feeding at the resource	R

Table 3.2: Transition rates in the ABM with a resource. Note that S ants that quit transition to state N if in Ω_N, and T otherwise. B.I. represents a transition that occurs with a "boundary interaction".

Transition	Rate
N $\rightarrow$ S	$w_N + \xi E_{tot}$
S $\rightarrow$ T	q_S
S $\rightarrow$ N	q_S
S $\rightarrow$ Q	v
T $\rightarrow$ N	$B.I.$
E $\rightarrow$ S	w_E
Q $\rightarrow$ B	$\alpha_0(A0 - B_{tot})$
Q $\rightarrow$ T	w_Q
B $\rightarrow$ R	w_B

Table 3.3: Parameter values used in the ABM model.

Parameter	Description	Value(s) Used	Units
n	Number of ants	{500, 2000}	# Ants
w_N	Rate N-ants leave the nest	0.11	$\frac{1}{\text{hr}}$
w_E	Rate E-ants leave the nest	36	$\frac{1}{\text{hr}}$
q_S	Rate S-ants quit searching	$\{1, 2\}$	$\frac{1}{\text{hr}}$
w_B	Rate B-ants take a bite	12	$\frac{1}{\text{hr}}$
w_Q	Rate Q-ants quit the bait	1	$\frac{1}{\text{hr}}$
ξ	Recruitment rate	0.02	$\frac{1}{\text{hr}\cdot\text{Ant}}$
δ	Pheromone decay rate	$\{5, 10\}$	$\frac{\text{marks}}{\text{hr}}$
ℓ	Pheromone marking rate	800	$\frac{\text{marks}}{\text{hr}\cdot\text{Ant}}$
v	$S \rightarrow Q$ rate in Ω_B	13	$\frac{1}{\text{hr}}$
α_0	Baseline finding rate of feeding sites	30	$\frac{1}{\text{hr}\cdot\text{site}}$
A_0	Total number of feeding sites on resource	{100}	sites

Table 3.4: Movement bias values used in the ABM model.

Parameter	Description	Value(s) Used	Units
κ_T	T state bias parameter	1.80	-
κ_R	R state bias parameter	1.80	-
k_m	S state maximum bias parameter per step	$\{1.4, 2.96\}$	-
P_0	Half-max pheromone level	$\{10, 100\}$	$\frac{\text{marks}}{\text{m}^2}$
$\hat{\rho_T}$	T state mean steplength	0.061	m
$\hat{\rho_R}$	R state mean steplength	0.061	m
$\hat{\rho_S}$	S state mean steplength	0.062	m

Table 3.5: Parameter values used in the PDE system, as calculated from the individual movement attributes displayed above. The magnitude of $\mathbf{c}_S$ is pheromone dependent.

Parameter	Description	Value(s) Used	Units
D_S	Diffusion coefficient of state S	0.68	$\frac{\text{m}^2}{\text{hr}}$
D_i	Diffusion coefficient of state i. i $\in \{T, R\}$	0.66	$\frac{\text{m}^2}{\text{hr}}$
$\lvert\mathbf{c}_i\rvert$	Magnitude of Adv. vector, state $i \in \{T, R\}$	16.4	$\frac{\text{m}}{\text{hr}}$
$\lvert\mathbf{c}_S\rvert$	Magnitude of S Adv vector	$\frac{I_1(\kappa_S(P))}{I_0(\kappa_S(P))}\frac{\hat{\rho}_S}{\tau}$	$\frac{\text{m}}{\text{hr}}$

CHAPTER 4

MODEL PARAMETERIZATION AND VALIDATION

The goal of this chapter is to validate the potential for subsequent autocorrelated resource finds during recruitment in an empirical system, and validate model predictions regarding the find times of autocorrelated resources for *Tetramorium caespitum*. The latter requires fitting the PDE model developed in Chapter 3. Parameter values of *T. caespitum* are estimated from literature when possible; when not possible, parameters of other ants are used (with the source noted). Movement parameters are obtained via field observations and maximum likelihood estimates. After parameterization, experiment 1 is used to understand how the finding rate of resources varies with distance from the nest when the colony is in its null searching distribution and subsequently estimate the parameter q_S, which describes the rate at which searching ants quit searching to return to the nest. Experiment 2 is used to understand how the finding rate of *T. caespitum* decreases with distance from a focal resource that is being recruited to using a series of Cox proportional hazard models. Specifically, the analysis answers the following questions: do subsequent, autocorrelated resource finds occur more quickly than the original focal bait finds? Does the model predict the relative finding hazards of autocorrelated baits?

4.1 Parameters obtained from literature

Colony size in *T. caepsitum* probably varies widely; values range from $n = 2500$ to $n = 14,000$ [8, 18]. The fraction of the colony that actively engages in foraging is typically unknown, but generally decreases with overall colony size [45]. Colony sizes were set to 500 and 2000 to encompass the uncertainty in this value.

Pheromone evaporation rate is known to be temperature and substrate dependent [38, 71]. Experimentally derived values for *T. caespitum* could not be found; however, Collignon and Detrain (2010) use the value $\delta = 18\frac{1}{\text{hr}}$ for *T. caespitum* without explanation [17].

Using a Y-bridge experimental setup, Jeanson, et al. (2003) measured how the bias of *Monomorium pharaonis* ants varied over time, and estimated $\delta = 6.7\frac{1}{hr}$ on plastic, and $\delta = 20\frac{1}{hr}$ on paper [38]. Preliminary work shows $\delta = 10$ and $\delta = 18$ give similar results; the results presented are simulated with the value $\delta = 18\frac{1}{hr}$.

Pheromone deposition rates of *T. caespitum* have not been found in the literature. *Lasius niger*'s deposition rates have been carefully studied on a simple experimental bridge setup and found to vary across individuals, resource quality, and the number of foraging trips [6]. This study finds 2 - 6 marks per 20 cm bridge length; using their estimates of 2.7 - 4.1 cm/s and the estimate that roughly 1/3 of foragers lay pheromone, I derive $300 \leq \ell \leq 1500\frac{marks}{hr}$, and use the value $\ell = 800\frac{1}{hr}$ as a reasonable estimate.

w_N was estimated using Collignon and Detrain's (2010) estimate that an ant spontaneously exits every 13 s. Assuming 2500 foragers have the same probabilistic rate of spontaneously leaving, this gives an estimate of $w_N = 0.11\frac{1}{hr}$. The parameter $w_E = 36\frac{1}{hr}$ is also used in this paper, and used throughout this thesis for simulations [17].

4.2 Movement parameter estimation

The following data were collected near the Farmington Bay Waterfowl Management Area in Farmington, UT, with *T. caepsitum* ants that occurred along an abandoned road with dirt-gravel substrate. Preliminary analysis of individuals' paths showed that the level of bias by searching and returning ants changed throughout the recruitment process. In an effort to document this change, paths of recruiting ants were analyzed at the beginning of the recruitment process, and after it had equilibrated for 1 hour.

Individuals' paths were recorded by placing small aquarium stones at their position at 10 s intervals for as long as the individual could be followed. Recording ceased when the ant's location was lost (usually due to it moving into deep grass), it switched behavioral states (it found a resource or returned to the nest), or because it began inspecting one of the aquarium stones. When recording ceased, the step lengths and step directions were measured with a ruler and protractor. 10 s intervals were used to reduce interstep correlation in direction, as required by the assumptions of the random walk model presented in Chapter 3.

Measurements involving searching ants included those outside the nest without any obvious trailing activity (S.NP, "no pheromone"), those following a pheromone trail laid by

exactly 1 returning excited ant (S.LP, "low pheromone"), and those involved in the recruitment process 1 hour after recruitment began (S.HP, "high pheromone"). The returning excited ants were classified as the R.NP type, which consisted of the first ant that found a bait (before any trailing activity was started), and R.HP, which consisted of returning excited ants in the recruitment process 1 hour after recruitment began. To measure all HP ant movements, a pecan sandy bait was laid near a searching ant to allow easy finding, and the recruitment process was allowed to equilibrate for an hour.

The S data consisted of 55 hops (steps and directions) of 7 searching NP ants, 155 hops from 32 LP ants, and 114 hops from 28 HP ants. The R data consisted of 85 hops from 8 NP individuals, and 63 hops from 15 HP individuals. All told, 324 hops were recorded from 67 searching ants, and 148 hops were recorded from 23 returning excited ants.

Let θ_i^k,ρ_i^k be the step directions and lengths on the k^{th} step of the random walk of individual i, $i \in \{1, 2, ..., N\}$, $k \in \{1, 2, ..., n_i\}$. I assume that each individual's steplengths are drawn from an exponential distribution with a fixed mean steplength, $\hat{\rho}_i$. Regarding turning angle distributions, I assume that all individuals choose from a von Mises distribution with fixed concentration parameter and bias angle specific to that individual; denote these κ_i and $\hat{\theta}_i$.

$$Pr(\kappa_i, \hat{\theta}_i) = \prod_{k=1}^{n_i} \frac{e^{\kappa_i \cos(\theta_i^k - \hat{\theta}_i)}}{2\pi I_0(\kappa_i)} \tag{4.1}$$

The maximum likelihood estimate of $\hat{\rho}_i$ is simply the mean of steps taken by individual i. The maximum likelihood estimates of $\hat{\theta}_i, \kappa_i$, denoted $\bar{\theta}_i$ and $\bar{\kappa}_i$, satisfy

$$\bar{\theta}_i = \text{atan2}\left(\sum_{k=1}^{N} \cos(\theta_i^k), \sum_{i=1}^{N} \sin(\theta_i^k)\right) \tag{4.2}$$

$$\frac{I_1(\bar{\kappa}_i)}{I_0(\bar{\kappa}_i)} = \frac{1}{n_i} \sum_{k=1}^{n_i} \cos(\theta_i^k - \bar{\theta}_i) \tag{4.3}$$

where atan2(x, y) is the generalized arctangent. The maximum likelihood estimates are used to calculate each $\bar{\rho}_i$, $\bar{\theta}_i$ and $\bar{\kappa}_i$ for individual i. Boxplots of $\bar{\rho}_i$ and $\bar{\kappa}_i$ estimates for each group are shown in Figure 4.1; between-group differences in means were tested at the 0.05 significance level using an ANOVA in the statistical package R.

Mean step lengths of different groups were not significantly different from each other (F = 0.938, p = 0.446). Means of $\bar{\kappa}$ differed between groups (F = 13.87, p = 1.83e-08). A multiple-comparisons test was performed using Tukey's honest significant difference test.

Significant differences were found between the following pairs: R.HP-R.NP ($p < 0.001$), S.NP-R.HP ($p < 0.001$), S.LP-R.HP ($p < 0.001$), S.HP-R.HP ($p < 0.001$); S.HP-S.NP were almost significantly different (p = 0.07). Estimates and 95% confidence intervals of the means are shown in Table 4.1.

The model presented in Chapter 3 assumed the step length distribution was exponential. Distributions of lumped S and R types are shown in Figure 4.2 and are roughly exponential, justifying the model assumptions. The mean step lengths of lumped S and R types are 0.062 m and 0.061 m respectively. With the diffusion limit assumptions, these give diffusion coefficient estimates of $D_S = 0.68\frac{m^2}{hr}$ and $D_R = 0.66\frac{m^2}{hr}$. Paired with the bias parameter estimates in Table 4.1, the average R-state advection magnitude is calculated as $|\mathbf{c_R}| = \frac{I_1(\kappa)}{I_0(\kappa)}\frac{\hat{\rho}_R}{\tau} = 16.4\frac{m}{hr}$. Ants in the T behavioral state are assumed to return to the nest with the same movement attributes as R-ants. Thus, $D_T = 0.66\frac{m^2}{hr}$, $|\mathbf{c_T}| = 16.4\frac{m}{hr}$.

The estimates of κ for low-pheromone and high-pheromone S-ants are used to fit the concentration function in the S-ants' von Mises distribution, $\kappa(P) = \frac{k_m P}{P + P_0}$. I assume that the bias parameter measured from HP ants is the maximum value possible, thus $k_m = 2.96$, and related parameter $b_m = 50.7$.

To measure P_0, I use the κ estimate of 23 S.LP ants and some approximations of the density of pheromone present from 1 R-ant's return. The 23 ants chosen were those for which time-since-pheromone-deposition was recorded, allowing pheromone evaporation to be accounted for. Assume R-ants lay pheromone at rate $\ell\frac{1}{hr}$. Assuming pure advection back to the nest, the R-ant will lay a trail with line density ℓ/c, where c is the R-ant's velocity. Suppose ant i's bias was recorded τ_i hours into the recruitment process. Assuming a decay rate of $\delta = 18$, the pheromone density in a 0.2 m wide region around the trail is roughly $P = \frac{\ell}{c \cdot 0.2} e^{\delta \tau_i}$.

A single P_0 value is assumed for all ants; $\kappa(P)$, with the k_m approximation above, was fit through the measured k_i (the bias measured for the i^{th} S.LP ant). P_0 was chosen as the value that minimized the sum squared error with c set to $16.4\frac{m}{hr}$. This method gives a rough estimate of $P_0 = 5.6$.

4.3 v estimate

To estimate the finding rate in the bait region, find times of a roughly circular, 1 cm diameter piece of pecan sandy were observed when initially placed 1, 3, 5, or 10 cm away from an ant; 10 observations were performed with each distance. Time was tracked while the ant searched within a 20×20 cm^2 region around the bait, and stopped when the bait was found or the ant left the bait region. A find-time function $T(x)$ was fit through the average time to find at each distance using a cubic spline (sum of the times in the resource region for all trials at the given initial distance divided by the number of finds), and the requirement $T(0) = 0$. The mean of this function was calculated over a 20×20 cm^2 square, and the inverse of the mean was used as the average find rate in the bait region. The estimate obtained is $v = 13\frac{1}{\text{hr}}$; this quantity is assumed to scale with the number of ants in the bait region. A similar procedure with a 10×10 cm^2 resource region resulted in $v = 25\frac{1}{\text{hr}}$. As expected, the finding rate in the smaller region is greater, as the initial condition has the ant closer to the resource.

4.4 Experiment 1: null searching state

Experiment 1 compared find times at two resource distances from 5 different colonies. A total of 6 baits were laid around each colony used in the study; 3 were laid 50 cm from the entrance, and 3 at 100 cm. All baits were watched for 30 minutes, and the times at which the baits were discovered were recorded. Upon discovery, the path of the ant was tracked for 10 cm to verify that the ant was heading towards the focal colony; discovery times of ants that did not head toward the focal colony were ignored. After verification, the ant was aspirated to prevent recruitment.

4.5 Experiment 2: ARS searching state

In experiment 2, ants of 6 different colonies were allowed to recruit to baits placed 50 or 100 cm away (3 colonies for each distance); these will be referred to as “focal baits”, with corresponding distance from the nest termed the “focal distance”. The recruitment process was allowed to equilibrate for 60 minutes, after which the number of ants passing an imaginary line perpendicular to the trail over a two-minute period was recorded, as well as the number at the bait. Up to 9 small additional baits were placed 5, 10, or 20 cm from

the bait being recruited to; these will be referred to as "subsequent baits". For 10 minutes, recruited ants that made contact with these supplementary baits were aspirated, and the find times were recorded.

4.6 Data Analysis

The Cox proportional hazards test is a semiparametric test that allows for comparison of survival times by assuming that the hazard functions under different experimental treatments differ by a constant scaling term. The standard Cox model describes the hazard with independent variable(s) $\mathbf{x}$, coefficient(s) β, and an *unspecified* baseline hazard $h_0(t)$ as

$$h(t, \mathbf{x}, \beta) = h_0(t)e^{\mathbf{x}\cdot\beta}, \tag{4.4}$$

where $\cdot$ denotes the dot product. Fitting is carried out via maximum likelihood techniques [37]. In the case $\mathbf{x} = x$, a scalar, the interpretation of two treatments $x_1 < x_2$ is that the hazard under condition x_2 is $h_0(t)exp\left[(x_2 - x_1)\beta\right]$, or $exp\left[(x_2 - x_1)\beta\right]$ that of the hazard under condition x_1.

In the present study, colonies may have different find times of resources due to heterogeneity in unmeasured variables, such as colony size, motivation to forage, or local substrate. To account for these differences, a colony-specific frailty term is included in the hazard term. The frailty model is

$$h(t, \mathbf{x}_i, \beta) = z_i h_0(t)e^{\mathbf{x}_i\cdot\beta}, \tag{4.5}$$

where $\mathbf{x_i}$ are the independent variables measured for individual i, and z_i is the frailty term for individual i; the frailties of the data are assumed to be gamma distributed with mean 1 and variance parameter θ [37]. A significant θ indicates that individual-specific differences in baseline hazards exist.

For experiment 1, a Cox proportional hazards test was used to estimate the ratio of the baseline hazards with bait distance (DIST) as an independent variable, and colony ID as a frailty term. For experiment 2, a Cox proportional hazards model was fit with DIST, BTYPE (focal or subsequent baits), and colony ID as a frailty term to determine whether subsequent baits were found more quickly than focal baits in experiment 1 for a given focal distance. Finally, discovery times of baits were analyzed with focal bait distance (DIST),

and distance (BDIST) from the focal resource (5, 10, and 20 cm) as continuous variables. Analyses were carried out in R using the "survival" package [67].

4.7 Results

In the null searching state data, distance was found significant (p = 0.0036) with a coefficient of -0.02274; temperature and frailty were not (p = 0.36, p = 0.94 respectively). With 50 cm focal distance as the baseline hazard, the coefficient is interpreted as follows: for every unit focal resource distance beyond 50 cm, the hazard of the resource is reduced by $\exp(-0.02274x)$; written another way, for focal distance x, the hazard is reduced by $\exp(-0.02274(x-50)) = 0.9775^{(x-50)}$. The lower and upper 95% confidence intervals on the exponentiated value were (0.9627, 0.9926). Thus, 100 cm baits are found approximately $0.9775^{100-50} = 0.32$ as quickly as 50 cm baits. This value is later used to estimate q_S.

Preliminary analysis involving subsequent baits showed temperature did not play a significant role, thus it is excluded. A Cox model with experimental bait type as a factor (BTYPE), focal bait distance (DIST), and colony ID frailty shows significance of all 3 ($p < 0.001$); log-likelihood ratio tests show that both experimental bait type and distance are significant ($p < 0.001$, $p = 0.013$). Lumped subsequent baits were found 3.326 times faster than focal baits of experiment 1 at 50 cm, and 4.95 times faster at 100 cm from the nest.

A Cox model and post hoc log-likelihood test showed DIST, BDIST, and colony frailty significant ($p < 0.001$, $p = 0.001$, and $p < 0.001$ respectively). The coefficient estimates are presented in Table 4.2. The log of the hazards ratio of the model is

$$-0.06618 \cdot \triangle\text{BDIST} + 0.1931 \cdot \triangle DIST, \tag{4.6}$$

where $\triangle BDIST$ and $\triangle$DIST are the differences in subsequent and focal bait distances that are being compared. The 5 cm subsequent baits with 50 cm focal distance are used as the baseline hazard. The model implies that 10 cm and 20 cm subsequent baits are found 0.72 and 0.37 times as quickly as 5 cm subsequent baits with 50 cm focal distance; for 100 cm focal baits, 5 cm, 10 cm and 20 cm subsequent baits are found 2.63, 1.89 and 0.97 times as quickly. For fixed BDIST, the Cox model predicts subsequent baits with focal distance 100 cm are found 2.56 times more quickly than those with focal bait distance of 50 cm.

4.8 Model prediction

The full PDE model described in Chapter 3 was parameterized with the values described in this section. Nest size was fixed at $n = 500$ and $n = 2000$. Steady-state searching distributions were found for resources 50 cm and 100 cm away from the nest; all resources had $A_0 = 100$. The model was simulated on the same habitat described in Chapter 3, with grid discretization of 0.1 m. Searching distributions were uploaded, and interpolated at points corresponding to 5, 10, and 20 cm away from the focal bait; these were used to obtain model predictions of finding rates according to $vn \iint_{\Omega_B} S^* \mathrm{dA}$.

For both 500-ant and 2000-ant colonies, the proportional hazards for 10 cm and 20 cm baits were the same to 2 decimal places. Only 500-ant colonies were used, as the predicted survival functions of subsequent baits generally matched the empirical data better. As in the empirical work, the baseline hazard is chosen as the subsequent baits 5 cm from the focal bait, with focal bait at 50 cm. For 50 cm focal baits, the predicted hazard ratios are 0.67 and 0.21 for 10 and 20 cm baits, respectively. For 100 cm focal baits, the predicted hazard ratios are 1.88, 1.22, and 0.36 for 5, 10, and 20 cm subsequent baits, respectively. With fixed BDIST, the model predicts 5, 10, and 20 cm subsequent baits at 100 cm focal distance are found 1.88, 1.83, and 1.73 times faster than 50 cm focal distance.

The survival curves of subsequent baits at various focal bait distances are plotted in Figure 4.3 for the empirical data and the model prediction with 500 ants.

4.9 q_S Estimate

Assuming an unbiased random walk (concentration parameter $\kappa_S = 0$), the equilibrium distribution of searching ants is found by setting $\frac{\partial S}{\partial t} = 0$ in Equation (3.10b). Denoting the searching steady-state by S^*, and the nest population steady-state as N^* yields

$$0 = D_S \Delta S^* - q_S S^* + \frac{I_N}{A_N} w_N N^* \tag{4.7}$$

Introduce the following nondimensionalized variables ξ and σ, and parameters γ and $\hat{A}_N$

$$\hat{S}^* = \frac{D_S}{q_S} S^* \quad x = \sqrt{\frac{D_S}{q_S}}\, \xi \quad y = \sqrt{\frac{D_S}{q_S}}\, \sigma \quad \gamma = \frac{w_N}{q_S} \quad \hat{A}_N = \frac{q_S A_N}{D_S} \tag{4.8}$$

The system becomes

$$-\Delta \hat{S}^* + \hat{S}^* = \frac{\gamma I_N N^*}{\hat{A}_N} \tag{4.9}$$

Equation (4.9) can be solved using Fourier transform techniques [28]. To simplify matters, I assume the nest area, $\hat{A}_N$, limits to 0; in this limit, $\frac{I_N}{\hat{A}_N} = \delta(x, y)$, the 2D delta-function. In dimensional variables, the solution is

$$S^*(r) = \frac{w_N N^*}{4\pi D_S} \int_0^\infty \frac{e^{-t - q_S \frac{r^2}{4tD_S}}}{t}\, dt$$

where r is the radial distance from the nest; $r = \sqrt{x^2 + y^2}$. This solution can be used to numerically find the q_S term that best matches our requirement $S^*(1)/S^*(0.5) = 0.32$. The term $w_N N^*$ scales out of this ratio, and need not be known to solve for q_S. Substituting in the estimate of $D_S = 0.68$, I find $q_S = 2.08\frac{1}{\text{hr}}$. Unfortunately, there were not enough data to robustly estimate a q_S for each colony.

4.10 Discussion

In this chapter, an empirical study was devised that assessed the ability of a colony to find autocorrelated "subsequent" baits 5, 10, and 20 cm away from a focal bait that ants are exploiting through recruitment. The focal bait was either 50 cm or 100 cm from the nest; this is termed the "focal distance". The full PDE model was parameterized through literature searches and field work, and the experimental study was replicated by simulating a colony recruiting to a resource either 50 cm or 100 cm away from the nest. The hazard rates of the empirical work were estimated using a Cox proportional hazards model with distance of subsequent bait from focal bait (BDIST) and distance of focal bait to the nest (DIST) as explanatory variables. The corresponding hazard ratios were calculated from the PDE's steady-state searching ant distribution for comparison.

The model correctly predicted that subsequent baits are found faster for focal distance of 100 cm compared to 50 cm. The exponentiated DIST coefficient in the Cox proportional hazards model was 1.019, meaning that subsequent baits with fixed distance from a focal bait are found 2.56 times more quickly than their 50 cm focal bait counterparts; the 95% confidence interval includes values (1.36, 5.14). The PDE model captured the trend of increased finding rate with focal distance (Figure 4.3); 5, 10, and 20 cm subsequent baits were found 1.88, 1.83, and 1.73 times as quickly when the focal bait is at distance 100 cm than when the focal bait is at distance 50 cm.

With focal distance fixed, the Cox model predicts that 10 cm and 20 cm baits are found $0.9360^5 = 0.72$, and $0.9360^{15} = 0.37$ times as quickly as the corresponding 5 cm subsequent bait at the same focal distance, with 95% confidence intervals of (0.60, 0.86) and (0.22, 0.63). The model predicts 0.67 and 0.21 at 50 cm, and 0.63 and 0.19 at 100 cm focal distance. Thus, the PDE model underestimates the hazards for subsequent baits 20 cm from the focal bait. In turn, this means the model underestimates the density of searching ants at 20 cm from a resource.

Although it captures the qualitative trend, the model underestimated the density of searchers away from the focal bait. The simplest reason for the discrepancy is parameter estimation, and error in the PDE steady-state solution. Better parameter estimates will eventually come from laboratory studies that track individual movements with video recordings, and studies with larger sample sizes. It is not believed that a poor estimate of colony size resulted in this discrepancy, as both 500-ant and 2000-ant colonies gave similar predictions for the proportional hazards. The scheme used to find the steady states is a first-order method, and might not adequately describe the true solution when the discretization is coarse relative to the focal bait distance. This can be checked by finding the steady states on finer grids, however this is difficult because the habitat must be defined on a large enough grid that precludes significant boundary interaction. A solution might be to find steady states of a simpler model with a constant flux of ants from the nest, and zero boundary conditions on a grid more tightly concentrated on the region between the nest and bait. Another solution is to use a grid with variable mesh-width, with a finer mesh near the trail.

The model's predictions could also suffer from the diffusion limit used to derive the PDE. This particular derivation assumes that the directional bias of individuals becomes 0 as the timestep becomes 0, while capturing the average bias over large timescales. At small timescales, the predicted positional variance in the PDE will be greater than that of the empirical system. This error might predict less bias in the walk of searching ants than in the empirical system, and in turn result in less directed motion in searching ants. This error should be greatest when the resource is 50 cm away from the nest, as the foragers might not take enough steps before reaching the resource for the positional spread in the walk to average out as it would on large timescales.

More interestingly, the model probably simplifies the possible behavioral states of individuals in the colony. Searching individuals that have lost a pheromone trail might have different movement patterns than individuals that never found a pheromone trail. Ants that lose the trail near the resource might undergo a more sinuous random walk, either by slowing down or turning more, to increase the chance that the trail is found again. Ants are known to change their searching behavior when informed of a resource's position, and even tailor their searching distribution to the type of resource [63]. The behavior of ants that "lose" the pheromone trail has not been adequately described in the literature, and is an important future research direction.

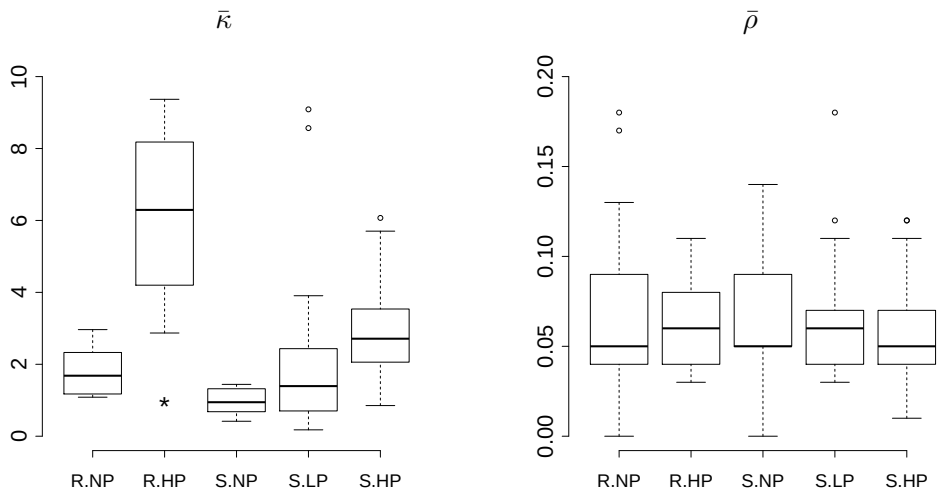

Figure 4.1: Boxplots of κ and ρ maximum likelihood estimates calculated for each individual.

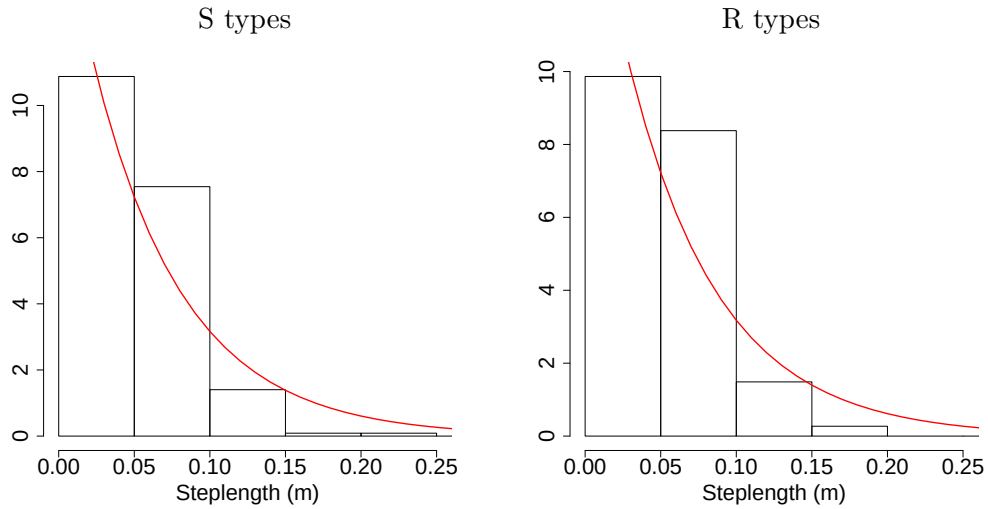

Figure 4.2: Histograms of $\bar{\rho}$ maximum likelihood estimates calculated for S and R individuals. Exponential distribution plots are added with mean $\frac{1}{\bar{\rho}}$.

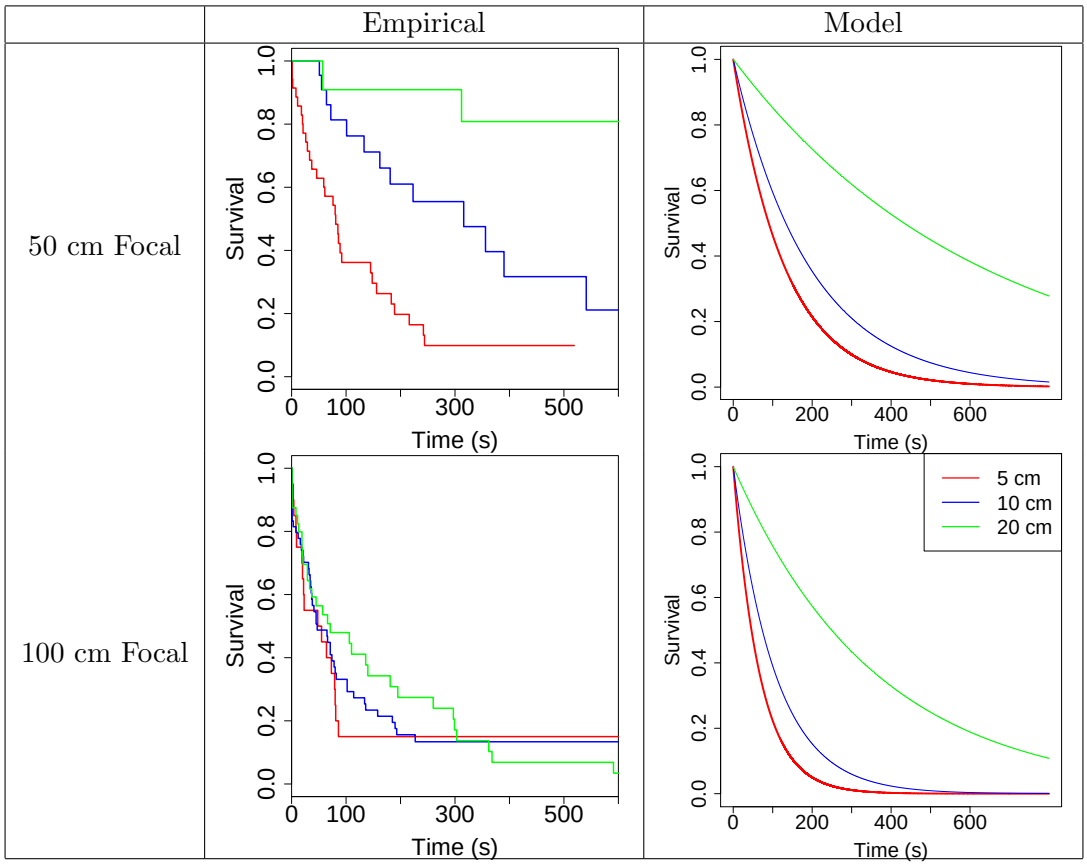

Figure 4.3: Survival plots of empirical data and the model prediction for a 500-ant colony; focal bait distance is 50 cm (top row) or 100 cm (bottom row). The model correctly predicts the qualitative trend of subsequent baits being found faster at a focal bait distance of 100 cm.

Table 4.1: Maximum likelihood estimates of step lengths ($\hat{\rho}$) and concentration parameters ($\bar{\kappa}$), 95% confidence intervals, and significance grouping of $\bar{\kappa}$ estimates for ants in different behavioral types in the ANOVA model. The first letter of Type indicates behavioral state (S: Searching, R: Returning excited), the second two letters indicate the observation period (NP: No pheromone, LP: Low pheromone, HP: High pheromone).

Type	$\bar{\rho}_x$	$\bar{\kappa}$	$\bar{\kappa}$ Int.	$\bar{\kappa}$ Sig. Group
S.NP	0.078 m	0.97	(0, 2.29)	A, B
S.LP	0.066 m	1.90	(1.28, 2.53)	A, B
S.HP	0.058 m	2.96	(2.22, 3.70)	B
R.NP	0.059 m	1.80	(0.57, 3.04)	A, B
R.HP	0.067 m	6.19	(5.08, 7.29)	C

Table 4.2: Results of experiment 2. The table categories are variables, the estimated coefficients, exponentiated coefficients, confidence intervals of exponentiated coefficients, and p-values. The independent variables are distance from focal bait to subsequent bait, focal distance.

Var.	Coef.	Exp[Coef.]	Conf. Int.	P-value
BDIST	-0.06618	0.936	(0.9038, 0.9693)	< 0.001
DIST	0.01931	1.019	(1.0062, 1.0329)	< 0.001

CHAPTER 5

MECHANISM AND BENEFITS OF COLONY-WIDE ARS

A major focus in optimal foraging theory is understanding how individuals should allocate foraging effort in space to maximize food collection [65]. The marginal value theorem, for example, investigates the optimal amount of time that a rate-maximizing forager should spend foraging in a patch [15]. The optimal time is a tradeoff between time spent traveling between patches, and diminishing returns within a patch. A more mechanistic understanding of spatial allocation of foraging activity comes from the study of area-restricted search (ARS), which connects information-use by individuals to subsequent changes in movement patterns while a forager is searching [4, 41]. In patchy resource distributions, a forager should focus its searching effort on areas in which prey are most concentrated. However, this information is typically not available; instead, the forager can use the number of prey that have been found in an area as a cue to increase or decrease the intensity of its search effort [41]. The value of ARS strategies depend critically on the resource distribution; ARS is most valuable when resources are autocorrelated, as the discovery of a resource gives information about the probable location of others [61].

A typical ant colony may comprise thousands of individuals; the ability of a colony to organize its foraging effort in a particular region depends on the actions by individual ants in response to local information, and feedbacks generated by these actions [22, 24]. Positive feedbacks and stimulus decay result in nonlinear scaling of individual behavioral changes at the colony level; small changes in individual behavior can result in drastic changes in the behavioral state of the colony [26]. An important colony-wide behavior present in many ants is pheromonal recruitment, a process used to efficiently exploit a resource. During pheromonal recruitment, an ant that discovers a resource lays a pheromone trail as it returns to the nest. At the nest, the founder ant prompts other ants to exit and follow the

trail to the resource. Subsequent ants led to the resource repeat the process, resulting in positive feedback in information spread and efficient colony-wide exploitation [35].

Although recruitment is classically considered a means by which a colony efficiently exploits a resource, it may also benefit a colony by directing searching effort to profitable regions of the environment, i.e., areas in which other resources are likely to occur due to autocorrelation in the resource distribution. Large species-specific differences in the ability of individual ants to follow their pheromone trails have been shown to exist, for example between *Tetramorium caespitum* and *Tapinoma erraticum* [23]. *T. caespitum* (previously called *T. impurum*) has been noted for its lack of trail fidelity; in an empirical experiment, Deneubourg et al. (1983) found only 18% of recruited ants reached a food source 10 cm from the nest entrance. In contrast, 73% of recruited individuals of the ant *Tapinoma erraticum* made it to the resource in a similar experiment.

Using a spatially implicit ODE model, Deneubourg et al. (1983) show that having a low trail fidelity increases the ability of an ant colony to locate autocorrelated resources. In the model, ants are recruited to a particular resource with a "noise" parameter that determines the proportions of ants that make it to the focal resource or become lost while following the pheromone trail. Lost ants are directed to regions around the resource, where they can contribute to the colony's foraging efforts by finding autocorrelated resources. Deneubourg et al. (1983) conclude that error-prone trail following allows the colony to flexibly multitask between exploiting a resource and searching the vicinity for new resources.

The goal of this chapter is to develop a mechanistic, 2D, spatially explicit simulation model, analogous to Deneubourg et al. (1983)'s experimental setup, and investigate whether natural selection could tune ants' trail fidelity to capitalize on autocorrelated resource hotspots. Such hotspots could represent one of several autocorrelated food sources that ants are known to use, including groups of aphids, groups of bird droppings originating from a bird nest, or even an autocorrelated grouping of urban waste that is continually renewed. The results focus primarily on how trail fidelity could be tuned to resource autocorrelation, and extend previous findings by incorporating an explicit mechanism by which trail fidelity changes the spatial distribution of ants in the colony. Addressing this question will yield insight into how natural selection might tune individual behavioral responses to pheromone to specific resource types.

Agent-based models (ABMs) have been used extensively to model the collective foraging dynamics of many individuals in a colony. Smolke (2009) and Cook et al. (2013), for example, use ABMs to understand how colony structure influences food collection abilities [19,62]. However, ABMs can suffer from long simulation times, and may benefit by mathematical approximations of the dynamics. Plowes et al. (2014) develop a model that spatially tracks the foraging effort of *Messor pergandei* colonies without tracking individuals; instead, simple foraging distributional forms are assumed each time a colony exploits a particular region of space, but no attempt is made to justify the foraging distributions using individual dynamics. The model presented here is similar in that it tracks colony foraging effort without tracking individuals, but the foraging distributions are chosen as equilibria of a PDE model derived from an ABM that describes individuals transitioning through a full set of behavioral states.

The model is constructed in the methods section. The simulations investigate how individual trail fidelity influences the ability of a colony to captilize on a resource hotspot a fixed distance from the colony. Future modifications to the simulation are outlined in Appendix C.

5.1 Methods

In Chapter 3, a continuum (PDE) model was built to describe the distribution of behavioral states and spatial locations of ants within a colony. Steady states of the PDE gave the approximate equilibrial behavior of the colony while recruiting to a resource, as well as in the absence of a resource. Here, these equilibrial distributions will be used to describe the distribution of colony-wide searching activity (with or without recruitment occurring), as well as the collection rate of a colony recruiting to a specified distance from the nest.

The distributions used in Chapter 3 described probabilities of individuals being in different behavioral states as functions of space and time. In the absence of a resource, the model tracked searching ants outside the nest (behavioral class S), ants returning home unexcited after quitting searching (class T), and unexcited nest ants (class N). With a resource present, searching ants could find the resource and become queued for exploitation (class Q), then actively take a bite (class B), and return home excited (class R) while laying

pheromone. Once at the nest, returning excited ants become excited ants at the nest (class E) that prompt nonexcited ants to leave the nest to search.

The focus in this chapter is colony activity at various steady states, and hence the time dependence of these terms is eliminated. In addition, this model uses numerical densities, hence the probability densities will be multiplied by the number of ants in the colony to get the expected number of ants in the various behavioral states and locations. For example, letting N^* denote the equilibrium probability of a colony member being in state N, the expected number of ants in state N at equilibrium is nN^*. Spatial probability densities are now used to predict numerical density. $nS^*(\mathbf{x})$, for example, describes the expected number density of ants in the searching class at position $\mathbf{x} = (x, y)$. Capital letters denote behavioral states (i.e., S, T, R, N, B, Q), and capital letters with superscripted asterisks denote the probability density functions obtained from the PDE system at steady state (i.e., $S^*, T^*, R^*, N^*, B^*, Q^*$), with spatial function arguments omitted unless necessary.

5.1.1 Simulation overview

The simulation models a single colony foraging in a 2D $L^H \times L^H$ m^2 habitat termed Ω_H, chosen large enough to preclude significant boundary effects on the distribution of foragers; pointwise resources fall into the habitat at rate ρ and disappear at rate μ. The mass of each resource is initiated at B_0. As described in Chapter 3, centered around each resource is an $L^B \times L^B$ box, termed the "resource region" and denoted $\Omega_B(\mathbf{x})$ for the resource centered at position $\mathbf{x}$. The resource region describes that area of space in which searching density can contribute to resource finding.

The spatial location of resources that appear in the environment is drawn from a 2D normal distribution with mean $\mathbf{x_0}$ and standard deviation σ_r meters, denoted $B(\mathbf{x_0}, \sigma_r)$. The mean resource position is chosen at the beginning of, and fixed throughout any one simulation.

5.1.2 Non-ARS strategy

A colony of n ants is assumed to switch between two equilibrial states: recruiting and searching. During the searching state ants transition through the searching (S), returning unexcited (T), and nest (N) behavioral states, the dynamics that occur without a resource region present in the PDE model (described by equation set (3.10)). Denote

$S_N^*(\mathbf{x}) = nS^*(\mathbf{x})$ as the equilibrium *number density* of searching ants in this process (the null searching process). Transitions from searching to recruiting occur when a resource is found by searching ants in the colony. The rate at which a resource is discovered is proportional to the expected number of ants in the resource region: a resource with resource region centered at position $\mathbf{x} = (x, y)$ is found at rate $v \iint_{\Omega_B(\mathbf{x})} S_N^*(\mathbf{y})\, d\mathbf{y}$, where v is the probabilistic rate of discovery for ants in the resource region $\Omega_B(\mathbf{x})$, and $d\mathbf{y}$ is the area differential.

After the colony finds a resource, it transitions to the recruiting state specific to that resource. For example, if the resource is a distance r from the nest, the PDE is used to find the equilibrial dynamics of the colony when individuals transition between the full set of behavioral states (S,T,E,R,N,B,Q) in the PDE model with a resource region centered at that distance. The steady-state of the PDE gives equilibrial number densities of ants in states S,T,R, and expected numbers of individuals in states E, N, B, and Q. The dynamics between the searching and recruiting equilibrial states are assumed to occur quickly, and are thus omitted from the simulation.

While recruiting, the colony collects food at a rate proportional to the equilibrial number of ants exploiting the resource, as predicted by the PDE dynamics. Let b be the resource mass that an individual ant is capable of removing from the resource in one bite; the colony-wide hourly collection rate is $b\, w_B\, n\, B^*(r)$, where $B^*(r)$ is the equilibrial number of exploiting ants for a resource at distance r. The resource is exploited until it is depleted, at which point the colony instantly transitions back into the searching state and searches according to S_N^*.

5.1.3 ARS simulation

To assess the effect of area-restricted search guided by pheromone trails, the simulation above was modified to include the following: additional resources can be discovered by ants in the S behavioral state while recruiting. During recruitment to a resource centered at $\mathbf{x}_r$, a resource with resource region $\Omega_B(\mathbf{x})$ is found at rate $v \iint_{\Omega_B(\mathbf{x})} S_R^*(\mathbf{y}, \mathbf{x}_r)\, d\mathbf{y}$, where $S_R^*(\mathbf{y}, \mathbf{x}_r)$ denotes the number density of searching ants during recruitment to a resource at position $\mathbf{x}_r$. When the currently exploited resource is consumed, the colony is allowed to instantly transition to a resource that has been discovered during exploitation if that resource has

not disappeared. If multiple resources have been discovered during exploitation and are still present after the focal resource is depleted, that which was found first is recruited to. If no resources are discovered during exploitation, or remain present when the colony finishes exploiting a resource, the colony switches back to the searching state and searches according to $S_N^*(\mathbf{x})$. As in the Non-ARS model, if multiple equilibria exist for a given resource distance, that with the highest level of resource exploitation is chosen.

5.1.4 PDE steady states and searching distributions

The simulation model requires much numerical solving for equilibria of the PDE system presented in Chapter 3. Several computational shortcuts were taken to make the simulation feasible. Steady states were solved for each set of parameter values over a finite set of distances prior to simulation and stored in a lookup directory. Resources in the PDE searching distributions were always located on the positive x-axis; distances used ranged from 0.2 m to 20 m at 0.4 m intervals. Numerical solving of the PDE for each of these distances was performed similarly to Chapter 3's method, with a grid discretization of 0.2m $\times$ 0.2m, which was also the area chosen for the nest and resource regions.

When a recruitment event occurred, the found resource distance is rounded to that value nearest the discretized distances for which equilibria were found, and used to upload the appropriate steady-state searching distribution and number of exploiting ants from saved text-files. Finally, the searching distribution is rotated to account for the angle of the resource relative the nest.

5.1.5 Parameter values

All parameters are listed in Table 5.1. Nonmovement parameter values describing the behavior of ants are heavily based on *T. caespitum*, with derivations and sources described in Chapter 4. Resource descriptors are generally more difficult to estimate. Rather than attempt to link specific diets to parameters, a range of parameter values are simulated over to understand what trail fidelity allows ants to capitalize on resources that differ qualitatively in level of autocorrelation (σ_r), and renewal and disappearance rates (ρ and μ, respectively). The distance from the resource-hotspot centers and the nest is denoted r_c, and set to either 2 or 5 m.

Trail fidelity was varied by varying b_m, the maximal bias per steplength in searching

ants in the presence of pheromone. b_m relates to the von Mises distribution concentration parameter by the relationship $\kappa_m = b_m \rho_S$, where $\rho_S = 0.62m$ is the average 10-second step length of ants in the S class. Mathematical details of b_m and κ_m are found in Chapter 3; for a given amount of pheromone, increasing b_m increases the proportion of an individual's step that is in the direction of the resource resulting in a more directed random walk. In the PDE model, increasing b_m increases the advection component of the Fokker-Planck equation.

5.1.6 Simulations

The resource hotspot center is positioned 2 or 5 m away from the colony to assess the ability of a colony to capitalize on a resource hotspot near and far from the colony. The ARS and non-ARS versions of the simulation are compared across habitats to understand the benefit of the pheromone-induced ARS. 50 simulations were run with a timestep of $\tau = 0.01$ days for 200 days of simulation time to ensure that the collection rates equilibrated for each set of parameter values. Collection rates were calculated for the 50 runs and used to assess collection abilities of colonies with different behavioral and resource parameters.

5.1.7 Data analysis

ARS and non-ARS collection rates were compared using the Wilcoxon test on the 50 realizations of collection rate for each parameter set. The Wilcoxon test allows comparisons of the average magnitude of two sets of numbers; as a nonparametric test, it makes no assumptions on the distributions from which the numbers are drawn. This test is used as an indicator of whether the ARS model collection rates are larger than non ARS collection rates.

5.2 Results

Boxplots of the collection rates with $r_c = 2$ obtained from 50 simulations are depicted in Figure 5.1 for 500-ant colonies, and a resource hotspot with $\sigma_r = 5$; white and gray boxplots denote ARS and non-ARS simulation results, respectively. At these close resource hotspot distances, both ARS and non-ARS models predict an increase in collection rate with increasing trail fidelity, and exhibit little difference between the two search strategies. Collection rates reach an asymptote relatively quickly; a trail fidelity of $b_m = 20$ achieves

approximately the same collection rate as $b_m = 50$. Reducing σ_r from 5 to 1 resulted in similar trends (Figure 5.2).

Significant differences in collection rates occurred across a wide range of trail fidelities when μ and ρ are large, and $\sigma_r = 1$ for both $r_c = 2$ m and $r_c = 5$ m (Figures 5.2 and 5.3). At close distances ($r_c = 2$ m), the difference between ARS and non-ARS simulations was small; large differences were observed when the resource hotspot is far from the colony ($r_c = 5$ m), and ρ is large (Figure 5.3).

For certain small $b_m \leq 20$ values, the ARS model colonies tended to find a series of resources, ever farther from the nest, resulting in very small collection rates when b_m was small. This resulted in these colonies spending much time collecting from far resources at a slow rate. Unexpectedly, the non-ARS colonies realized a higher collection rate, as they only found resources close to the nest that could be collected at a faster rate. This scenario only occurred when the resource hotspot was close, and b_m small, and is evident in Figures 5.2 and 5.3.

The ARS strategy collection rates increase monotonically with b_m when $r_c = 2$, but exhibit a local optimum when $r_c = 5$. In the latter case, a colony achieves a higher collection rate when its workers have a lower trail fidelity, with the optimum near $b_m = 20$ ($k_m = 1.2$). At larger colony sizes, the optimal b_m is attained at lower trail fidelities (Figure 5.4).

Generally, at far resource hotspot distances the ARS strategy benefited the colony most when resources appearance rates were high ($\rho = 5$); at low rates of appearance and high rates of disappearance, no clear optimal strategy exists.

5.3 Discussion

Autocorrelated resource distributions, or "resource hotspots", have been known to influence the evolution of ant colonies, most notably through colony structure [21]. For example, *Camponotus gigas* ants use a polydomous colony structure to set up new nest sites in areas under bird nests to capitalize on regular bird droppings, as well as near trees with large trophobiont populations to capitalize on autocorrelated honeydew sources [57]. Here, the ability of a colony of ants to capitalize on an autocorrelated resource distribution through modified trail fidelity is investigated.

This chapter uses a spatially explicit simulation of a colony foraging on various resource

hotspot scenarios to understand how modifying trail fidelity of individual ants modifies the ability of a colony to capitalize on an autocorrelated resource distribution. The simulation describes a colony that transitions between a searching and a recruiting state during which a resource is exploited. The degree of exploitation of the focal resource and the distribution of searching ants in the searching and recruiting state are derived as steady states of the mechanistic, spatially explicit PDE model built in Chapter 3.

When the resource hotspot is close to the colony, resource-discovery during recruitment does not greatly increase the collection rate of the colony (Figures 5.1 and 5.2). At these distances, a higher trail fidelity results in a greater collection rate by resulting in a faster rate of exploitation on discovered resources, and the colony-wide ARS is relatively unimportant. In contrast, a lower trail fidelity results in a substantially higher collection rate when the resource hotspot is autocorrelated and far from the nest; in this case, the colony benefits by directing its searching effort around a resource being recruited to, even at the cost of exploiting the focal resource (Figure 5.3 and 5.5). The benefit of colony-wide ARS increases with colony size (Figure 5.5). For autocorrelated resource distributions, the model predicts that a lower optimal trail fidelity for autocorrelated resource distributions occurs in larger colonies (Figure 5.4).

Deneubourg et al. (1983) use the low trail fidelity of the pavement ant *T. caespitum* to argue that this species has evolved to capitalize on autocorrelated resource distributions. The results obtained in this work suggest otherwise; *T. caepsitum*'s measured trail fidelity ($b_m \approx 50$) indicate that this species does not receive a large advantage in its collection rate from harvesting autocorrelated resources, and instead is more suited to environments that require rapid exploitation and are close to the nest. The model suggests that ant species that use resources that are distributed approximately normally with standard deviation 1 m will have substantially lower trail fidelities than *T. caespitum* (Figure 5.5).

The simulation model could be improved upon in several ways. Important future directions will include incorporating the bistable nature of the recruitment process (outlined in Appendix C), and simulating the average collection rate of a colony in environments where the hotspot falls at a random location; preliminary work shows simulations with the resource hotspot placed at random locations in the habitat result in high variance in collection rates, making interpretation of the results difficult. Another important addition will come from

allowing the colony to exploit multiple resources simultaneously, however this may require substantial changes in simulation framework, or reverting back to the agent-based model (ABM) upon which the dynamics of the PDE are based.

The ability of a colony to change its behavioral state through positive feedbacks can come at a cost of flexibility in the colony response. In a classic experiment, Beckers et al. (1990) showed that pheromonal recruitment in *Lasius niger* allows a colony to allocate its foraging effort to choose a 1M sucrose solution over a 0.1M sucrose solution when presented with the choices simultaneously; however, when recruitment to the 0.1M solution has begun, the colony is unable to switch recruitment to a 1M resource introduced later [7]. The colony becomes "stuck" recruiting to the lower quality resource, and is unable to track changes to its environment.

By interpreting an ant colony as a dynamical system, mathematical models have been used to understand how natural selection may have tuned the recruitment process at the individual level to combat inflexibility in tracking environmental changes. One source of flexibility is in the pheromone dynamics used in recruitment; Tabone et al. (2010) use a system of ODEs to understand how pheromone properties, such as evaporation rate, could be tuned by natural selection. The model predicts that a high evaporation rate increases collection rates in environments in which resources are ephemeral. High evaporation rates allow the colony to quickly "turn off" the recruitment process after resources disappear or are depleted [66].

This work seeks to understand how "noise" in the recruitment dynamics, provided by low trail fidelity of individuals, adds flexibility to the recruitment process by allowing simultaneous ARS during exploitation. Social insects that rely on positive feedbacks for collective action can benefit from noise made by individuals through increased flexibility in colony-wide response. An example similar to that investigated here exists in honey bees (*Apis mellifera*): the so called "tuned error hypothesis", where individuals intentionally introduce errors when recruiting via the waggle dance to nearby flower patches; these errors serve to spread foraging effort to the general vicinity of the patch rather than sending all individuals to the same flower, resulting in self-competition and diminishing returns [69,76]. It seems likely that similar mechanisms could have evolved in ants, especially those species with large colonies that may suffer from diminishing returns at a specific resource. Carefully

documenting movement parameters of individuals, as done in the honey bee studies, is required to rigorously document similar traits of collective ant systems.

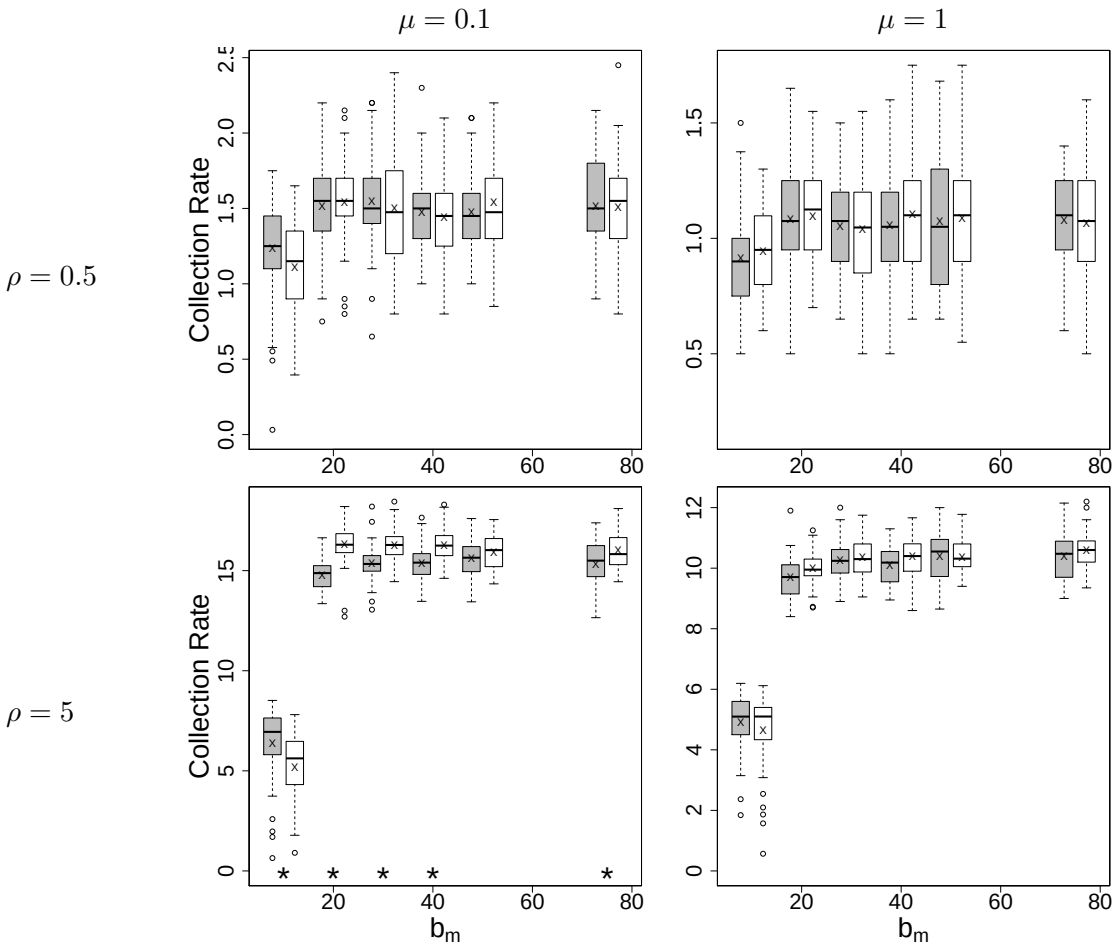

Figure 5.1: Boxplots of collection rates from 50 simulations of each parameter set with $r_c = 2$, $A_0 = 100$, $\sigma_r = 5$, and $n = 500$. Gray and white boxplots denote results from search-recruit model non-ARS and ARS simulations, respectively; asterisks below denote collection rates with significant differences between with and without ARS at the p = 0.01 level.

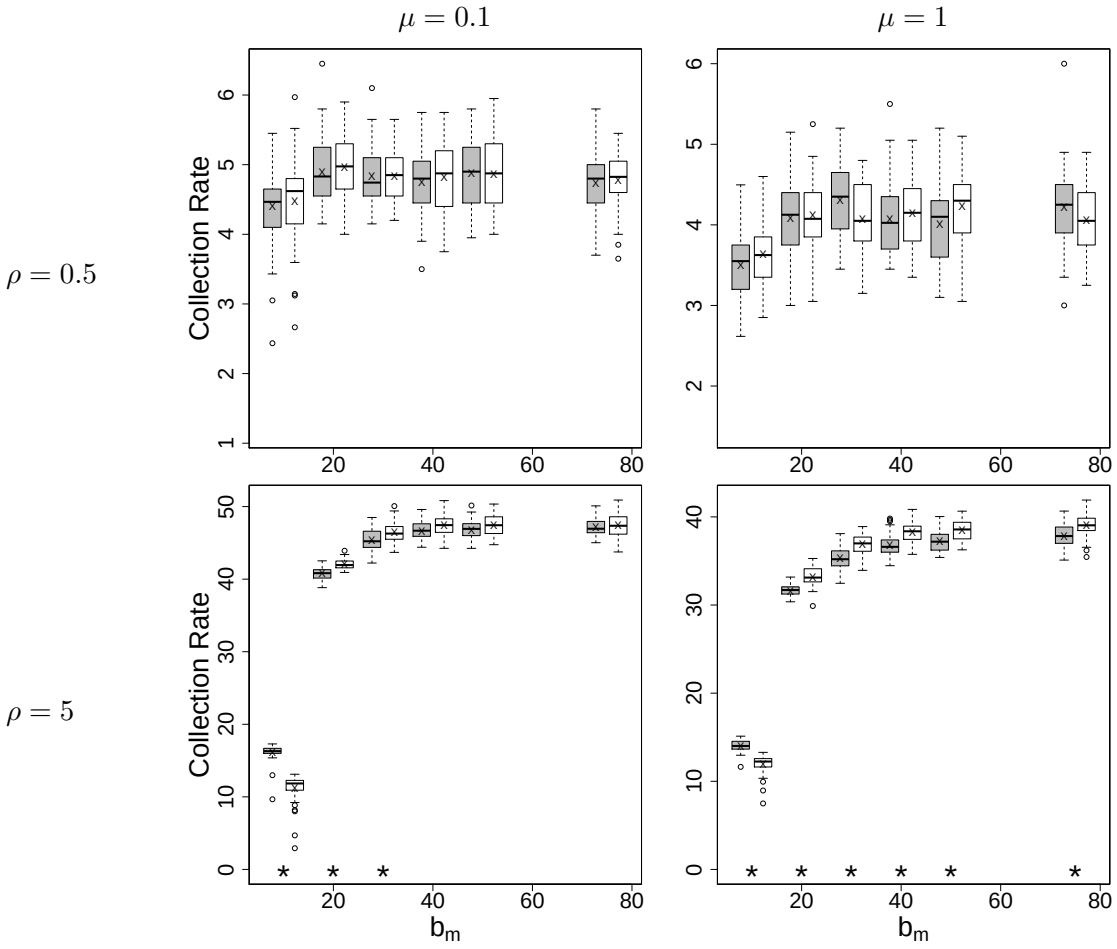

Figure 5.2: Boxplots of collection rates from 50 simulations of each parameter set Parameters as in Figure 5.1 but with $\sigma_r = 1$.

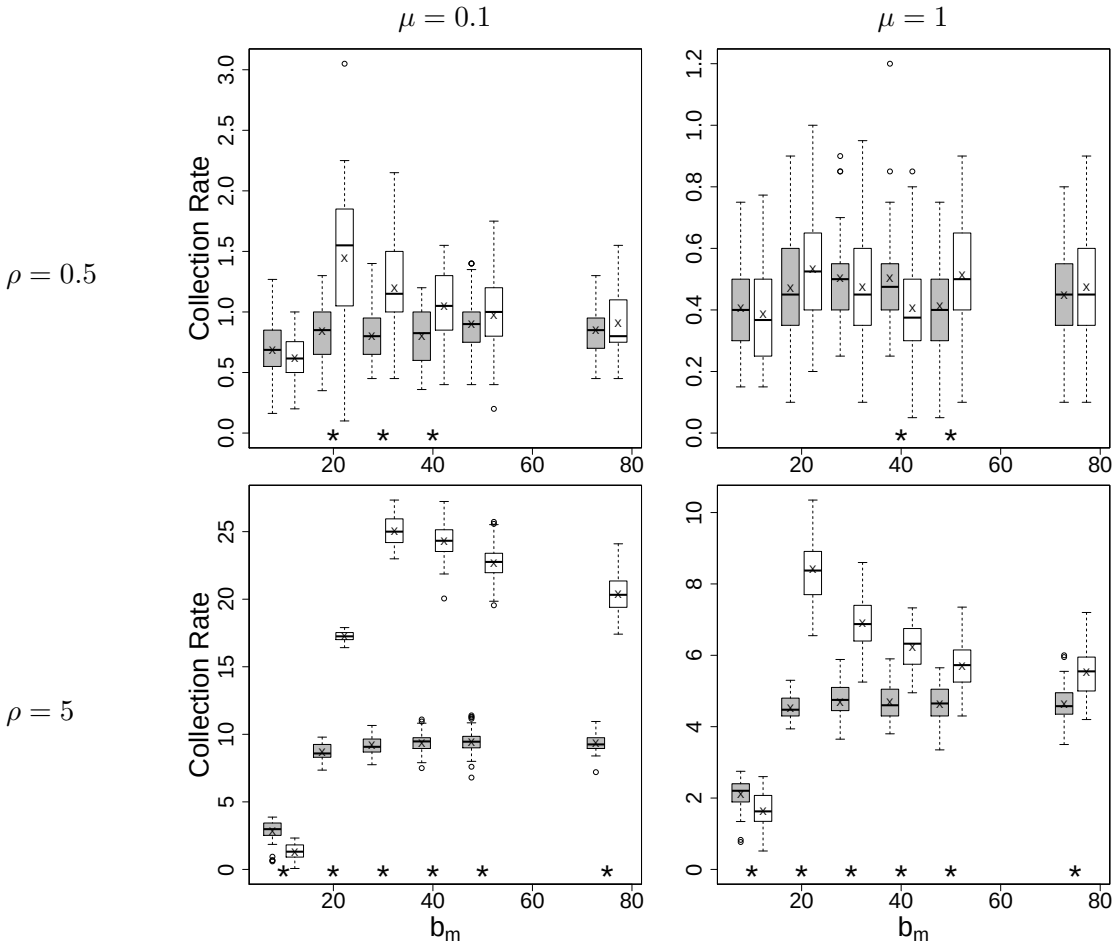

Figure 5.3: Boxplots of collection rates from 50 simulations of each parameter set Parameters as in Figure 5.1, but with $\sigma_r = 1$, and $r_c = 5$ m.

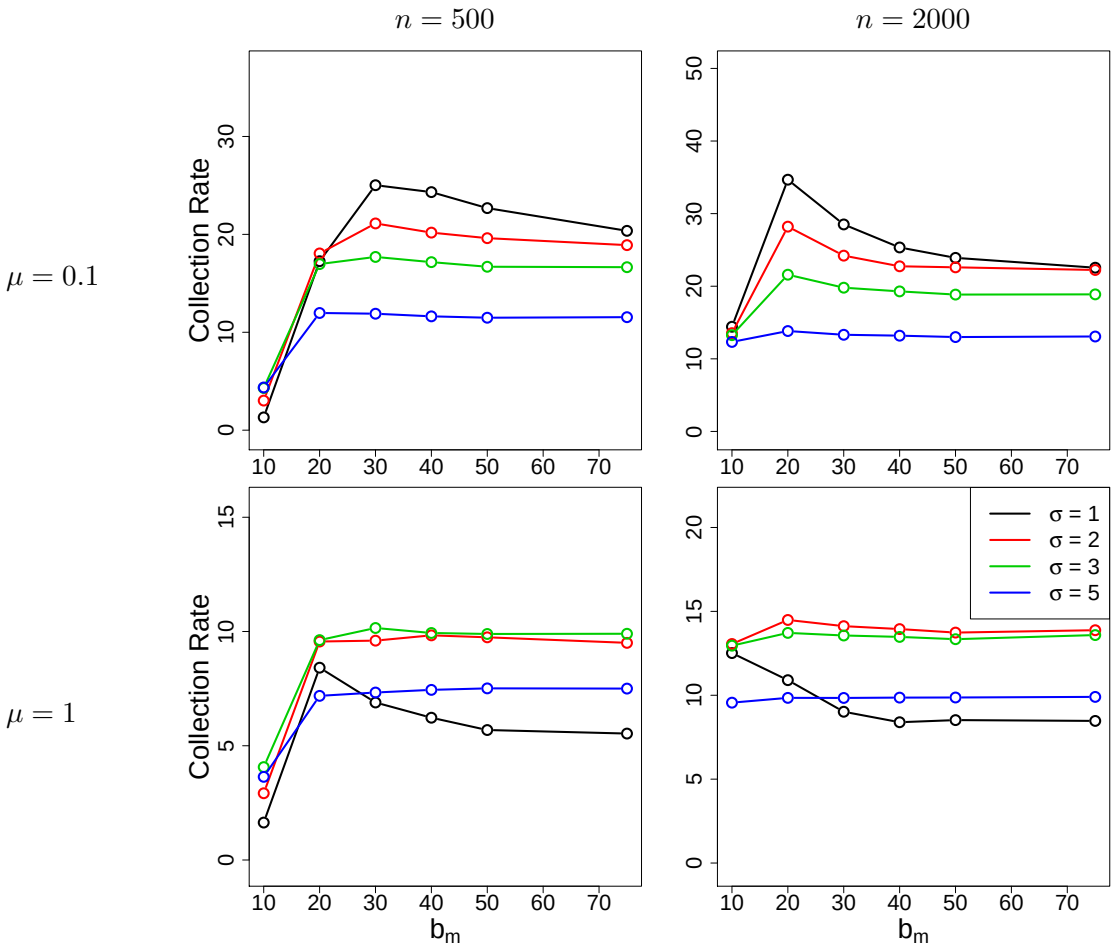

Figure 5.4: Mean collection rates of 500-ant and 2000-ant colonies with $r_c = 5$, $\rho = 5$, and various σ_r values.

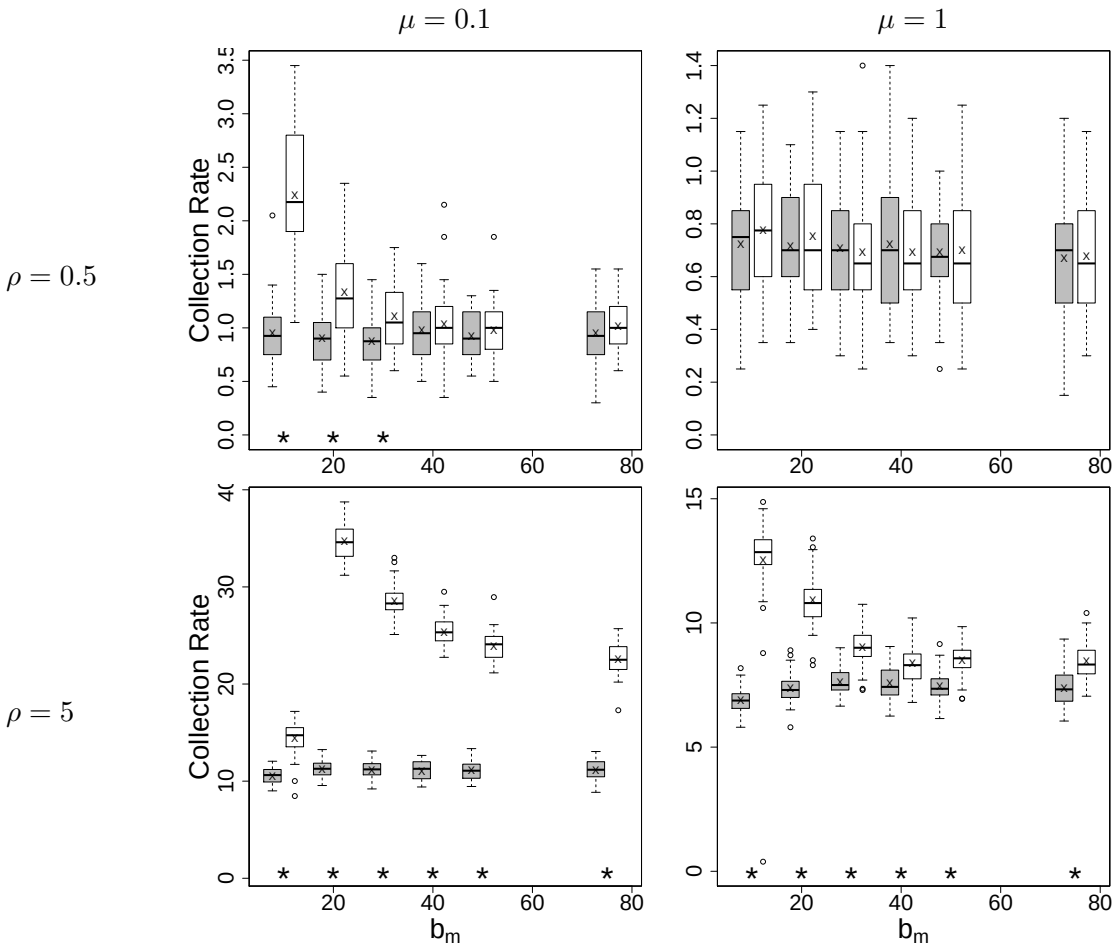

Figure 5.5: Boxplots of collection rates from 50 simulations of each parameter set with $r_c = 5$, $A_0 = 100$, and $n = 2000$. Gray and white boxplots denote results from search-recruit model non-ARS and ARS simulations, respectively; asterisks below denote collection rates with significant differences between with and without ARS at the p = 0.01 level.

Table 5.1: Parameters of the Search-Recruit model. Ant behavioral parameters are shown in time units of hours for clarity, and converted to units of days in the simulation.

Par's	Description	Value(s) Used	Units
r_c	Distance to resource hotspot	$\{2, 5\}$	m
ρ	Rate of resource appearance	$\{0.5, 5\}$	$\frac{1}{\text{day}}$
μ	Rate of resource disappearance	$\{0.1,\ 1\}$	$\frac{1}{\text{day}}$
σ_r	Standard deviation of resource PDF	$\{1, 2, 3, 5\}$	m
b	Grams ingested per ant per resource visit	$\{0.04\}$	g
A_0	Total number of feeding sites per resource	$\{100\}$	#
n	Number of ants	$\{500,\ 2000\}$	#
w_N	Rate N-ants leave the nest	0.11	$\frac{1}{\text{hr}}$
w_E	Rate E-ants leave the nest	36	$\frac{1}{\text{hr}}$
q_S	Rate S-ants quit searching	2	$\frac{1}{\text{hr}}$
w_B	Rate B-ants take a bite	12	$\frac{1}{\text{hr}}$
w_Q	Rate Q-ants quit the bait	1	$\frac{1}{\text{hr}}$
ξ	Recruitment rate	0.02	$\frac{1}{\text{hr}\cdot\text{Ant}}$
δ	Pheromone decay rate	10	$\frac{\text{marks}}{\text{hr}}$
ℓ	Pheromone marking rate	800	$\frac{\text{marks}}{\text{hr}\ \cdot\ \text{Ant}}$
v	$S \to Q$ rate in Ω_B	13	$\frac{1}{\text{hr}}$
α_0	Baseline finding rate of feeding sites	30	$\frac{1}{\text{hr}\cdot\text{site}}$

APPENDIX A

NUMERICAL CALCULATIONS IN CHAPTER 2

Evaluation of the analytical expressions requires calculating $\chi^*(x,y)$, the longterm equilibrial distribution of finding a resource at (x,y). Recall $\chi^*(x,y)$ satisfies

$$\chi^*(x,y) = \int_{-\infty}^{\infty}\int_{-\infty}^{\infty} \chi^*(\hat{x},\hat{y})\, P(\hat{x},\hat{y},x,y)\, d\hat{x}\, d\hat{y} \tag{A.1}$$

Numerically estimating this function in turn requires estimation of

$$P(\hat{x},\hat{y},x,y) = \int_0^{\infty} \frac{f(\hat{x},\hat{y},x,y) r B(x,y)}{\delta(\delta + f(\hat{x},\hat{y},x,y))} \left(\delta + f(\hat{x},\hat{y},x,y) e^{-(\delta+f(\hat{x},\hat{y},x,y))t}\right) e^{-R(t,\hat{x},\hat{y})} dt \tag{A.2}$$

One way of approximating $P(\hat{x},\hat{y},x,y)$ is to discretize space; let patch j be the square with center (x_j, y_j) and area $(\triangle y)^2$. We will refer to the previously exploited patch as i, with location $(\hat{x}_i, \hat{y}_i)$.

Define the matrix $\hat{P}$ with elements

$$\hat{P}_{i,j} = P(\hat{x}_i, \hat{y}_i, x_j, y_j)\, (\triangle y)^2 \tag{A.3}$$

The j^{th} column of $\hat{P}$ is a probability distribution of moving to patch j conditional on being at patch i. Of course, we assume the appropriate discretizations and rescalings of the probability distributions f and B as well. Equation A.1 can be approximated as

$$\hat{\chi}_j^* \;\; = \sum_{i=1}^{N} \hat{P}_{i,j}\, \hat{\chi}_i^* \tag{A.4}$$

where N is the number of patches in the discretized environment, and $\hat{\chi}^*$ is a vector approximation of χ^* ($\hat{\chi}_j^* \approx \chi^*(x_j, y_j)$). This can be written more succinctly as

$$\hat{\chi}^* = \hat{\chi}^* \cdot \hat{P} \tag{A.5}$$

where $(\cdot)$ indicates matrix multiplication. $\hat{P}$ is a transition matrix of a finite discrete time Markov chain [2]. Since any transition from patch i must result in the forager moving

somewhere, $\hat{P}$ has the property $\sum_{j=1}^{N} \hat{P}_{i,j} = 1$. From Equation (A.5), we note that $\hat{\chi}$ is a left eigenvector of $\hat{P}$ with eigenvalue 1. Since $\hat{P}$ is a stochastic matrix (rows sum to 1), such a $\hat{\chi}$ is guaranteed to exist.

We can refine this method to take advantage of the radially symmetric resource distribution and only track the annuli of the resource finds. Discretize space into N annuli with average radial distance ρ_j from the origin, and radial width $\triangle\rho$. Since the model is radially symmetric, we can always take the forager's previous resource find in (ρ, θ) space to be at $(\hat{\rho}_m, 0)$. Define

$$\begin{aligned} P_{pol}(\hat{\rho}, \rho, \theta) &= P(\hat{\rho}\cos\hat{\theta}, \hat{\rho}\sin\hat{\theta}, \rho\cos\theta, \rho\sin\theta) \\ &= P(\hat{\rho}, 0, \rho\cos\theta, \rho\sin\theta) \end{aligned} \tag{A.6}$$

Now, define a matrix $\hat{P}$ with elements $\hat{P}_{m,n}$ describing the probability of transitioning from annulus m to annulus n. We have

$$\hat{P}_{m,n} = 2\rho_n \triangle\rho \int_0^{\pi} P_{pol}(\hat{\rho}_m, \rho_n, \theta)\, \mathrm{d}\theta \tag{A.7}$$

Equation (A.5) again gives $\hat{\chi^*}$ as a function of annular distance. $T(\hat{x}, \hat{y})$ can likewise be simplified to depend on ρ only, allowing $\hat{T}$ to be calculated via Equation (2.21) with integration over $\hat{\rho}$.

APPENDIX B

COMPUTATION AND DIFFUSION LIMIT OF CHAPTER 3

Appendix B describes finite difference methods, steady-state solving, and the diffusion limit assumptions found in Chapter 3.

B.1 Finite Difference Methods

The steady states were found using finite-difference methods (FDMs) in R, the statistical language [46,60]. When applying FDMs to linear steady-state problems, the time derivatives in the system are set to 0 while the right-hand side is approximated with finite difference approximations of the spatial derivative terms. The result is a large, sparse, linear system of equations. To illustrate the idea, consider a generalized version of the steady-state PDE describing S ants from Equation (3.10) with no-flux boundary conditions on $\partial\Omega_H$.

$$-f(x,y) = -\nabla \cdot [\nabla (D_S S) - \mathbf{c}(x,y)S)] - q_S(x,y)S. \tag{B.1}$$

The source term from the nest is generalized as $f(x,y)$ and moved to the left-hand side. Discretize the x-coordinate into N_x partitions with $x_i = \frac{2i-1}{2}\triangle x$, $i \in \{1,2,...,N_x\}$, where $\triangle x = \frac{L_x}{N_x}$. Similarly, discretize the y-coordinate into N_y partitions with $y_j = \frac{2j-1}{2}\triangle y$, $j \in \{1,2,...,N_y\}$, and $\triangle y = \frac{L_y}{N_y}$. Let $S_{i,j}(t)$ be an approximation of the solution inside the box centered at (x_i, y_j), with width and height $\triangle x$ and $\triangle y$, respectively. Let $c^1_{i+\frac{1}{2},j} = c_1(x_i + \frac{\triangle x}{2}, y_j)$ denote the x-direction advection between nodes (i,j) and $(i+1,j)$, and $c^2_{i,j+\frac{1}{2}} = c_2(x_i, y_j + \frac{\triangle y}{2})$. c^1 and c^2 are nicely represented as $(N_x+1)\times N_y$ and $N_x \times (N_y+1)$ matrices respectively; however, the fractional subscripts will be kept.

Building the finite difference scheme requires estimating the flux across each edge of the grid. Let $\mathbf{J} = \langle J_1, J_2 \rangle$ denote the flux vector: $J_1 = -D_S\frac{\partial S}{\partial x} + c_1(x,y)S$, $J_2 = -D_S\frac{\partial S}{\partial y} + c_2(x,y)S$. Define $F^1_{i+\frac{1}{2},j}$ as the flux estimate on the edge connecting nodes (x_i, y_j) and x_{i+1}, y_j, and similarly $F^2_{i,j+\frac{1}{2}}$ for the edge connecting the nodes at (x_i, y_j) and (x_i, y_{j+1}).

The finite difference approximations of the fluxes are

$$F^1_{i+\frac{1}{2},j} = D_S \frac{S_{i+1,j} - S_{i,j}}{\triangle x} + c^1_{i+\frac{1}{2},j} \left(S_{i,j}(c^1_{i+\frac{1}{2},j} \geq 0) + S_{i+1,j}(c^1_{i+\frac{1}{2},j} < 0) \right) \tag{B.2a}$$

$$F^2_{i,j+\frac{1}{2}} = D_S \frac{S_{i,j+1} - S_{i,j}}{\triangle y} + c^2_{i,j+\frac{1}{2}} \left(S_{i,j}(c^2_{i,j+\frac{1}{2}} \geq 0) + S_{i,j+1}(c^2_{i,j+\frac{1}{2}} < 0) \right) \tag{B.2b}$$

Note the advection terms only use data upwind of the advection direction. Upwind advection schemes generally enhance the stability of finite difference methods [46]. Though simple to implement, this scheme has local truncation error of $\mathcal{O}(h)$, where $h = max(\triangle x, \triangle y)$.

Next, we plug the flux estimates from Equations (B.2) into Equation (B.1), using finite difference approximations of the divergence operator. Discretizing the left-hand side of Equation (B.1) by defining $f_{i,j} = f(x_i, y_j)$ gives

$$-f_{i,j} = -\left(\frac{F^1_{i+\frac{1}{2},j} - F^1_{i-\frac{1}{2},j}}{\triangle x} + \frac{F^2_{i,j+\frac{1}{2}} - F^2_{i,j-\frac{1}{2}}}{\triangle y} \right) - q_S S_{i,j} \tag{B.3}$$

To incorporate the boundary conditions, we add "ghost points" to $S_{i,j}$. As an example, the left boundary of the habitat requires $\mathbf{J} \cdot \langle -1, 0 \rangle = 0$; in the approximation, this implies $F^1_{\frac{1}{2},j} = 0$ for each j. The ghost points $S_{0,j}$ satisfy this condition if

$$D_S \frac{S_{1,j} - S_{0,j}}{\triangle x} + c^1_{\frac{1}{2},j} \left(S_{0,j}(c^1_{\frac{1}{2},j} \geq 0) + S_{1,j}(c^1_{\frac{1}{2},j} < 0) \right) = 0,$$

which gives

$$S_{0,j} = \frac{(D_S S_{1,j} + \triangle x c^1_{\frac{1}{2},j}(c^1_{\frac{1}{2},j} < 0) S_{1,j})}{(D_S - \triangle x c^1_{\frac{1}{2},j}(c^1_{\frac{1}{2},j} \geq 0))}$$

Having characterized the boundary condition, the approximation (B.3) can be solved for each of the $S_{i,j}$ using a numerical solver.

B.2 Steady-State of the Null Searching Distribution

Linearity and conservation of the system (3.10) allow the steady-state to be found by matching inflow and outflow between states and requiring the sum of the state probabilities to be 1. We start by setting the derivatives in system (3.10) to 0. Since the system conserves probability mass, the equations describing the dynamics are linearly dependent; we work

with the S and T. Additionally, we define $\hat{S} = S^*/(w_N N^*)$ and $\hat{T} = T^*/(w_N N^*)$, with N^* the unknown equilibrium of the N equation. The modified system can be written as

$$0 = D_S \Delta \hat{S} - \nabla \left(\mathbf{c}_S \hat{S} \right) - q_S \hat{S} + \frac{I_N}{A_N} \tag{B.4a}$$

$$0 = D_T \Delta \hat{T} - \nabla \left(\mathbf{c}_T \hat{T} \right) + q_S \hat{I}_N \hat{S} \tag{B.4b}$$

Finite difference methods from Section B.1 are used to solve for $\hat{S}$, which in turn is used to solve for $\hat{T}$. Because the original system was linear, the true steady-state solutions S^*, T^* are simply multiples of $\hat{S}$ and $\hat{T}$, respectively. The remaining work is to find what these scaling factors are. Define

$$\begin{aligned} \hat{S}^T &= \iint_{\Omega_H} \hat{S}\, dA \qquad c = \frac{1}{\hat{S}^T} \iint_{\Omega_N} \hat{S}\, dA \qquad \hat{T}^T = \iint_{\Omega_H} \hat{T}\, dA \\ \hat{\mathbf{J}}_T &= \frac{\mathbf{J}_T}{w_N N^*} \qquad \delta_T = -\frac{\oint_{\partial \Omega_N} \hat{\mathbf{J}}_T \cdot \vec{n}_N \, ds}{\hat{T}^T}. \end{aligned} \tag{B.5}$$

Recall $\mathbf{J}_I = -D_I \nabla I + \mathbf{c}_I I$ for I $\in$ {T, R}. The constant δ_T describes how flux from state T to N depends on the total probability mass in the T state; because the T equation is linear, δ_T remains unchanged if the input $\hat{S}$ is multiplied by a scalar. c describes the ratio of mass in the nest region to total mass, and does not change with a scalar change in the $\hat{S}$ state source term, $\dfrac{I_N}{A_N}$.

Next, we integrate Equations (3.10) with time derivatives set to 0 over Ω_H and use the divergence theorem, paired with the definitions in (B.5), to give

$$0 = -q_S S^T + w_N N^* \tag{B.6a}$$

$$0 = -\delta_T T^T + q_S (1 - c) S^T. \tag{B.6b}$$

Here, S^T and T^T denotes the total probability mass in state S and T at equilibrium, respectively. Equations (B.6) can be solved for S^T and T^T:

$$S^T = \frac{w_N N^*}{q_S} \tag{B.7a}$$

$$T^T = \frac{(1 - c)\, w_N N^*}{\delta_T} \tag{B.7b}$$

The sum requirement $S^T + T^T + N^* = 1$ becomes $w_N N^* \left(\dfrac{1}{q_S} + \dfrac{(1-c)}{\delta_T} + \dfrac{1}{w_N} \right) = 1$ Thus,

$$S^T = \frac{1}{q_S}\left[\frac{1}{q_S} + \frac{(1-c)}{\delta_T} + \frac{1}{w_N}\right]^{-1} \tag{B.8a}$$

$$T^T = \frac{(1-c)}{\delta_T}\left[\frac{1}{q_S} + \frac{(1-c)}{\delta_T} + \frac{1}{w_N}\right]^{-1} \tag{B.8b}$$

$$N^* = \frac{1}{w_N}\left[\frac{1}{q_S} + \frac{(1-c)}{\delta_T} + \frac{1}{w_N}\right]^{-1} \tag{B.8c}$$

Finally, S^*, T^* are found by rescaling $\hat{S}$ and $\hat{T}$, giving

$$\begin{aligned} S^* &= \frac{\hat{S}}{\iint\limits_{\Omega_H} \hat{S}\, dA} S^T \\ T^* &= \frac{\hat{T}}{\iint\limits_{\Omega_H} \hat{T}\, dA} T^T \end{aligned} \tag{B.9}$$

B.3 Steady States of the Recruitment Searching Distribution

Finding the equilibrium of the recruitment dynamics is more difficult due to nonlinearity, as well as the increased number of equations. If the advection term in the S dynamics were constant, the equilibrium could be found by a procedure similar to that described in Section B.2. A similar method as before is used to incorporate advection as a nonlinear function of pheromone levels.

Suppose $P^T = \iint\limits_{\Omega_H} P^*\, dA$ is the total amount of pheromone present at equilibrium. Define a function *ss.cost* that takes the total amount of pheromone present as input, computes the amount of returning excited ants for that amount of pheromone present at equilibrium, $R^T = \iint\limits_{\Omega_H} R^*\, dA$, and returns $n\frac{\ell}{\delta}R^T - P^T$. Steady states of the system correspond to roots of *ss.cost*. Once formed, all steady states can be found using a root-solving procedure such as uniroot in the RootSolve package in R [64].

The function *ss.cost* works as follows: given P^T

1. Initialize pheromone distribution, fix S-state advection terms
2. Solve scaled versions of the spatial equations
3. Solve system (3.17), return $n\frac{\ell}{\delta}R^T - P^T$.

1. Initialize pheromone distribution, fix S-state advection terms:

   The total amount of pheromone is given as P^T; the equilibrium distribution satisfies $P^* = n\frac{\ell}{\delta}R^*$, but R^* is unknown. It is known that R^* is a scaled version of $\hat{R}$, where $\hat{R}$ satisfies the equation

$$0 = D_R \Delta \hat{R} - \nabla \left(\mathbf{c}_R \hat{R} \right) + \frac{I_B}{A_B}, \tag{B.10}$$

   with $\hat{R} = 0$ on Ω_N, and no-flux boundaries on $\partial\Omega_H$. This linear PDE can be numerically solved using the finite difference methods outlined in Section B.1. Set $P^G = \dfrac{\hat{R}}{\iint\limits_{\Omega_H} \hat{R}\, dA} P^T$. With P^T pheromone present at equilibrium, P^G is the pheromone distribution. We fix the searching advection terms (assumed to be constant in time) to $\mathbf{c}_P := \mathbf{c}_P(P^G)$.

2. Solve scaled versions of the spatial equations:

   Solve a system analogous to (B.4) and compute terms analogous to equation group (B.5). For the following to work, the T-state equation is broken up into two components: T_1 describes that part of T that has a source from state S; T_2 describes the part of T with source from state Q. Solve the scaled equations below for $\hat{S}, \hat{T_1}, \hat{T_2}$, and $\hat{R}$ using finite difference methods.

$$0 = D_S \Delta \hat{S} - \nabla \left(\mathbf{c}_P \hat{S} \right) - q_S \hat{S} + \frac{I_N}{A_N} - v\, \frac{I_B}{A_B} \hat{S} \tag{B.11a}$$

$$0 = D_T \Delta \hat{T_1} - \nabla \left(\mathbf{c}_T \hat{T_1} \right) + \hat{I}_N \hat{S} \tag{B.11b}$$

$$0 = D_T \Delta \hat{T_2} - \nabla \left(\mathbf{c}_T \hat{T_2} \right) + \frac{I_B}{A_B} \tag{B.11c}$$

$$0 = D_R \Delta \hat{R} - \nabla \left(\mathbf{c}_R \hat{R} \right) + \frac{I_B}{A_B} \tag{B.11d}$$

   These equations are solved with no-flux boundary conditions on $\partial\Omega_H$, and $\hat{T_1} = 0$, $\hat{T_2} = 0$, $\hat{R} = 0$ on Ω_N. The true steady-state distributions S, T_1, T_2, R are simply scaled versions of $\hat{S}, \hat{T_1}, \hat{T_2}, \hat{R}$.

3. Solve system (3.17) for the steady-state, given P^T. Return $n\frac{\ell}{\delta}R^T - P^T$:

   Using the previous solutions, define the following:

$$\hat{I}^T = \iint\limits_{\Omega_H} \hat{I}\, dA,\ \hat{I} \in \{\hat{S}, \hat{T}_1, \hat{T}_2, \hat{R}\} \qquad c = \frac{1}{\hat{S}^T} \iint\limits_{\Omega_N} \hat{S}\, dA \qquad \delta_S = \frac{v}{\hat{S}^T} \iint\limits_{\Omega_B} \hat{S}\, dA$$

$$\hat{\mathbf{J}}_T^1 = -D_T \nabla \hat{T}_1 + \mathbf{c}_T \hat{T}_1 \qquad \delta_T^1 = -\frac{1}{\hat{T}_1^T} \oint\limits_{\partial\Omega_N} \hat{\mathbf{J}}_T^1 \cdot \vec{n}_N\, ds$$

$$\hat{\mathbf{J}}_T^2 = -D_T \nabla \hat{T}_2 + \mathbf{c}_T \hat{T}_2 \qquad \delta_T^2 = -\frac{1}{\hat{T}_2^T} \oint\limits_{\partial\Omega_N} \hat{\mathbf{J}}_T^2 \cdot \vec{n}_N\, ds$$

$$\hat{\mathbf{J}}_R = -D_R \nabla \hat{R} + \mathbf{c}_R \hat{R} \qquad \delta_R = -\frac{1}{\hat{R}^T} \oint\limits_{\partial\Omega_N} \hat{\mathbf{J}}_R \cdot \vec{n}_N\, ds \tag{B.12}$$

Now, we integrate the spatial equations of system (3.17) over Ω_H and use the definitions in (B.12) to derive the following system of algebraic equations (recall $()^*$ denotes equilibria of ODE states, and $()^T$ denotes the equilibrial total probability mass in the superscripted state):

$$0 = c\, q_S S^T + \delta_T^1 T_1^T + \delta_T^2 T_2^T - w_N N^* - \xi n E^* N^* \tag{B.13a}$$

$$0 = -\delta_S S^T - q_S S^T + w_N N^* + \xi n E^* N^* + w_E E^* \tag{B.13b}$$

$$0 = -\delta_T^1 T_1^T + q_S (1-c) S^T \tag{B.13c}$$

$$0 = -\delta_T^2 T_2^T + w_Q Q^* \tag{B.13d}$$

$$0 = -\delta_R R^T + w_B B^* \tag{B.13e}$$

$$0 = \delta_R R^T - w_E E^* \tag{B.13f}$$

$$0 = \delta_S S^T - \alpha_0 (A_0 - n B^*) Q^* - w_Q S \tag{B.13g}$$

$$0 = \alpha_0 (A_0 - n B^*) Q^* - w_B B^* \tag{B.13h}$$

When paired with the conservation equation, $S^T + T^T + E^* + R^T + N^* + Q^* + B^* = 1$, these equations can be solved uniquely for the 7 unknowns. Even more, paired with some algebra (omitted), this system can be reduced to a one-variable equation which, solved numerically, gives the other 6 unknowns. We solve this system for the 7 unknowns, and return $n\frac{\ell}{\delta} R^T - P^T$.

We apply a root-solving scheme to *ss.cost* to find the P^T values that result in a steady-state (roots of *ss.cost*). Once found, the P^T value can be used to find all other states. To

accomplish this, we use the P^T value to solve for $\hat{S}, \hat{T}$, and $\hat{R}$, then solve for S^T, T^T, and R^T. Finally, the properly scaled equilibrium solutions are

$$\begin{aligned} S^* &= \frac{\hat{S}}{\iint\limits_{\Omega_H} \hat{S}\, dA} S^T \\ T^* &= \frac{\hat{T}}{\iint\limits_{\Omega_H} \hat{T}\, dA} T^T \\ R^* &= \frac{\hat{R}}{\iint\limits_{\Omega_H} \hat{R}\, dA} R^T \end{aligned} \tag{B.14}$$

B.4 Continuum limit of a general space-jump random walk in 2D

To understand how the colony's trail fidelity influences the searching distribution, a random walk description of movement and the resulting Focker-Planck equation from the diffusion limit are developed. Next, the effect of pheromone is incorporated in the random walk, and modifications to the Fokker-Planck equation are described. We begin with a derivation of the probability distribution of an individual's position in 2D space. Divide space into small, nonoverlapping boxes of width $\triangle x$ and height $\triangle y$, and define box

$$b_{i,j} = \{(x, y) : x_i \leq x < x_i + \triangle x \ \ \& \ \ y_j \leq y < y_j + \triangle y\}$$

with $x_i = i \triangle x, y_j = j \triangle y$. Define $\hat{S}(i, j, t)$ as the discrete probability density function of the ant's position at time t; the probability the ant is in box $b_{i,j}$ at time t is $\hat{S}(i, j, t) \triangle x \triangle y$, and $\sum\limits_{i=-\infty}^{\infty} \sum\limits_{j=-\infty}^{\infty} S(i, j, t) \triangle x \triangle y = 1$ for all t.

Every τ units of time, the ant hops to a different box, or remains in its current box; define $\hat{K}(i', j', i, j)$ as the discrete probability density of the individual moving from position (i', j') to position (i, j). We require $\sum\limits_{i=-\infty}^{\infty} \sum\limits_{j=-\infty}^{\infty} \hat{K}(\hat{i}, \hat{j}, i, j) \triangle x \triangle y = 1$, since an individual currently at position $(\hat{i}, \hat{j})$ moves *somewhere* with probability 1.

To derive an equation for $\hat{S}(i, j, t)$, we sum all of the ways an ant can end up at position (i, j) over a single timestep, τ:

$$\hat{S}(i, j, t + \tau) = \sum_{i=-\infty}^{\infty} \sum_{j=-\infty}^{\infty} \hat{S}(i, j, t) \hat{K}(\hat{i}, \hat{j}, i, j) \triangle x \triangle y \tag{B.15}$$

This is the discrete version of the so-called Master Equation of the random walk process. Replace (i, j) and (i', j') with (x_i, y_j) and $(\hat{x}_i, \hat{y}_j)$, respectively. Letting $\triangle x$, $\triangle y \to 0$, x_i and y_j become the continuous variables x and y.

Define $S(t, x, y) = \hat{S}(i, j, t)$, and replace the right-hand side of (B.15) with the integral to obtain the continuous version of the Master equation,

$$S(t+\tau, x, y) = \int_{-\infty}^{\infty}\int_{-\infty}^{\infty} S(t, x', y')K(x', y', x, y)\ \mathrm{d}x'\ \mathrm{d}y'. \tag{B.16}$$

For clarity, we redefine $K(x', y', x, y)$ as $K(x', y', a_1, a_2)$, where (x', y') is the starting position, and $a_1 = x - x'$, $a_2 = y - y'$ are the jump distances in the x and y direction, respectively. Equation (B.16) becomes

$$S(t+\tau, x, y) = \int_{-\infty}^{\infty}\int_{-\infty}^{\infty} S(t, x-a_1, y-a_2)K(x-a_1, y-a_2, a_1, a_2)\ \mathrm{d}a_1\ \mathrm{d}a_2. \tag{B.17}$$

Assuming that the starting and ending points of a jump are close together, Equation (B.17) can be Taylor expanded around $a_1 = 0$, $a_2 = 0$ in the starting position argument. The right-hand side becomes:

$$\begin{aligned}
&= \iint_{\Omega_H} S(x-a_1, y-a_2, t)K(a_1, a_2, x, y)\ \mathrm{d}a_1\ \mathrm{d}a_2 \\
&= \iint_{\Omega_H} \left(S - a_1S_x - a_2S_y + \frac{a_1^2}{2}S_{xx} + a_1a_2S_{xy} + \frac{a_2^2}{2}S_{yy} + H.O.T.\right)\cdot \\
&\left(K - a_1K_x - a_2K_y + \frac{a_1^2}{2}K_{xx} + a_1a_2K_{xy} + \frac{a_2^2}{2}K_{yy} + H.O.T.\right)\ \mathrm{d}a_1\ \mathrm{d}a_2.
\end{aligned} \tag{B.18}$$

with terms order 3 and higher (in a_1, a_2) denoted H.O.T (Higher Order Terms). Expanding all terms, and taking a limit as $\tau \to 0$, the equation can be rearranged to yield

$$\frac{dS}{\partial t} = -\nabla\cdot(\mathbf{c}S) + \frac{\partial^2}{\partial x^2}\left(d_{xx}S\right) + \frac{\partial^2}{\partial y^2}\left(d_{yy}S\right) + \frac{\partial^2}{\partial x\partial y}\left(d_{xy}S\right). \tag{B.19}$$

where $\mathbf{c} = \langle c_1, c_2\rangle$, and

$$
\begin{aligned}
c_1 = &\quad \lim_{\tau\to 0}\frac{1}{\tau}\iint\limits_{\Omega_H} a_1 K(a_1,a_2,x,y)\ \mathrm{d}a_1\ \mathrm{d}a_2 \\
c_2 = &\quad \lim_{\tau\to 0}\frac{1}{\tau}\iint\limits_{\Omega_H} a_2 K(a_1,a_2,x,y)\ \mathrm{d}a_1\ \mathrm{d}a_2 \\
d_{xx} = &\quad \lim_{\tau\to 0}\frac{1}{2\tau}\iint\limits_{\Omega_H} a_1^2 K(a_1,a_2,x,y)\ \mathrm{d}a_1\ \mathrm{d}a_2 \\
d_{xy} = &\quad \lim_{\tau\to 0}\frac{1}{\tau}\iint\limits_{\Omega_H} a_1 a_2 K(a_1,a_2,x,y)\ \mathrm{d}a_1\ \mathrm{d}a_2 \\
d_{yy} = &\quad \lim_{\tau\to 0}\frac{1}{2\tau}\iint\limits_{\Omega_H} a_2^2 K(a_1,a_2,x,y)\ \mathrm{d}a_1\ \mathrm{d}a_2
\end{aligned}
\tag{B.20}
$$

are assumed to exist. This assumption requires the first and second moments of $K(a_1, a_2, x, y)$ (with respect to a_1 and a_2) to approach 0 at order τ or faster as $\tau \to 0$; it is also assumed that higher order moments go to 0 in the limit. Equation (B.19) is called the Fokker-Planck equation, and describes the time evolution of the positional probability distribution when τ is arbitrarily small [52].

B.5 Angular and steplength distributions

To continue the analysis, it is necessary to choose a specific form of the jump distribution K. Switching the stepsize variables a_1, a_2 to polar coordinates, define $K(\rho, \theta, x, y)$ as the probability of hopping length ρ in direction θ when at position (x, y). A convenient form is $K(\rho, \theta, x, y) = \frac{1}{\rho} f(\rho) k(\theta, \hat{\theta})$, where $f(\rho)$ describes the distribution of steplengths, and $k(\theta, \hat{\theta})$ describes a turning angle distribution symmetric around $\hat{\theta}$. Let $f(\rho) = \frac{1}{\hat{\rho}} exp\left[-\frac{1}{\hat{\rho}}\rho\right]$, the exponential distribution with mean steplength $\hat{\rho}$.

The direction of each step is drawn from a von Mises distribution; this distribution is popularly used to model random directions that exibit bias, can be fitted to data, and has well-known properties [5, 29]. The von Mises distribution is defined as

$$k(\theta, \hat{\theta}) = \frac{e^{\kappa\, cos(\theta - \hat{\theta})}}{2\pi I_0(\kappa)}.$$

$k(\theta, \hat{\theta})$ is symmetric about its mode, $\hat{\theta}$, and has dispersion proportional to $\frac{1}{\kappa}$. As κ increases, the distribution becomes more biased toward $\hat{\theta}$. $I_0(\kappa)$ is a modified Bessel function of order 0 that acts as a normalizing term, $I_0(\kappa) = \frac{1}{2\pi}\int\limits_{-\pi}^{\pi} e^{\kappa\, cos(\theta)}\, d\theta$. More generally, the Bessel function of order n, $I_n(\kappa)$, is defined as

$$I_n(\kappa) = \frac{1}{2\pi} \int_{-\pi}^{\pi} e^{\kappa cos\theta} cos(n\theta)\, \mathrm{d}\theta \tag{B.21}$$

[5].

B.6 Explicit advection and diffusion terms

The specific values of (B.20) are now calculated with the von Mises directional distribution and exponential steplength distribution. To calculate c_1, first rewrite the integral $\iint_{\Omega_H} a_1 K(a_1, a_2, x, y)\ \mathrm{d}a_1\ \mathrm{d}a_2$ in polar coordinates. To simplify the discussion, define $k_0(\theta) = k(\theta, 0)$ as the von Mises with mean 0; the von Mises with bias $\hat{\theta}$ can be written $k_0(\theta - \hat{\theta})$, with k_0 an even function of $\theta - \hat{\theta}$.

$$\begin{aligned}
\iint_{\Omega_H} a_1 K(a_1, a_2, x, y)\ \mathrm{d}a_1\ \mathrm{d}a_2 &= \int_0^{\infty}\int_{-\pi}^{\pi} \rho\, \cos(\theta) K(\rho, \theta, x, y) \rho\, \mathrm{d}\theta\ \mathrm{d}\rho \\
&= \int_0^{\infty}\int_{-\pi}^{\pi} \rho\, \cos(\theta)\, \frac{1}{\rho} f(\rho)\, k_0(\theta - \hat{\theta})\, \rho\, \mathrm{d}\theta\ \mathrm{d}\rho \\
&= \int_0^{\infty} \rho\, f(\rho) \mathrm{d}\rho \int_{-\pi}^{\pi} \cos(\theta - \hat{\theta} + \hat{\theta})\, k_0(\theta - \hat{\theta})\, \mathrm{d}\theta \\
&= \hat{\rho} \int_{-\pi}^{\pi} \cos(\theta - \hat{\theta} + \hat{\theta})\, k_0(\theta - \hat{\theta})\, \mathrm{d}\theta \\
&= \hat{\rho} \int_{-\pi}^{\pi} \cos(\theta - \hat{\theta}) \cos(\hat{\theta})\, k_0(\theta - \hat{\theta}) - \sin(\theta - \hat{\theta}) \sin(\hat{\theta})\, k_0(\theta - \hat{\theta})\, \mathrm{d}\theta \\
&= \hat{\rho} \int_{-\pi}^{\pi} \cos(\theta - \hat{\theta}) \cos(\hat{\theta})\, k_0(\theta - \hat{\theta})\, \mathrm{d}\theta \\
&= \hat{\rho} \cos(\hat{\theta}) \int_{-\pi}^{\pi} \cos(\theta - \hat{\theta})\, k_0(\theta - \hat{\theta})\, \mathrm{d}\theta \\
&= \hat{\rho} \cos(\hat{\theta}) \frac{I_1(\kappa)}{I_0(\kappa)}
\end{aligned} \tag{B.22}$$

The above calculation uses the cosine property $\cos(\alpha + \beta) = \cos(\alpha)\cos(\beta) - \sin(\alpha)\sin(\beta)$; it also uses $\int_{-\pi}^{\pi} \sin(\theta - \hat{\theta}) \sin(\hat{\theta})\, k_0(\theta - \hat{\theta})\, \mathrm{d}\theta = 0$, since the integral of an odd function over its period is 0. k_0 is even, and $\sin(\theta - \hat{\theta})$ is odd, so the product is odd and integrates to 0. Finally, the definition of the Bessel function of order 1, found in Equation (B.21), is used.

Similarly,

$$\begin{aligned}
\iint_{\Omega_H} a_2 K(a_1,a_2,x,y)\ \mathrm{d}a_1\ \mathrm{d}a_2 &= \int_0^\infty \int_{-\pi}^{\pi} \rho\ \sin(\theta) K(\rho,\theta,x,y)\rho\,\mathrm{d}\theta\ \mathrm{d}\rho \\
&= \int_0^\infty \int_{-\pi}^{\pi} \rho\ \sin(\theta)\ \frac{1}{\rho} f(\rho)\, k(\theta-\hat{\theta})\,\rho\,\mathrm{d}\theta\ \mathrm{d}\rho \\
&= \int_0^\infty \rho\, f(\rho)\mathrm{d}\rho \int_{-\pi}^{\pi} \sin(\theta-\hat{\theta}+\hat{\theta})\, k(\theta-\hat{\theta})\,\mathrm{d}\theta \\
&= \hat{\rho} \int_{-\pi}^{\pi} \sin(\theta-\hat{\theta}+\hat{\theta})\, k(\theta-\hat{\theta})\,\mathrm{d}\theta \\
&= \hat{\rho} \int_{-\pi}^{\pi} \sin(\theta-\hat{\theta})\cos(\hat{\theta})\, k(\theta-\hat{\theta}) + \cos(\theta-\hat{\theta})\sin(\hat{\theta})\, k(\theta-\hat{\theta})\,\mathrm{d}\theta \\
&= \hat{\rho} \int_{-\pi}^{\pi} \cos(\theta-\hat{\theta})\sin(\hat{\theta})\, k(\theta-\hat{\theta})\,\mathrm{d}\theta \\
&= \hat{\rho}\sin(\hat{\theta}) \int_{-\pi}^{\pi} \cos(\theta-\hat{\theta})\, k(\theta-\hat{\theta})\,\mathrm{d}\theta \\
&= \hat{\rho}\sin(\hat{\theta}) \frac{I_1(\kappa)}{I_0(\kappa)}
\end{aligned} \tag{B.23}$$

Thus $\mathbf{c}(x,y) = \lim_{\tau\to 0} \frac{\hat{\rho}}{\tau}\frac{I_1(\kappa)}{I_0(\kappa)} \left\langle \cos(\hat{\theta}), \sin(\hat{\theta}) \right\rangle$

The diffusion coefficients can be analyzed in a similar manner.

$$\begin{aligned}
\iint_{\Omega_H} a_1^2 K(a_1,a_2,x,y)\ \mathrm{d}a_1\ \mathrm{d}a_2 &= \int_0^\infty \int_{-\pi}^{\pi} \rho^2\ \cos^2(\theta) K(\rho,\theta,x,y)\rho\,\mathrm{d}\theta\ \mathrm{d}\rho \\
&= \int_0^\infty \int_{-\pi}^{\pi} \rho^2\ \cos^2(\theta)\ \frac{1}{\rho} f(\rho)\, k(\theta-\hat{\theta})\,\rho\,\mathrm{d}\theta\ \mathrm{d}\rho \\
&= \int_0^\infty \rho^2\, f(\rho)\mathrm{d}\rho \int_{-\pi}^{\pi} \cos^2(\theta-\hat{\theta}+\hat{\theta})\, k(\theta-\hat{\theta})\,\mathrm{d}\theta \\
&= 2\hat{\rho}^2 \int_{-\pi}^{\pi} \frac{1}{2}(1+\cos(2(\theta-\hat{\theta}+\hat{\theta}))\, k(\theta-\hat{\theta})\,\mathrm{d}\theta \\
&= \hat{\rho}^2 \left(1 + \int_{-\pi}^{\pi} \cos(2(\theta-\hat{\theta}))\cos(2\hat{\theta})\, k(\theta-\hat{\theta})\,\mathrm{d}\theta \right) \\
&= \hat{\rho}^2 \left(1 + \int_{-\pi}^{\pi} \cos(2(\theta-\hat{\theta}))\cos(2\hat{\theta})\, k(\theta-\hat{\theta})\,\mathrm{d}\theta \right) \\
&= \hat{\rho}^2 \left(1 + \frac{I_2(\kappa)}{I_0(\kappa)}\cos(2\hat{\theta}) \right)
\end{aligned} \tag{B.24}$$

Here, the calculation $\int_0^\infty \rho^2 f(\rho)\mathrm{d}\rho = 2\hat{\rho}^2$ was used. Similar calculations give

$$\begin{aligned} \iint_{\Omega_H} a_1 a_2 K(a_1, a_2, x, y)\ \mathrm{d}a_1\ \mathrm{d}a_2 &= 2\hat{\rho}^2 \frac{I_2(\kappa)}{I_0(\kappa)} \sin(2\hat{\theta}) \cos(2\hat{\theta}) \\ \iint_{\Omega_H} a_2^2 K(a_1, a_2, x, y)\ \mathrm{d}a_1\ \mathrm{d}a_2 &= \hat{\rho}^2 \left(1 - \frac{I_2(\kappa)}{I_0(\kappa)} \cos(2\hat{\theta})\right) \end{aligned} \tag{B.25}$$

These expressions can be further simplified by specifying a form of κ; set $\kappa = b\hat{\rho}$. This assumes the bias in the turning angle distribution is small, and scales with average stepsize as $\tau \to 0$; thus the bias observed over each timestep is small. Now, we approximate Bessel functions $I_0(\kappa)$, $I_1(\kappa)$, and $I_2(\kappa)$ with

$$I_0(\kappa) = 1 + \frac{\kappa^2}{4} + H.O.T. \tag{B.26}$$

$$I_1(\kappa) = \frac{\kappa}{2} + H.O.T. \tag{B.27}$$

$$I_2(\kappa) = \frac{\kappa^2}{8} + H.O.T. \tag{B.28}$$

which can be obtained by a Taylor expansion of Equation (B.21) around $\kappa = 0$.

Putting it all together,

$$\begin{aligned} d_{xx} &= \lim_{\tau \to 0} \frac{1}{2\tau} \iint_{\Omega_H} a_1^2 K(a_1, a_2, x, y)\ \mathrm{d}a_1\ \mathrm{d}a_2 \\ &= \lim_{\tau \to 0} \frac{1}{2\tau} \hat{\rho}^2 \left(1 + \frac{I_2(\kappa)}{I_0(\kappa)} \cos(2\hat{\theta})\right) \\ &= \lim_{\tau \to 0} \frac{1}{2\tau} \hat{\rho}^2 \left(1 + \frac{\kappa^2}{8} \cos(2\hat{\theta}) + H.O.T.\right) \\ &= \lim_{\tau \to 0} \frac{1}{2\tau} \hat{\rho}^2 \left(1 + \frac{b^2\hat{\rho}^2}{8} \cos(2\hat{\theta}) + H.O.T.\right) \end{aligned} \tag{B.29}$$

Keeping the highest order term gives $d_{xx} = \lim_{\tau \to 0} \frac{1}{2\tau} \hat{\rho}^2$. Similar calculations give

$$\begin{aligned} d_{xx} &= D = d_{yy} = \lim_{\tau \to 0} \frac{\hat{\rho}^2}{2\tau} \\ d_{xy} &= 0 \end{aligned} \tag{B.30}$$

assuming this limit exists. To ensure that the PDE model can track the average advection in the ABM, we must allow τ to approach 0 while keeping the magnitude of the advection, $\lim_{\tau\to 0} \frac{\hat{\rho}}{\tau}\frac{I_1(\kappa)}{I_0(\kappa)}$, constant. Thus, the advection is

$$\mathbf{c} = \lim_{\tau\to 0} \frac{I_1(\kappa)}{I_0(\kappa)}\frac{\hat{\rho}}{\tau}\left\langle \cos(\hat{\theta}), \sin(\hat{\theta})\right\rangle \tag{B.31}$$

With these forms, Equation (B.19) becomes

$$\frac{\partial S}{\partial t} = \Delta\left(DS\right) - \nabla\left(\mathbf{c}S\right) \tag{B.32}$$

Note that Equation (B.32) contains a diffusive term describing change in the pdf due to random motion, as well as an advection term that describes deterministic motion due to directional bias.

APPENDIX C

SIMULATION ADD-ON TO CHAPTER 5

This appendix outlines future additions to the colony area-restricted search simulation built in Chapter 5.

C.1 ARS with transition probabilities

The ARS simulation with transition probabilities (shortened to ARS.TP from hereon) is identical to the ARS simulation except that discovered resources have probabilities of successful recruitment. In these simulations, the colony transitions to the recruiting state with a distance-specific transition probability. The transition probabilities for various resource distances are estimated from the agent-based model developed in Chapter 3. For each resource distance r used in the PDE, 10 simulations are performed with the colony dynamics initiated at the PDE equilibrium corresponding to no resource present, except for the presence of 1 ant at the resource in the B behavioral class at a resource r m from the nest. The ABM is run for 5 hours of simulation time, after which pheromone levels are used to classify the colony as being in the recruiting state or not; simulations that end with at least 100 units of pheromone present in the environment are classified as successful recruitment. This value is somewhat arbitrary, however after 5 hours of simulation time the amount of pheromone was typically either in the thousands or close to 0, 100 gives a reasonable cut off for classifying a colony as recruiting.

To understand the influence of local searching ant density on the propensity of successful recruitment, the ABM simulation described above was performed with 1, 5, 10, 50, or 100 returning unexcited ants in the colony (the T behavioral state) initiated in a 1×1 m square centered around the resource (termed the "Sval" number).

Prior to the full ARS.TP simulation for a given parameter set, a logistic regression was used to understand how Sval and resource distance influenced the ability of the colony to recruit. The response variable used was the proportion of successful recruitment events for

the 10 trials, weighted by the number of trials. Briefly, the logistic regression model assumes a "success" in a binary response variable comes from a Bernoulli trial with probability p, which in turn is a function of the explanatory variables [47]. In this model p is assumed a linear function of Sval and resource distance r, described by

$$p = \frac{exp(a_0 + a_1 Sval + a_2 r)}{1 + exp(a_0 + a_1 Sval + a_2 r)}, \tag{C.1}$$

where a_i are determined via maximum likelihood techniques. This model is intended as an estimate of the probability that a colony is able to recruit to a newly discovered resource, given a particular number of searching ants in the vicinity. The logistic regression function was found using the statistical package R with the "glm" function prior to a simulation.

Each time a resource is found during the simulation, the current searching distribution is used to calculate the Sval number (the number of searching ants in a $1m^2$ box around the resource), after which the "predict" function is used to retrieve the expected probability p of successful recruitment for the given resource distance and Sval number. A random number RAND is chosen uniformly between 0 and 1; the colony transitions to recruiting at the resource if $RAND < p$, otherwise the simulation proceeds as if the resource were not found.

REFERENCES

[1] F. Adler and D. Gordon, *Information collection and spread by networks of patrolling ants*, The American Naturalist, 140 (1992), pp. 373–400.

[2] L. Allen, *An Introduction to Stochastic Processes with Applications to Biology*, CRC Press, 2010.

[3] P. Amorim, *Modeling ant foraging: a chemotaxis approach with pheromones and trail formation*, Journal of Theoretical Biology, 385 (2015), pp. 160–173.

[4] F. Bartumeus and J. Catalan, *Optimal search behavior and classic foraging theory*, Journal of Physics A: Mathematical and Theoretical, 42 (2009), p. 434002.

[5] E. Batschelet, *Circular statistics in biology*, vol. 371, Academic press London, 1981.

[6] R. Beckers, J. Deneubourg, and S. Goss, *Trail laying behaviour during food recruitment in the ant* Lasius niger (L.), Insectes Sociaux, 39 (1992), pp. 59–72.

[7] R. Beckers, J. Deneubourg, S. Goss, and J. Pasteels, *Collective decision making through food recruitment*, Insectes Sociaux, 37 (1990), pp. 258–267.

[8] R. Beckers, S. Goss, J. Deneubourg, and J. Pasteels, *Colony size, communication, and ant foraging strategy*, Psyche, 96 (1989), pp. 239–256.

[9] M. Beekman, D. Sumpter, and F. Ratnieks, *Phase transition between disordered and ordered foraging in pharaoh's ants*, Proceedings of the National Academy of Sciences, 98 (2001), pp. 9703–9706.

[10] S. Benhamou and P. Bovet, *How animals use their environment: a new look at kinesis*, Animal Behaviour, 38 (1989), pp. 375–383.

[11] A. Bernadou and V. Fourcassié, *Does substrate coarseness matter for foraging ants? An experiment with* Lasius niger *(Hymenoptera; Formicidae)*, Journal of Insect Physiology, 54 (2008), pp. 534–542.

[12] E. Boissard, P. Degond, and S. Motsch, *Trail formation based on directed pheromone deposition*, Journal of Mathematical Biology, 66 (2013), pp. 1267–1301.

[13] P. Bovet and S. Benhamou, *Spatial analysis of animals' movements using a correlated random walk model*, Journal of Theoretical Biology, 131 (1988), pp. 419–433.

[14] V. Calenbuhr and J. Deneubourg, *A model for osmotropotactic orientation (i)*, Journal of Theoretical Biology, 158 (1992), pp. 359–393.

[15] E. Charnov, *Optimal foraging, the marginal value theorem*, Theoretical Population Biology, 9 (1976), pp. 129–136.

[16] J. Cherry and F. Adler, *How to make a biological switch*, Journal of Theoretical Biology, 203 (2000), pp. 117–133.

[17] B. Collignon and C. Detrain, *Distributed leadership and adaptive decision-making in the ant tetramorium caespitum*, Proceedings of the Royal Society B: Biological Sciences, 277 (2010), pp. 1267–1273.

[18] B. Collignon, J. Louis Deneubourg, and C. Detrain, *Leader-based and self-organized communication: modelling group-mass recruitment in ants*, Journal of Theoretical Biology, (2012).

[19] Z. Cook, D. Franks, and E. Robinson, *Exploration versus exploitation in polydomous ant colonies*, Journal of Theoretical Biology, (2013).

[20] J. Cresswell, *A comparison of bumblebees movements in uniform and aggregated distributions of their forage plant*, Ecological Entomology, 25 (2000), pp. 19–25.

[21] G. Debout, B. Schatz, M. Elias, and D. McKey, *Polydomy in ants: what we know, what we think we know, and what remains to be done*, Biological Journal of the Linnean Society, 90 (2007), pp. 319–348.

[22] J. Deneubourg and S. Goss, *Collective patterns and decision-making*, Ethology Ecology & Evolution, 1 (1989), pp. 295–311.

[23] J. Deneubourg, J. Pasteels, and J. Verhaeghe, *Probabilistic behaviour in ants: a strategy of errors?*, Journal of Theoretical Biology, 105 (1983), pp. 259–271.

[24] C. Detrain and J. Deneubourg, *Self-organized structures in a superorganism: do ants behave like molecules?*, Physics of Life Reviews, 3 (2006), pp. 162–187.

[25] L. Edelstein-Keshet, *Simple models for trail-following behaviour; trunk trails versus individual foragers*, Journal of Mathematical Biology, 32 (1994), pp. 303–328.

[26] L. Edelstein-Keshet, J. Watmough, and B. Ermentrout, *Trail following in ants: individual properties determine population behaviour*, Behavioral Ecology and Sociobiology, 36 (1995), pp. 119–133.

[27] D. Eifler, K. Baipidi, M. Eifler, D. Dittmer, and L. Nguluka, *Influence of prey encounter and prey identity on area-restricted searching in the lizard* Pedioplanis namaquensis, Journal of Ethology, 30 (2012), pp. 197–200.

[28] L. Evans, *Partial differential equations*, Graduate Studies in Mathematics, 19 (1998).

[29] N. Fisher, *Statistical analysis of circular data*, Cambridge University Press, 1995.

[30] V. Fourcassié and J. Traniello, *Effects of experience on food-searching behavior in the ant* Formica schaufussi *(Hymenoptera: Formicidae)*, Journal of Insect Behavior, 6 (1993), pp. 287–299.

[31] D. Gillespie, *Exact stochastic simulation of coupled chemical reactions*, The Journal of Physical Chemistry, 81 (1977), pp. 2340–2361.

[32] M. Greene and D. Gordon, *How patrollers set foraging direction in harvester ants*, The American Naturalist, 170 (2007), pp. 943–948.

[33] T. Hillen and K. Painter, *A users guide to pde models for chemotaxis*, Journal of Mathematical Biology, 58 (2009), pp. 183–217.

[34] T. Hills, P. Brockie, and A. Maricq, *Dopamine and glutamate control area-restricted search behavior in* Caenorhabditis elegans, The Journal of Neuroscience, 24 (2004), pp. 1217–1225.

[35] B. Hölldobler and E. Wilson, *The Ants*, Belknap Press, 1990.

[36] E. Holmes, *Are diffusion models too simple? a comparison with telegraph models of invasion*, American Naturalist, (1993), pp. 779–795.

[37] D. Hosmer and S. Lemeshow, *Applied survival analysis: Regression modelling of time to event data*, Eur Orthodontic Soc, 1999.

[38] R. Jeanson, F. L. Ratnieks, and J. Deneubourg, *Pheromone trail decay rates on different substrates in the Pharaoh's ant, Monomorium pharaonis*, Physiological Entomology, 28 (2003), pp. 192–198.

[39] L. Johnson, S. Hubbell, and D. Feener, *Defense of food supply by eusocial colonies*, American Zoologist, 27 (1987), pp. 347–358.

[40] P. Kareiva and G. Odell, *Swarms of predators exhibit "preytaxis" if individual predators use area-restricted search*, American Naturalist, (1987), pp. 233–270.

[41] P. Kareiva and N. Shigesada, *Analyzing insect movement as a correlated random walk*, Oecologia, 56 (1983), pp. 234–238.

[42] A. Kay, *Applying optimal foraging theory to assess nutrient availability ratios for ants*, Ecology, 83 (2002), pp. 1935–1944.

[43] E. Keller and L. Segel, *Initiation of slime mold aggregation viewed as an instability*, Journal of Theoretical Biology, 26 (1970), pp. 399–415.

[44] ——, *Model for chemotaxis*, Journal of Theoretical Biology, 30 (1971), pp. 225–234.

[45] S. I. Kramer, B.H. and S. Foitzik, *The role of per-capita productivity in the evolution of small colony sizes in ants*, Behavioral Ecology and Sociobiology, 68 (2014), pp. 41–53.

[46] R. LeVeque, *Finite difference methods for ordinary and partial differential equations: steady-state and time-dependent problems*, vol. 98, Siam, 2007.

[47] J. Matthiopoulos, *How to be a quantitative ecologist: the'A to R'of green mathematics and statistics*, John Wiley & Sons, 2011.

[48] H. McKenzie, E. Merrill, R. Spiteri, and M. Lewis, *How linear features alter predator movement and the functional response*, Interface focus, 2 (2012), pp. 205–216.

[49] G. McNickle and J. Cahill, *Plant root growth and the marginal value theorem*, Proceedings of the National Academy of Sciences, 106 (2009), pp. 4747–4751.

[50] P. Moorcroft and M. Lewis, *Mechanistic home range analysis.(MPB-43)*, Princeton University Press, 2013.

[51] J. Murray, *Mathematical Biology. II Spatial Models and Biomedical Applications: Interdisciplinary Applied Mathematics V. 18*, Springer-Verlag New York Incorporated, 2001.

[52] A. Okubo and S. Levin, *Diffusion and ecological problems: modern perspectives*, vol. 14, Springer Science & Business Media, 2013.

[53] M. Onsum and C. Rao, *Calling heads from tails: the role of mathematical modeling in understanding cell polarization*, Current Opinion in Cell Biology, 21 (2009), pp. 74–81.

[54] V. Paiva, P. Geraldes, I. Ramírez, S. Garthe, and J. Ramos, *How area restricted search of a pelagic seabird changes while performing a dual foraging strategy*, Oikos, 119 (2010), pp. 1423–1434.

[55] J. Pearce-Duvet, C. Elemans, and D. Feener, *Walking the line: search behavior and foraging success in ant species*, Behavioral Ecology, 22 (2011), pp. 501–509.

[56] J. Pearce-Duvet and D. Feener, *Resource discovery in ant communities: do food type and quantity matter?*, Ecological Entomology, 35 (2010), pp. 549–556.

[57] M. Pfeiffer and K. Linsenmair, *Contributions to the life history of the Malaysian giant ant Camponotus gigas (Hymenoptera, Formicidae)*, Insectes Sociaux, 47 (2000), pp. 123–132.

[58] G. Pyke, *Optimal foraging in hummingbirds: testing the marginal value theorem*, American Zoologist, 18 (1978), pp. 739–752.

[59] R Core Team, *R: A Language and Environment for Statistical Computing*, R Foundation for Statistical Computing, Vienna, Austria, 2012. ISBN 3-900051-07-0.

[60] ——, *R: A Language and Environment for Statistical Computing*, R Foundation for Statistical Computing, Vienna, Austria, 2015.

[61] I. Scharf, B. Kotler, and O. Ovadia, *Consequences of food distribution for optimal searching behavior: an evolutionary model*, Evolutionary Ecology, 23 (2009), pp. 245–259.

[62] A. Schmolke, *Benefits of dispersed central-place foraging: An individual-based model of a polydomous ant colony*, The American Naturalist, 173 (2009), pp. 772–778.

[63] P. Schultheiss and K. Cheng, *Finding food: outbound searching behavior in the Australian desert ant* Melophorus bagoti, Behavioral Ecology, (2012), p. ars143.

[64] K. Soetaert and P. M. Herman, *A practical guide to ecological modelling: using R as a simulation platform*, Springer Science & Business Media, 2008.

[65] D. Stephens and J. Krebs, *Foraging theory, 1986*, Princeton: Princeton University Press, 1, p. 100.

[66] M. Tabone, B. Ermentrout, and B. Doiron, *Balancing organization and flexibility in foraging dynamics*, Journal of Theoretical Biology, 266 (2010), pp. 391–400.

[67] T. Therneau, *A Package for Survival Analysis in S*, 2015. version 2.38.

[68] A. Thiel and T. Hoffmeister, *Knowing your habitat: linking patch-encounter rate and patch exploitation in parasitoids*, Behavioral Ecology, 15 (2004), pp. 419–425.

[69] W. Towne and J. Gould, *The spatial precision of the honey bees' dance communication*, Journal of Insect Behavior, 1 (1988), pp. 129–155.

[70] J. Traniello, A. Kozol, and M. Fournier, *Resource-Related Spatial Patterns of Search in the Ant* Formica schaufussi*: a Field Study*, Psyche, 99 (1992), pp. 87–93.

[71] L. Van O., E. Billoir, R. Boulay, C. Bernstein, and X. Cerda, *Temperature limits trail following behaviour through pheromone decay in ants*, Naturwissenschaften, 98 (2011), pp. 1009–1017.

[72] J. Verhaeghe and J. Deneubourg, *Experimental study and modelling of food recruitment in the anttetramorium impurum (hym. form.)*, Insectes sociaux, 30 (1983), pp. 347–360.

[73] A. Visser, *Lagrangian modelling of plankton motion: From deceptively simple random walks to Fokker–Planck and back again*, Journal of Marine Systems, 70 (2008), pp. 287–299.

[74] E. Wajnberg, X. Fauvergue, and O. Pons, *Patch leaving decision rules and the marginal value theorem: an experimental analysis and a simulation model*, Behavioral Ecology, 11 (2000), pp. 577–586.

[75] J. Watmough and L. Edelstein-Keshet, *A one-dimensional model of trail propagation by army ants*, Journal of Mathematical Biology, 33 (1995), pp. 459–476.

[76] A. Weidenmüller and T. Seeley, *Imprecision in waggle dances of the honeybee (Apis mellifera) for nearby food sources: error or adaptation?*, Behavioral Ecology and Sociobiology, 46 (1999), pp. 190–199.

[77] H. Weimerskirch, D. Pinaud, F. Pawlowski, and C. Bost, *Does prey capture induce area-restricted search? a fine-scale study using gps in a marine predator, the wandering albatross*, The American Naturalist, 170 (2007), pp. 734–743.

[78] E. Wilson, *The organization of colony defense in the ant Pheidole dentata Mayr (Hymenoptera: Formicidae)*, Behavioral Ecology and Sociobiology, 1 (1976), pp. 63–81.

[79] P. Zollner and S. Lima, *Search strategies for landscape-level interpatch movements*, Ecology, 80 (1999), pp. 1019–1030.